Numerical Investigation of Solar Vapor Absorption Refrigeration System Integrated with Phase Change Material for Industrial Application

By

Natnale Sitotaw Asefa

A Thesis Submitted to the Department of Thermal and Aerospace Engineering

School of Mechanical, Chemical, and Material Engineering

Presented in partial fulfillment of the Requirement for the degree of Master of Science in Thermal Engineering

Adama Science and Technology University

Adama, Ethiopia

September 2019

Numerical Investigation of Solar Vapor Absorption Refrigeration System Integrated with Phase Change Material for Industrial Application

By: Natnale Sitotaw Asefa

Advisor: Dr. Gezahegn Habtamu

A Thesis Submitted to the Department of Thermal and Aerospace Engineering

School of Mechanical, Chemical, and Material Engineering

Presented in partial fulfillment of the Requirement for the degree of Master of Science in Thermal Engineering

Adama Science and Technology University

Adama, Ethiopia

September, 2019

CANDIDATE'S DECLARATION

First, I hereby declare that this M.Sc. thesis entitled **"Numerical Investigation of Solar Vapor Absorption Refrigeration System Integrated with Phase Change Material for Industrial Application"** is my bona fide work and that all sources of materials used for this thesis have been duly acknowledged. This thesis has been submitted in partial fulfillment of the requirements for M.Sc. degree in **Thermal Engineering** at Adama Science and Technology University, **School of Mechanical, Chemical and Material Engineering**. I solemnly declare that this thesis is not submitted to any other institution anywhere for the award of any academic degree, diploma, or certificate.

Brief quotations from this thesis are allowable without special permission provided that accurate acknowledgement of source is made. Requests for permission for extended quotation from or reproduction of this manuscript in whole or in part may be granted by the Head of the major department or the Dean of the School when in his or her judgment the proposed use of the material is in the interests of scholarship. In all other instances, however permission must be obtained from the author.

_____	_____	_____
Candidate	Signature	Date of Submission

ADVISOR'S APPROVAL SHEET

This is to certify that the thesis entitled **"Numerical Investigation of Vapor Absorption Refrigeration System Integrated with Phase Change Material for Industrial Application"** submitted in partial fulfillment of the requirements for the degree of **Master of Science in Thermal Engineering**, Graduate Program to the Department of **Thermal Engineering** and has been carried out by **Natnale Sitotaw Asefa, (A/PR15410),** under my supervision. Therefore, I recommend that the student has fulfilled the requirements and hence hereby he can submit the thesis to the department.

_____	_____	_____
Name of Advisor	Signature	Date

APPROVAL OF BOARD OF EXAMINERS

We, the undersigned members of the Board of Examiners of the final open defense by **Natnale Sitotaw Asefa** have read and evaluated his thesis entitled **"Numerical Investigation of Vapor Absorption Refrigeration System Integrated with Phase Change Material for Industrial Application"** and examined the candidate. Therefore, this is to certify that the thesis has been accepted in partial fulfillment of the requirement of the Degree of Masters in Thermal Engineering.

_____	_____	_____
Internal Examiner	Signature	Date
_____	_____	_____
External Examiner	Signature	Date
_____	_____	_____
Chairperson	Signature	Date

DEDICATION

I dedicate this project to Jesus Christ Almighty my creator, my strong pillar, my source of inspiration, wisdom, knowledge, and understanding. He has been the source of my strength throughout this program and on His wings only have I soared. I also dedicate this work to my family and to those who have been affected in every way possible by this quest. Thank you. God bless you.

ACKNOWLEDGMENTS

First and above all, I praise the almighty God for his grace to do this work, blessings, wisdom, protection and helps me throughout my life. This Master's thesis is a product of the collaboration of many institutions, material and moral support of many individuals. All these people and institutions deserve heartfelt gratitude. My sincere apologies, if I fail to mention some who deserve to be acknowledged!

My Advisor Dr. Gezahegn Habtamu has been an enormous resource to me in all facets of my academic life during my Master's study. I'm grateful to him for his continuous encouragement and constructive comments from the beginning of the research up until the thesis was made to this final form including the final edition and proofreading. He made every effort possible to help me develop as a successful researcher in a multidisciplinary environment for which I'm sincerely indebted.

I extend my deep gratitude to Adama Science and Technology University for its willingness in providing and supporting me financially, and Bekas Chemical PLC and Ah-Wan Food Complex for their kind help and cooperation. At last but not least, I am grateful to extend my deepest and heartfelt gratitude towards my family who was always on my side in my academic life. This long academic life involved lots of ups and downs, hope and despair, and needed immense moral and material support. Thank you all for your persistent support all along.

ABSTRACT

Most industrial processes in the world need refrigeration and air conditioning, to create cold storage, pasteurized products, and a comfortable thermal zone. But, the conventional refrigeration and air conditioning system is one of the major consumer of electrical energy to use it for industrial applications. Solar energy have a comprehensive applicability as an energy resource, specifically for the heat requirement for the vapor absorption refrigeration system, and it is a promising technology to create a sustainable absorption system. However, the main drawback of this resource is the intermittency and unpredictability. The objective of this study is to construct and build solar vapor absorption refrigeration system which can operate in industrial processing units without these main drawbacks.

The system comprised of three main subsystems: the water LiBr absorption system, the evacuated heat pipe collector, and the latent heat thermal storage system. The mathematical modeling based on energy and exergy analysis, and component design is studied for the absorption system. Furthermore, a transient one-dimensional heat transfer model is developed for both the collector and the storage tank. For all of the three subsystems, a general python code program that can be applied for any industrial cooling capacity is developed.

Lastly, the applicability of the model for Bekas Chemical PLC and Ah-Wan Food Complex is studied, with a chiller capacity of 186.66 kW and 245 kW, respectively. Each components of the absorption system is designed for both industries. The result show that 242 units of heat pipe evacuated tube collector with a storage tank size of 4.917m height and 3.278m diameter is demanded for Bekas Chemical PLC. On the same routine for Ah-Wan Food Complex, 310 units of evacuated tube collector with a storage tank size of 5.334m height and 3.556m diameter is needed to satisfy the heat demand with supply.

Keywords: Absorption system, Evacuated heat pipe collector, Solar radiation, Thermal storage.

TABLE OF CONTENTS

Contents

LIST OF FIGURES

LIST OF TABLES

ABBREVIATIONS

COP	Coefficient of Performance
ETC	Evacuated Tube Collector
FDM	Finite Difference Method
FPC	Flat Plate Collector
HPETSC	Heat Pipe Evacuated Tube Solar Collector
HTF	Heat Transfer Fluid
HX	Heat Exchanger
COPex	Second Law Efficiency
LHS	Latent Heat Storage
LHTES	Latent Heat Thermal Energy Storage
LMTD	Log Mean Temperature Difference
PCM	Phase Change Material
SHS	Sensible Heat Storage
SHX	Solution Heat Exchanger
TES	Thermal Energy Storage
VARS	Vapor Absorption Refrigeration System

NOMENCLATURE

f	Circulation ratio
m	Mass (Kg) /molality (mol/Kg)
χ	Mass base concentration
y	Molar base concentration
$\bar{s}$	Entropy (W/K)
R	Universal gas constant (J/mol K)
T	Temperature (K)
P	Pressure (Pa)
h	Enthalpy (J)
e	Porosity /Exergy (W)

W	Work (J)
Q	Heat flow (W)
$\boldsymbol{Pr}$	Prundtle number
$\mathbf{h_{fg}}$	Latent heat of vaporization (kJ/kg)
R	Heat transfer resistance (W/m^2K)
D	Diameter (m)
L	Length (m)
k	Thermal conductivity (W/m K)
N	Number of solar collector /number of PCM layer
n	Day of the year
g	gravity (m/s^2)
Nu	Nusselt number
U	Overall heat transfer coefficient (m^2K/W)
F	Fin efficiency
A	Area (m^2)
Re	Reynold's number
H	Global daily radiation (W/m^2)
I	Global hourly radiation (W/m^2)
Ns	Day time duration
V	Velocity (m/s)
Ka	Kapitaz number
Ja	Jakobs number

GREEK SYMBOL

Δ	Change
ρ	Density (kg/m^3)
ΔЄ	Lost exergy (W)
β	Inclination angle (^{o})
$\boldsymbol{\delta}$	Declination angle (^{o})
$\boldsymbol{\theta}$	Angle of incidence (^{o})

ω	Hour angle (^{o})
θ_z	Zenith angle (^{o})
μ	Dynamic viscosity (kg/ms)
ε	Emissivity
σ	Stefan-Boltzmann constant
α	Thermal absorptivity
H	Efficiency
γ	Melt fraction of phase changing material
ν	Kinematic viscosity (m^2/s)

SUBSCRIPTS

sc	Solar constant
o	Extraterrestrial /Standard state
G	Global
D	Diffuse
B	Beam
max	Maximum
min	Minimum
T	Tilted surface
g	Generator /glass /ground
e	Evaporator
c	Condenser
exp	Expansion valve
a	Absorber
f	Liquid
v	Vapor
fg	Latent heat
ex	Exergetic efficiency
abs	Absorber glass
w	wind /working fluid

g-a	Glass to absorber
w-g	Inner to outer glass
ps	Specific heat
hp	Heat pipe
evap	Heat pipe evaporator
cond	Heat pipe condenser
mani	Manifold
c.film	Condensing film
b.film	Boiling film
amb	Ambient
ava	Average

CHAPTER 1: Introduction

1.1. Background

Recent studies in cooling technology have been concentrated toward the use of vapor absorption refrigeration systems. Less infusion of energy in the form of heat is an admirable advantage of the vapor Absorption systems. Waste heat and solar energy can be utilized and harnessed by installing the vapor absorption refrigeration system. Solar energy is a promising means of reducing fossil fuel, electrical energy consumption, and CO_2 emission into the atmosphere. However, solar energy has two shortcomings: intermittency and unpredictability. Meaning, efficient and economical heat storage is a vital factor in the utilization of solar energy to operate without these two drawbacks. Thermal energy storage (TES) as energy storage proved a great role in the use of solar energy. TES can be either sensible energy storage or a latent heat storage system. Unlike sensible storage materials such as water, masonry or rocks, phase change material (PCM) have high storage density with a smaller temperature difference between storing and releasing heat. This makes, PCM to be a more preferable, economical and compact form of storing units over the competing sensible heat storage system.

Regarding these, integrating solar power with PCM in the vapor absorption refrigeration system is a fortune technology toward creating a cost-effective and pollution-free world. During the low or no solar radiation hours, the PCM makes the refrigeration process to continue and maintains the cold compartment at constant required temperature for a long period of time without a great fluctuation of temperature. But, to have the required performance of the absorption systems, the system is critically dependent on the chemical and thermodynamic properties of the working fluid. A fundamental requirement of the absorbent-refrigerant combination is that it must have a margin of miscibility within the temperature range of the cycle. The mixture should also be chemically stable, non-toxic, and non-explosive (Srikhirin *et al*., 2001).

The commercial vapor absorption refrigeration system (VARS) utilized in industrial process use, either the ammonia water (NH_3-H_2O) or the water lithium bromide (H_2O -LiBr) absorbent-refrigerant combination. In most of the case, NH_3-H_2O solution gets its application for subzero degree Celsius temperature while the second one used for above zero level requirements. The

toxicity and low coefficient of performance behavior of NH_3-H_2O system makes it less preferable than the competing H_2O-LiBr solution (Raja *et al.,* 2016).

VARS with H_2O-LiBr solution is conventional in thermal-driven air conditioning systems and have too many benefits in comparison with another cooling system as their performance is good and the cost is low (Falahatkar and Assadi, 2011). The single effect water-LiBr absorption system is used for this study, as the system has low cost and require low generator temperature to operate. The single effect works at lower pressures that consist of a generator, condenser, absorber, evaporator, expansion valves, pumps and an external device (cooling tower). The operation takes place on four independent circuits: hot, cold, chilled water and the circuit of the water-LiBr solution (Antonio *et al*., 2014).

In this study, the absorption system with the integration of phase change material as a fill-in for the night time heat source is investigated. The coefficient of performance (COP) and exergetic efficiency is studied for a variable input parameter of each component to optimize the working temperature. The efficiency and total useful energy gain of solar collectors for the required capacity are also studied to ensure the sustainability of system operation. PCM as thermal storage for the night time operation makes the system to function throughout the day. The charging and discharging effectiveness of PCM are analyzed to ensure the sustainable operation of the system.

Lastly, a general python code that works for a variable capacity of a single effect water-LiBr solution is presented, with the application to the selected industry. The general working layout of the entire system is shown in Figure 1.1 below.

In this proposed system charging of the PCM is done during the day time when the solar radiation is present. During the charging period or day time, valve 1 is kept open while valve 2 is remained closed. The pressurized water from generator passes through the solar collector. Water takes heat from the solar collector and flow through the heat storage unit for charging the PCM. At the time of discharge during night time or in the absence of solar radiation, valve 1 is needed to be closed as it is not necessary to circulate water through the collector and valve 2 is opened to pass the water directly through the TES unit for discharging heat to the working fluid. Simultaneously, the PCM starts to be solidified and being fully solidified, this PCM can be used for charging again. This process is continued until the ends of the PCM thermal life cycle. In order to maintain

a constant output temperature, an electric heater is also attached to the PCM packed bed. The electric heater is essential to maintain the preferred temperature for comfortable use. Using a thermostat in the heater, the power consumption and temperature both can be controlled.

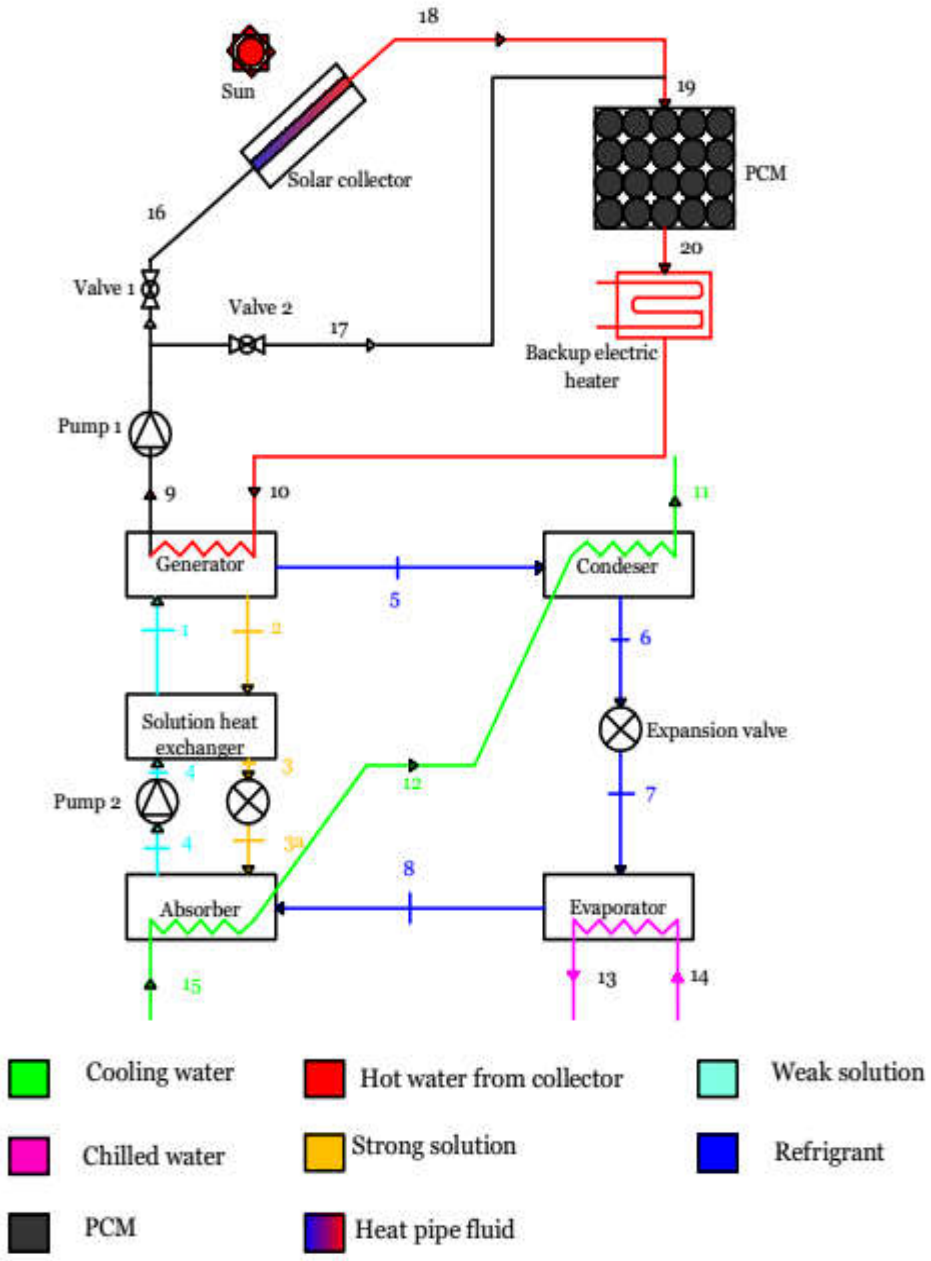

1. Weak solution from HX.
2. Strong solution from Generator
3. Weak solution from HX.
3a. Strong solution from Exp.valve.
4. Weak solution from absorber.
4a. Weak solution from pump.
5. Refrigerant leaving Generator and entering condenser.
6. Refrigerant leaving condenser and entering Exp.valve.
7. Refrigerant leaving exp. Valve and entering Evaporator.
8. Refrigerant leaving evaporator and entering absorber
9. Hot water leaving generator.
10. Hot water entering Generator.
11. Cooling water leaving condenser.
12. Cooling water leaving absorber.
13. Chilled water out.
14. Chilled water in
15. Cooling water from cooling tower
16 Hot water to solar collector.
17. Hot water to PCM.
18. Hot water from solar collector.
19. Hot water to PCM.
20. Hot water to backup electric heater.

Figure 1. 1: Schematic diagram of the solar vapor absorption refrigeration system integrated with PCM

1.2. Statement of the problem

The solar absorption refrigeration system is a promising technology to create a cost-effective and pollution-free world. But, the intermittency and unpredictable nature of solar energy is the major problem for its ongoing operation. To keep the operational stability of the system and energy supply with demand, thermal energy storage is a key issue to be addressed. Some experimental, as well as numerical research, have been conducted to analysis optimization, performance test, and design of the vapor absorption refrigeration system. But a little effort is contributed to overcome the unstable nature of the energy resources, typically the renewables energy resources. In addition, no work has been developed to design a compressive solar vapor absorption refrigeration system that can be applicable for a given industrial cooling capacity. Doing so, the study is mainly focus on to address the intermittent and unpredictable solar condition of the VARS by integrating solar thermal energy storage packed with phase change material, with creating general Python code which can be applied for a given industrial cooling capacity.

1.3. General objective

The general objective of this thesis is to design a solar vapor absorption refrigeration system integrated with a phase change material as a fill-in for the low or off solar radiation hours, by enhancing the working time of the system to meets the purpose of a 24 h operation.

1.4. Specific objective

- To make energy and exergy analysis for each components of the VARS.
- Component design and performance analysis of industrial scale VARS.
- Optimization of working temperature for variable input parameters
- To developed a numerical code that size the solar collector to fulfill the cooling load requirement.
- To size PCM thermal storage system for a given cooling capacity.

1.5. Scope and limitation

1.5.1. Scope of the study

This study mainly focuses on the transient numerical analysis of the solar collector and the phase change material, which is designed to fit on the VARS. The COP and exergetic efficiency of the absorption system is also studied for the different input parameters, followed by the design of each absorption system components.

1.5.2. Limitation of the study

As the thesis aim is to fill the gap for the intermittency and night condition of the absorption refrigeration systems, the work is entirely focused on the thermodynamic analysis and design of each component, whereas the hydrodynamic and cost-effectiveness analysis is not included.

1.6 Organization of the study

After going through a number of literature on each part of the system in chapter 2, a method for approaching the solution has been developed. The mathematical modeling for the VARS based on mass, energy and exergy balances will be studied in chapter 3, and the developed model will be validated against an experimental test conducted on the VARS. The effect of variable input parameter on the coefficient of performance and exergy efficiency is studied to design the components of the VARS.

Available solar radiation on a surface for different month of the year, and design of the heat pipe collector to size the collector area for the required capacity of VARS with the implementation of the model in Python script is studied in Chapter 4. And, Chapter 5 is focused on to develop a mathematical model for the latent heat storage unit based on the energy balances and heat transfer equations. Same as the absorption system, the model will be implemented in PYTHON software and the results will be validated on experimental test results from the works of literature. Charging and discharging time of latent heat storage integrated with the solar collector field and the absorption cooling system will be studied. Finally, from the cooling load and chilled water temperature of the selected industries in Ethiopia, the single effect absorption refrigeration system, the latent heat storage unit, and solar collector is designed in Chapter 6.

CHAPTER 2: Literature Review

2.1. Introduction

In this chapter, previous work on solar vapor absorption refrigeration technology integrated with thermal storage unit is reviewed on the base of three specific areas. The first and the second focuses on solar collector technology in use and thermal energy storage system, respectively. And, the last one is on the vapor absorption refrigeration system.

2.2. Solar Collector

Different types of renewable energy resources are available in nature such as – solar, wind, geothermal, tidal...etc. from those available renewable energies, solar energy is the most used form of energy, as it's vital and abundant in nature (Raghurajsinh and Kedar, 2016). To catch this vital resource, based on the required application, a flat or concentrating collectors are used. Solar collectors are a special kind of heat exchangers which transform solar radiation energy to internal energy of the transporting medium (Soteris, 2004). It is a device that absorbs incoming solar radiation, converts it into heat, and transfers that heat to a fluid (usually air or water) that flow through the collector. In all solar collectors, there are three characteristic energy processes: a collection of solar radiation, energy loss to the environment and the useful energy extracted from the collector (Zbysław, 2011). As solar radiation is only available during the daytime, energy must be collected efficiently to use it for the full-day.

There are two types of collector; stationary and tracking. The tracking collectors get their application in high-temperature requirement areas such as in industry and electricity production. Stationary collectors, however, are largely used in domestic and industrial cooling and heating processes (Raghurajsinh and Kedar, 2016). As the study is entirely focused on the industrial cooling process, the literature is concentrated on the technological development and application area of the stationary collectors.

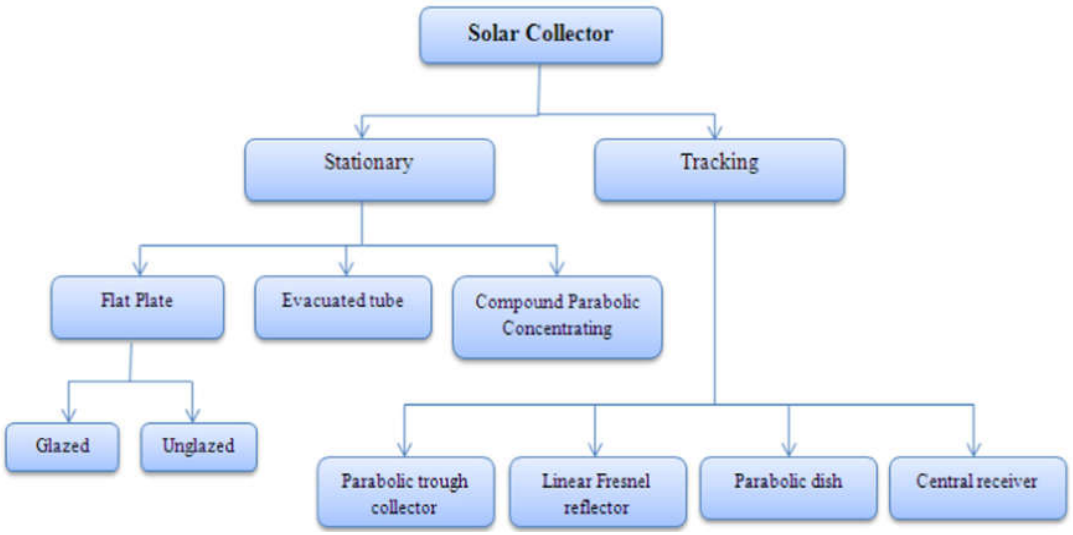

Figure 2. 1: Types of solar collectors (Sabiha *et al*., 2015).

The stationary collectors can be:

1. Flat plate or,
2. Evacuated tube collector

Both of the above stationary collectors are used in industry, but the evacuated tube collector is the most efficient for high temperature demanding applications, like industrial heating and cooling.

2.2.2. Evacuated Tube Collector

Evacuated tube solar collectors are commonly viewed as a device having significantly higher performance than the ordinary flat plate collectors (Zbysław, 2011), as shown in Table 2.1. The evacuated tube solar collectors are common and can achieve higher temperatures ranging from 50-200 ℃ (Sabiha *et al*., 2015). To ensure the required physical robustness, in a vacuum system the collectors are usually composed of cylindrical shape glass elements with the absorber placed inside a glass shield, consists of two tubes, one is inner and the other is an outer tube. The inner tube is coated with selective coating while the outer tube is transparent and the tube usually made from Borosilicate. Two categories of evacuated tube collectors are used, namely (Sabiha *et al*., 2015):

- single-walled glass evacuated-tube, and
- Dewar tube

Table 2. 1: Comparison between evacuated and flat plate collectors (Mingyang, 2014).

	Evacuated tube collector	**Flat plate collector**
1	Quick heat generation	Slow heat generation
2	Convection losses are negligible	High convection loss
3	Working temperature 50 to 200^{o}C	Working temperature 50 to 80^{o}C
4	Satisfactory performance in extreme cold condition (-18^{o}C).	Freezing of water takes place at high altitude causing damage to the collector.
5	The collector absorber being cylindrical the incident sun's rays on the tube is at 90^{o} throughout the day, Peak heat absorption always.	The collector fins and tubes being flat the incident sun's rays will be at 90^{o} at noon only for peak absorption.
6	In locations with an average availability of solar energy oversizing of the system, a glass tube collector is not required.	High system sizing is required to get the desired result, hence added cost.
7	Very easy to replace glass tube	Difficult and expensive to replace glass sheet
8	Has low maintenance	Required high maintenance

Single-walled glass evacuated tube usually composed of transparent single glass with a metallic absorber. Whereas the Dewar tube consists of inner and outer tubes with absorbance material which is embodied in the outside wall of the inner tube to collect solar energy (Aman and Pathak, 2016). For both cases, the convective loss is reduced by evacuating the layer between the inner and outer tubes.

Figure 2. 2: Dewar tube type evacuated glass tube (Raghurajsinh and Kedar, 2016).

The two basic types have a distinct difference. For instance, heat extraction can be through a U-pipe, heat pipe or direct liquid contact (Adel *et al*., 2016). Great efficiency in transferring heat and zero maintenance requirement of heat pipe evacuated tube collector makes it preferable over the other heat extraction method.

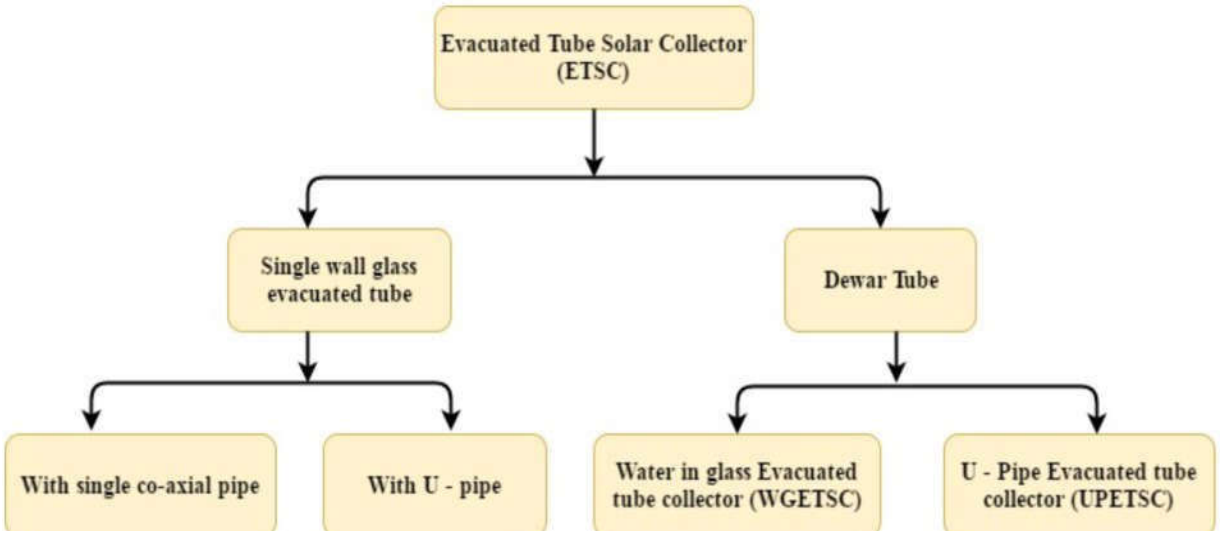

Figure 2. 3: Types of evacuated tube solar collectors (Ashutosh *et al.,* 2018).

2.2.2.1. Heat pipe evacuated tube collector (HPETC)

The HPETC is constructed with sealed borosilicate glass and a sealed metallic copper tube with a working fluid in it, and a metallic fin (usually aluminum). The selective coating is applied on the inner cover of the outer glass tube. The length of the inner metallic tube is divided into the lower evaporation section and the upper condenser section, or sometimes with an adiabatic section in between. The liquid pool in the evaporation section absorbs the transmitted heat and turns into vapor, which then rises to the upper condenser section, where the vapor returns to a liquid turned back to the liquid pool and flow down to evaporation section by gravity. It is the latent heat released by the working fluid that heats the fluid in the manifold (Chow *et al*., 2011).

The advantage of heat pipe over the U tube and the glass-glass (direct contact) collector is their great efficiency in transferring heat and contain no mechanical moving parts. When a single pipe element fails, no need to shut down the entire system. As the single element has a negligible effect over the entire system, doing so, heat pipe collectors require less maintenance (Raghurajsinh and Kedar, 2016).

2.2.3. Overviews on Evacuated Tube Collectors

Arabkoohsar et al., (2016) study the feasibility of employing evacuated tube solar thermal systems to supply the heating demand of a hybrid power plant. After detailed mathematical modeling, the solar heating units and other power plant components are properly sized. The results of simulations demonstrate that a total of 7000 evacuated tube collectors were required for the system, leading to the elimination of the air heater from the compressed air energy storage system (CAES) completely and 17.2% fuel saving at the city gate station (CGS). The internal rate of return (IRR) method was used to compare economically the proposed system with similar systems proposed previously, outperforming all of the other candidates with an IRR of 11.1%.

Bouzenadaa et al., (2016), presented a technical paper on collector array design including the use of flat-plate collectors (FPC), evacuated tube collector (ETC) and hybrid arrays consisting of both FPC and ETCs. Simulations were conducted for three cities including Toronto, Canada; Tunis, Tunisia; and Calcutta, India. To achieve comparable solar fractions to ETC arrays it was found that FPC arrays required approximately 15 m^2 more area than the ETC arrays in Toronto and Tunis, and 30 m^2 more in Calcutta. Tunis showed the best results for a hybrid system. A ratio of 30%

FPCs and 70% ETCs achieved the same solar fraction (i.e., 0.56) as the array consisting of only ETCs.

Mohamed et al., (2017), presents an experimental analysis for integrating a phase change material (PCM) in a typical direct flow evacuated tube solar water heater with a U-tube heat exchanger (HX). Each evacuated tube is filled with 0.8 kg of paraffin wax to store the absorbed incident solar energy. The proposed system is investigated under two configurations: un-finned and finned HX to investigate the effectiveness of adding the fin. The results show that the natural convection was the main heat transfer mechanism during the charging phase, with a higher system efficiency for the un-finned collector, about 14%. During the discharging phase, the presence of the fin helps to overcome the poor thermal conductivity of the solidified layer of the PCM and subsequently enhance the total effective energy discharged.

Neeraj and Gerardo (2011), investigated numerically the thermal performance of a novel minichannel based solar collector. The particular collector consists of a U-shaped flat-tube absorber with a selective coating on its external surface. The working fluid flows inside an array of minichannels located in the cross-section of the absorber along its length. The absorber is enclosed in an evacuated glass envelope to minimize convective losses. Performance and pressure drop are evaluated for different inlet temperatures and flow rates of the working fluid. The thermal performance of minichannel-based solar collector was compared to that of an evacuated tube collector without minichannels from the literature. The efficiency of the minichannel-based collector with a concentrator was sensitive to the gap loss which can be reduced by further optimizing the shape near the bottom of the concentrator.

Tong *et al*., (2016), presented in their technical paper the thermal performance of an individual pipe in an evacuated tube solar collector with a heat pipe using an analytical method based on energy balance. After comparing the simulation and experimental results, a discrepancy of about 0-6% was observed due to the simple assumptions in the simulation process and unavoidable human factors.

Ayompe and Duffy (2013), presents an analysis for the thermal performance of a solar water heating system with heat pipe evacuated tube collector using data obtained from a field trial installation over a year in Dublin, Ireland. The maximum recorded collector outlet temperature

was 70.3ºC while the water temperature at the bottom of the hot water tank was 59.5ºC. The result showed that for an annual global solar insolation on the collector surface of 11,760.3 MJ, a total of 7,435.1 MJ was collected while 6,121.1 MJ was delivered to the hot water tank.

Raghurajsinh and Kedar (2016), study a detail review on the application of solar energy by using an evacuated tube collector with heat pipe technology for hot water generation. The utilization of solar energy for hot water generation system by ETC would help to improve energy economics, energy consumption, and energy efficiency of the system. Their conclusion shows that evacuated tube collector with heat pipe has best performance among all other non-tracking collectors, and it can be used for hot water generation which is required in refrigeration system for horticulture product.

A HPETC is investigated theoretically and experimentally by Jafarkazemi and Abdi, (2012). Heat transfer formulas were used for theoretical modeling, and a test method was adopted from ISO 9806-1 to compare the theoretical model with the experimental results. The collector efficiency and useful heat gain were compared between the theoretical and experimental methods. It has been shown that the efficiency of the collector decreases as the ratio of the inlet temperature to the incident radiation increases. It is recommended that the inlet water temperature to be kept as near as possible to the ambient temperature to gain more heat and efficiency.
Farzad et al., (2016), studied a heat pipe evacuated tube solar collector both theoretically and experimentally. A detailed theoretical method for energy and exergy analysis of the collector is developed. The result show that increasing the difference between the water inlet and the ambient temperature leads to a decrease in energy efficiency, and increase in exergy efficiency of the collector. The same process is observed on the variations of water inlet mass flow rate. It is also concluded that increasing water inlet temperature while decreasing water mass flow rate results in a better exergetic efficiency.

2.3. Energy storage unit

As the supply of solar energy is time-dependent, a discrepancy may arise between solar energy supply and demand. To tackle this problem different form of energy storing method is used as shown in Figure 2.4.

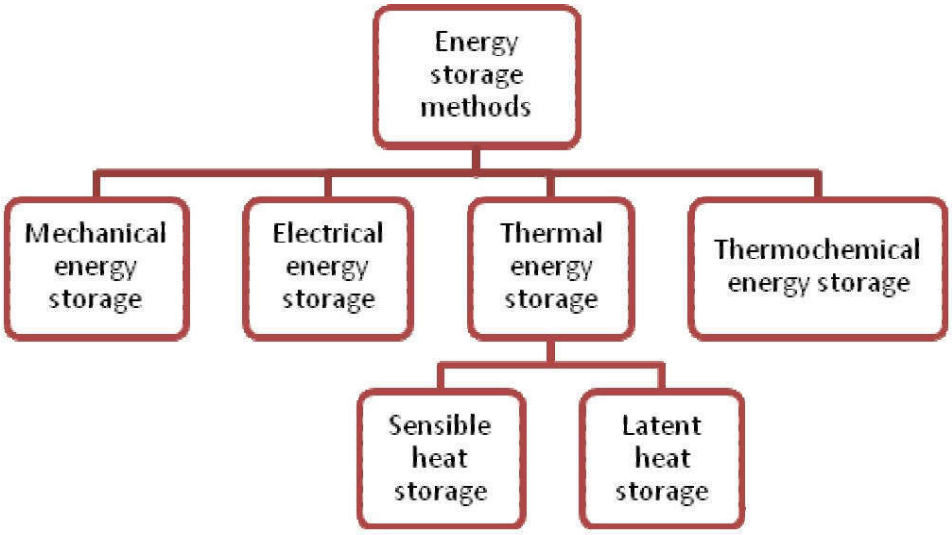

Figure 2. 4: Types of energy storage methods (Arun and Shukla, 2015).

From those methods of energy storing units, thermal energy storage (TES) is the simpler and energy-efficient way of storing the supplied energy. TES may cater to solar time-discrepancy by storing solar thermal energy during sunshine hours to use it for night condition (Shobo and Mawire, 2015). Basically, TES can be stored as a change in the internal energy of a material as sensible heat or latent heat storage (Abhay *et al*., 2013).

2.3.1. Thermal Energy Storage System

Thermal energy storage (TES) is defined as a temporary storage of heat energy at high or low temperatures (Dakuri and Hayavadana, 2014). TES systems can be classified as active or passive, the former can be direct or indirect. In the direct type, the storage medium is also the heat transfer fluid, whereas, in the indirect type, a second fluid is used for storing the heat. In passive TES systems, a solid material is used as the storage medium (packed bed) with the heat transfer fluid passes through the storage medium only during the charging and discharging phases (Shobo and Mawire, 2015).

TES can be classified as sensible heat storage (SHS), and latent heat storage (LHS). SHS store heat by raising the temperature of the storing medium, and it bases in the heat capacity and the change in temperature of the material during the charging and discharging process (Arun and Shukla, 2015). The amount of heat stored depends on the specific heat of the medium, the temperature change, and size of the storage tank. Whereas, LHS is based in the phase change process of the substance within a limited temperature change. LHS is one of the most efficient ways of storage medium compared to the competing SHS. It provide much higher storage density with a smaller temperature difference between storing and releasing heat, and it depends on the phase change process of the material (Dakuri and Hayavadana, 2014).

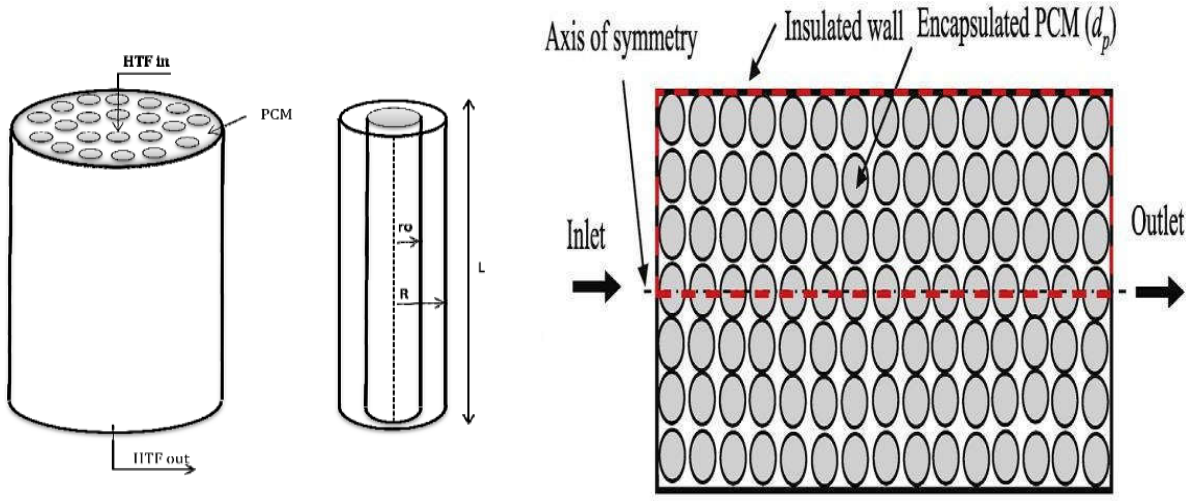

Figure 2. 5: Packed bed PCM (Bansal and Buddhi, 1992), a) cylindrical PCM b) spherical PC

Packed bed configurations as shown in Figure 2.5 have excellent heat transfer characteristics by providing a large surface area to enhance heat transfer process (Fortunato *et al*., 2012). The spherical geometry of PCM is preferred over the cylindrical one because of its larger area of heat transfer between the fluid and the bed. And, for the storing vessel, cylindrical shell makes the storage tank to have a greater packing density over the others (Shobo and Mawire, 2015).

2.3.2. Types of phase change material

PCM can be classified mainly according to their chemical composition and melting temperature. Based on melting Temperature PCM can be divided into low (below 120^{o}C), middle (between 120 and 200^{o}C) and high (above 200^{o}C) melting temperature PCM, as shown in Figure 2.6

(Gustavo *et al*., 2017).

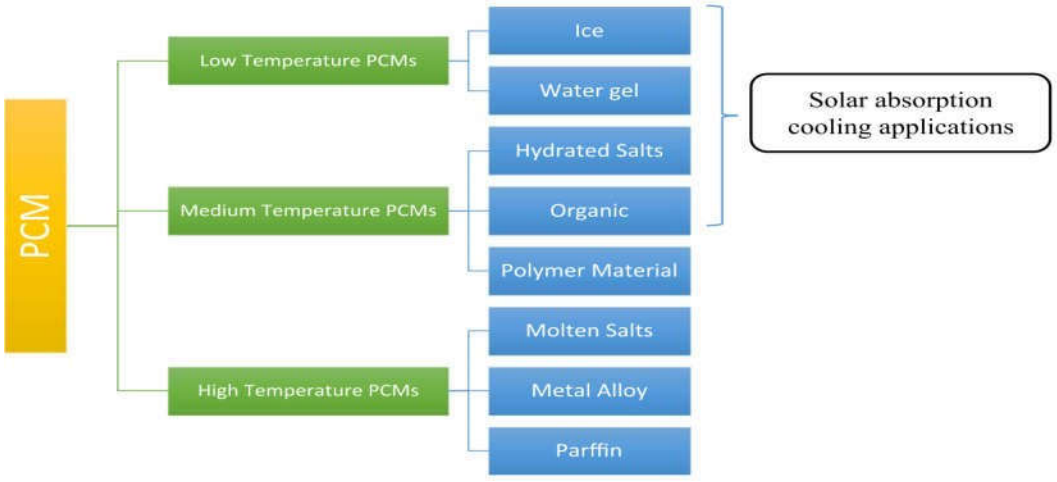

Figure 2. 6: Category of PCM based on melting temperature (Mohammed *et al.,* 2017).

PCM can also be classified based on their chemical composition as organic, inorganic and eutectic PCM, as shown in Figure 2.7.

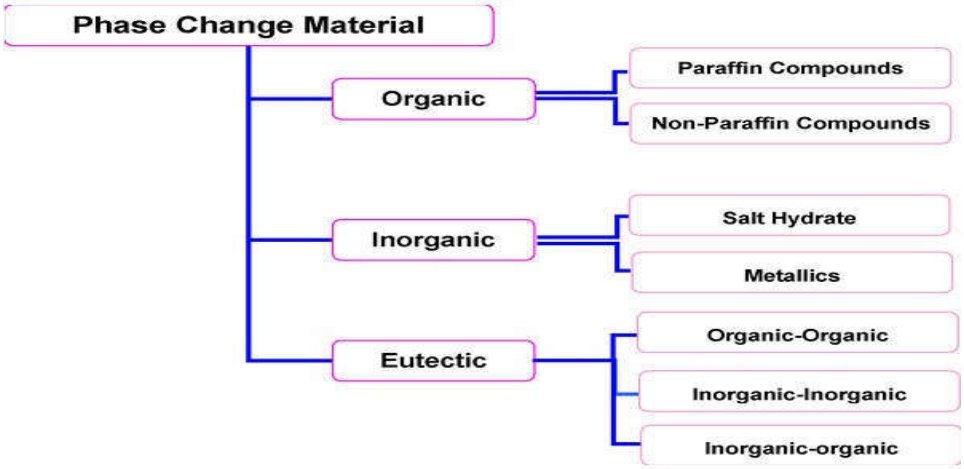

Figure 2. 7: Category based on chemical composition (Abdalla *et al.,* 2018).

Composition, Advantage and disadvantage of each category of PCM are described in Table 2.2 (Lingayat and Suple, 2013):

Table 2. 2: Merit and demerit of organic, inorganic and eutectic PCM

	Composition	Advantage	Disadvantage
Organic	consists of a mixture of straight-chain alkanes CH_3–n(CH_2)–CH_3 esters, fatty acids, alcohol's and glycol's	Safe, Reliable, Predictable, less expensive and non-corrosive, chemically inert and stable below 500^{o}C, show little volume changes on melting	Low thermal conductivity, Non-compatible with the plastic container and moderately flammable
Inorganic	Salts hydrate, salts, metals, and alloys	High latent heat of fusion, high thermal conductivity small volume changes on melting.	Irreversible melting–freezing of the salt hydrate, super-cooling, segregation
Eutectic	Composition of organic and inorganic compounds	Take the advantage of organic and inorganic PCM	

2.3.3. Charging and discharging of PCM

The charging process is happened in side the PCM when the HTF have a higher temperature than the bed. During the charging process the HTF is circulated continuously through the PCM storage tank. The Heat Transfer Fluid (HTF) exchanges its energy to the bed. At the beginning of the charging process, the temperature of the bed will be at ambient temperature, which is lower than the melting temperature. Initially the energy is stored inside the bed as sensible heat until the PCM reaches its melting temperature. As the charging process proceeds, energy storage is achieved by melting the PCM at a constant temperature and stored as latent heat. Then the charging process is continued until the paraffin temperature reaches the temperature of the HTF. Whereas the discharging processes is occur when the temperature of the HTF is lower than the PCM that circulate continuously through the storage tank to recover the stored heat energy.

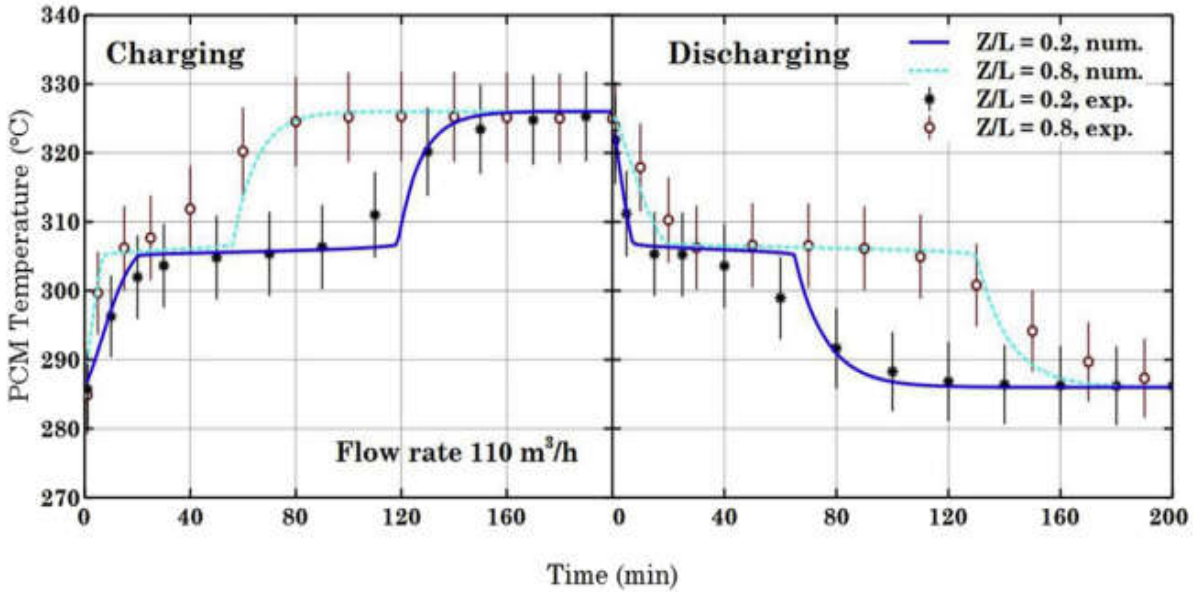

Figure 2. 8: Comparison of experimentally measured and numerically predicted PCM temperatures as a function of time (Bellan *et al*., 2015).

Figure 2.8 shows the comparison of numerically predicted and experimentally measured charging and discharging time of PCM (sodium nitrate) as a function of time by Bellan *et al*., (2015).where, Z is the axial length of the PCM and L is the height of PCM packed bed. It was found that the melting range of the PCM is between 305 ºC and 307 ºC. To perform the charging process, the air-blower was connected to the top port of the system at 110 m3/h flow rate, and the initial condition of the bed and the inlet HTF temperature were fixed at 286 ºC and 326 ºC respectively. For discharging the initial and the inlet temperatures were fixed at 326 ºC and 286 ºC respectively.

2.3.4. Criteria for the selection of PCM

Selection of PCM is mainly based in the melting temperature for a practical range of application but PCM selection also depends on a number of other factors, Table 2.3 describes the characteristics of a favorable PCM (Abhay and Yogesh, 2013):

Table 2. 3: Characteristics of favorable PCM (Abhay and Yogesh, 2013)

Properties	Descriptions
Thermal properties	• Suitable phase-transition temperature
	• High latent heat of transition
	• Good heat transfer
Physical properties	• Favorable phase equilibrium.
	• High density
	• Small volume change
	• Low vapor pressure
Kinetic properties	• No super cooling
	• Sufficient crystallization rate
Chemical properties	• Long-term chemical stability
	• Compatibility with materials of construction
	• No toxicity
	• No fire hazard
Economics	• Abundant
	• Available
	• Cost effective

The selection of an appropriate PCM requires the PCM to have a melting temperature within the practical range of application, so the selection was dictated by the generator temperature required for the efficient operation of the VARS. Since H_2O-LiBr absorption systems operate with generator temperatures in the range of 75- 100^oC, the PCM melting temperature should be higher than the generator temperature. Selected PCMs for an application of solar H_2O-LiBr absorption systems, with melting temperature in the range of 100- 150^oC is shown in Table 2.4 bellow (Hossien *et al.,* 2011).

Table 2. 4: List to be used in single effect solar H_2O-LiBr VARS.

PCM	Material type	Melting point (°C)	Heat of Fusion (kJ/kg)
Methyl fumarate	Organic (fatty acid)	102	242
$MgCl_2.\ 6H_2O$	Inorganic	115	165
Erythritol	Organic	118	339.8
HDEP	Organic	100- 150	200
RT 110	Organic (Paraffin)	112	213
Acetanilide	Organic(non-Paraffin)	118.9	222
Succinic anhydride	Organic(non-Paraffin)	119	204

2.3.4. Overview of the latent heat storage unit

Gonzalez *et al*., (2014), develop a two-dimensional two-phase model to study the dynamic behavior of a packed bed thermal energy storage system, which is composed of spherical packed bed PCM (sodium nitrate) and high-temperature heat transfer fluid- synthetic oil (Therminol 66). After model validation, the model is used to investigate the influence of capsule size, fluid temperature, tank size (length and diameter), fluid flow rate and the insulation layer thickness of tank wall on the performance of the system. The result shows that increasing the capsule size, fluid flow rate, or decreasing the Stefan number, results in an increase in the thermocline region which finally decreases the effective discharge time and the total utilization.

Shobo and Mawire, (2015), present a numerical model for a packed bed PCM to be utilized for a solar cooking application. Sunflower Oil is the heat transfer fluid (HTF) with spherical capsules filled with Erythritol, as a phase change material. The model uses dual-phase mathematical heat transfer equations while the phase change phenomena inside the PCM capsules are analyzed by using the effective heat capacity method. Results from the model were validated with experimental results from literatures.

Nallusamy *et al*., ((2006), studied experimentally the thermal performance of a packed bed latent heat TES unit integrated with a solar flat plate collector. Charging experiments were carried out at varying inlet fluid temperatures to examine the effects of porosity and the HTF flow rate on the efficiency of the storage unit. The results shows that the mass flow rate has a significant effect on the heat extraction rate from the solar collector, which in turn affects the rate of charging of the storage tank. Experiments were conducted for continuous and batch-wise discharging processes for both sensible heat storage and latent heat storage systems. It is concluded from the experimental results that the packed bed LHS system reduces the size of the storage tank and batch-wise discharging of hot water from the TES tank is best suited for applications where the requirement is intermittent.

Ponshanmugakumar *et al*., (2015), numerically investigated a vertical generator integrated with PCM (Erythritol) for forced convective boiling in an NH_3-H_2O solar absorption air-conditioning system connected to concentrating parabolic collector field. TRNSYS model to simulate a real stainless-steel generator with coaxial tubes of 1m length is developed. The hot water charging the PCM tubes in the generator is connected to a hot water storage tank and an auxiliary boiler. They found that the use of PCM can decrease the auxiliary heating source demand during the peak load and low radiation hour.

Muthukumar and Hakeem (2018), studied the thermal modeling and performance comparison of sensible and latent heat based TES systems using concrete and PCM encapsulated in containers of different geometrical configurations. An effective heat capacity method is applied to analyze the charging and discharging effectiveness of the PCM. Boussinesq approximation and Darcy law's source term are added in the momentum equation to incorporate the natural convection of molten PCM and nullify the velocities of solid PCM. 2D axisymmetric model equations are solved using COMSOL Multi-physics. Charging time of capsules in four different configurations spherical, cylindrical and novel cylindrical configurations were compared. The proposed novel cylindrical configuration yields 61 and 28% lesser charging times for SHS and LHS capsules, respectively, when compared with the cylindrical capsule.

Meenakshi *et al*,. (2012), presente experimental investigation of a combined sensible and latent heat TES system integrated with a different heat sources. Investigations are carried for different phase change materials (Paraffin and Stearic acid) by varying HTF flow rates and spherical

capsules size (68, 58, and 38 mm in diameter) in both charging and discharging processes. The results show that the 38 mm diameter shows better PCM performance compared to spherical capsules of other sizes.

Qarnia (2009), developed a theoretical model based on the energy equations to predict the thermal behavior and efficiency LHS unit, which consisting of a series of identical tubes embedded in the PCM. During charging mode the heat transfer fluid, from the solar collector, passes through the tubes and transfers the collected heat of solar radiation to the PCM. Later on, the heat stored in the liquid PCM is transferred to water during discharging mode to produce a heated water. A simulation program based on the finite volume approach was also developed to numerically evaluate the thermal performance of the LHS unit.

Kunal *et al*., (2016), experimentally investigated the thermal behavior and feasibility of a cylindrically encapsulated PCM as a latent heat thermal energy storage (LHTES) medium. A storage tank containing latent heat storage material was constructed to analyze the performance of the latent heat thermal energy storage system. Experiments have been carried out at a constant flow rate of HTF, so that, the thermal characteristics of the LHTES system and efficiency of the system was calculated. The discharging characteristics for batch-wise discharge were also studied.

Kondakkagari et *al*., (2014) did an experimental analysis on Phase Change Material. In their experiment, Sodium thiosulphate pentahydrate was used as the phase change material. The PCM was filled in stainless steel capsules of different shapes in order to analyze the best possible shape for better heat transfer. A heat transfer fluid (water) is used to transfer heat energy into the PCM capsules. According to their experimental results, a combination of latent heat and sensible heat storage with higher temperature and mass flow rate for a cylindrical capsule shape were the recommendations made for better heat transfer.

2.4. Vapor Absorption Refrigeration System (VARS)

Conventional cooling systems, which operate with vapor compression, have a negative impact on the sustainable environmental development issue. In addition to that, the conventional cooling system demands huge amounts of electric energy to operate; it has been estimated that around

15% of the electricity produced worldwide is used for air conditioning and cooling (Inzuza *et al*., 2013).

Vapor Absorption refrigeration system is an attractive method for using the low-grade energy directly for cooling. This is the favorability of VARS compared to the conventional vapor compression system which operates on high-grade energy (Vikas and Dinesh, 2017). However, the net efficiency of such units as well as exergetic efficiency is often lower than the vapor compression units, mainly due to high exergetic losses during isothermal boiling and condensation, and high parasitic load for heat rejection (Vaclav et al., 2017).

The working principle of the VARS is similar to that of the vapor compression system with two main differences. The first is that the VARS is a heat-driven thermal cycle, where only thermal energy is exchanged with the surrounding. No appreciable mechanical energy is transferred as in the case of the mechanical compression system. The second one is the existence of secondary fluid in addition to the refrigerant, known as liquid sorption medium or absorbent (Jerko *et al*., 2012).

2.4.1. Classification of VARS

The vapor absorption refrigeration system can be classified based on several criteria, but classification with respect to the working fluid is studied in this literature. From several working pairs of absorption systems, the most common and commercial one are water-lithium bromide (H_2O-LiBr) and ammonia-water NH_3-H_2O solutions.

2.4.1.1. Ammonia water VARS

Ammonia/water absorption system are similar to water/lithium bromide with some important differences such as ammonia's lower latent heat of vaporization compared to water, the volatility of the absorbent, and the different pressure and solubility ranges. The latent heat of ammonia is only about half that of water. Thus, for the same duty, the refrigerant and absorbent mass-circulation rates are roughly double that of H_2O-LiBr. As a result, the heat loss associated with heat exchanger approaches is greater (Ashrae handbook, 2009).

In an NH_3-H_2O absorption refrigeration system compared to H_2O-LiBr systems, three additional components are used: a rectification column, a dephlegmator, and a sub-cooling heat exchanger.

Furthermore, due to the boiling point difference between ammonia and water is not very high, both ammonia and water are generated from the solution in the generator.

Another important difference between NH_3-H_2O system and H_2O-LiBr systems are in the operating pressures. Water-lithium bromide systems operates under vacuum pressures, whereas, the ammonia-water system is operates at pressures much higher than the atmospheric pressure (Modahl *et al*., 2002). And also, unlike the refrigerant water, ammonia is both toxic and flammable.

2.4.1.2. Water-lithium bromide VARS

Vapor absorption refrigeration systems using the H_2O-LiBr pair are extensively used in medium and large-capacity air conditioning and refrigeration systems. In these systems, water is used as a refrigerant and a solution of lithium bromide in water is used as an absorbent. Since water is used as a refrigerant, using these systems it is not possible to provide refrigeration at sub-zero temperatures. Hence it is used only in applications requiring refrigeration at temperatures above 0^oC (Kharagpur, 2008).

The affinity of H_2O-LiBr makes it a suitable pair and preferred over ammonia-water mixture because of the unwanted behavior of NH_3-H_2O solution such as high pressure, volatility, toxic nature, and corrosive action. The lithium bromide and water combination is nonvolatile and eliminates the need for rectifier in the system (Abhishek and Babu, 2015).

2.4.2. Design of H_2O-LiBr VARS

2.4.2.1. Single-Effect VARS

A single-effect absorption refrigeration system is the simplest and most commonly used design. Evaporator, absorber, generator, condenser, solution heat exchanger (SHX) and pumps are the main components of this system (Falahatkar and Assadi, 2011). As shown in Figure 2.9, the cycle has two circuits: the refrigerant circuit (1-4) and the H_2O-LiBr solution circuit (5-10).

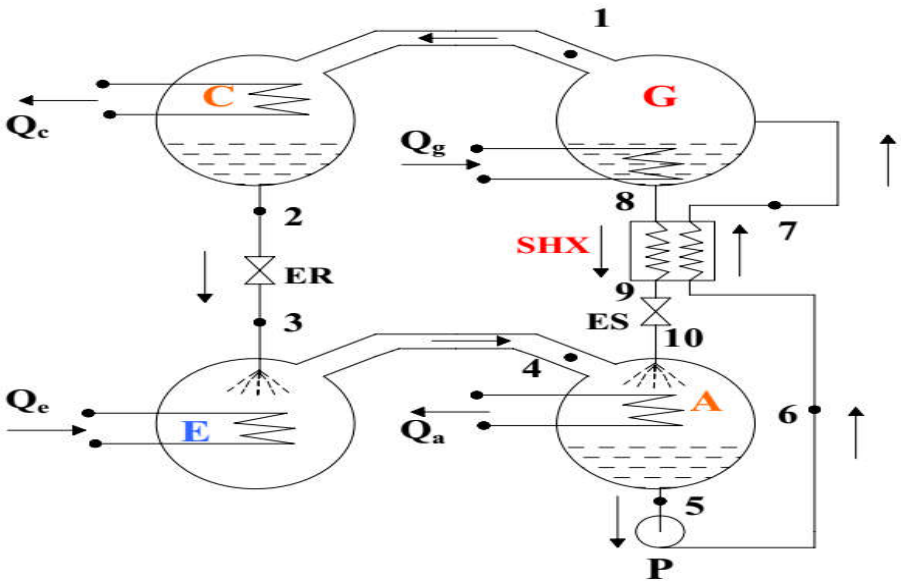

Figure 2. 9: Single effect water-LiBr absorption system.

A heat source (Q_g) supplies the generator, and H_2O-LiBr solution will be heated and the supplied heat evaporate refrigerant H_2O at high pressure (condenser pressure). Once the refrigerant evaporates it will be directed to the condenser and the condenser dissipate heat to the environment as the refrigerant changes its phases from vapor to liquid. Then, the refrigerant directed through an expansion valve to reduce its pressure and subsequently it's led to the evaporator. Finally, the cooling process takes place inside the evaporator by absorbing heat from the environment.

2.4.2.2. Multi-Effect VARS

Multistage cycles have one or more of the four basic exchangers (generator, absorber, condenser, and evaporator) that present at two or more places in the cycle at different pressures or concentrations (Ashrae handbook, 2009). Two or more single-effect absorption cycles, such as shown in Figure 2.10, can be combined to form a multistage cycle by coupling any of the components. The double-effect cycle, for example, is formed by pressure-staging two single-effect cycles.

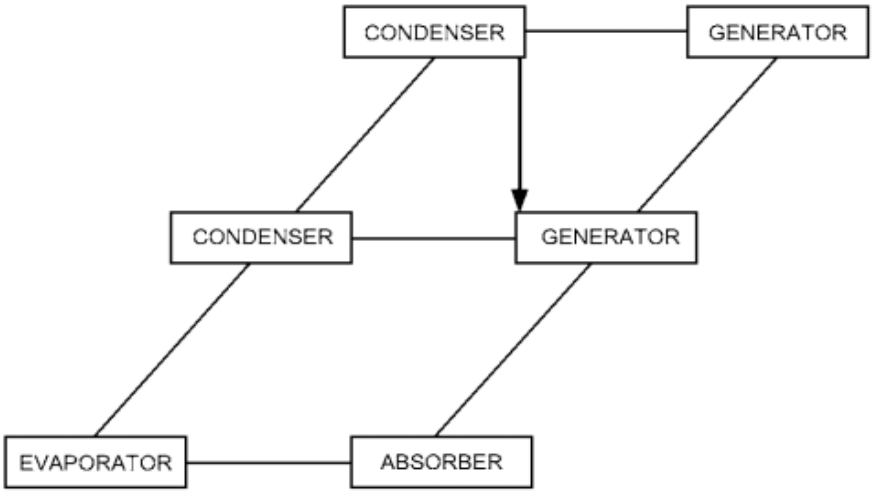

Figure 2. 10: Double-effect absorption cycle (Ashrae handbook, 2009).

2.4.3. Overview on VARS

Alvaro *et al*. (2014), studied theoretically the performance of a single-stage H_2O-LiBr absorption chiller, driven by hot water. The model equations were solved in the EES-32 program (engineering equation solver version 32). The program data generated by variation of the inlet temperature of the hot water were used for the determination of a range of values of energy and exergy COP system whose maximum were 0.7406 and 0.2409, respectively. His analysis revealed that the main irreversibility was found in the cooling tower, generator, and absorber with a values of 34, 32 and 16%, respectively.

Amir and M. Khalaji (2011), analyze solar single effect H_2O-LiBr absorption cooling system in a typical office building in Tehran. This system has been designed to supply the cooling load of a typical office building where the cooling load is 35.17 kW (10 tons of refrigerant) which events in the month of July. Results demonstrate that up to 2400 m^3/year Natural Gas energy can be saved by the use of a solar VARS. To achieving this, utilization of 16 evacuated tube collectors with 30 tubes for each is required. It was shown in their technical paper that the solar cooling fraction for the office building was 64.3% and the optimum solar heat pipe collector area was 45 m^2.

A H_2O-LiBr absorption refrigeration system for cooling and heating applications was analyzed by Shun and Sherif, (2001), on the basis of the first and second laws of thermodynamics. In the

parametric analysis of the VARS for cooling, it's found that low cooling water temperature yields both a higher cooling COP and a higher exegetic efficiency as expected. Increasing the heat source temperature can improve the cooling COP of the absorption system, but as the heat source temperature increases beyond a certain threshold, the COP of the system levels off and even decreased. For heating, it is evident that increasing the heat source temperature will increase both the heating COP and the exegetic efficiency.

An approach to use the PCM in the absorption system has been made by Vikas and Dinesh, 2017. The advantages and disadvantages of using PCM in the system, and exergy analysis have been discussed in their technical paper. It's observed that the cooling time of the system increased from 50 to 115 minutes in the case of pure ethylene glycol as compared with the conventional absorption system without any PCM material under switched off condition. Furthermore, refrigerating effect is also improved by installing the mixture of water and ethylene glycol as a PCM material that results in the rise of cooling time during system switched off condition.

Josef (2012), studied the theoretical modeling and design of LHS for a VARS. A shell and tube latent heat storage exchanger for retaining any excess solar thermal energy was selected. Here, solar thermal energy supplied by a collector is transferred to and sorted by the LHS. During low insolation stored thermal energy was transferred by a heat transfer fluid into the generator, a component of an ammonia absorption system, to ensure the efficiency of the cooling cycle.

François *et al*., (2012), developed the numerical and experimental thermally driven ammonia-water absorption chiller of 5 kW cooling capacity for solar cooling applications. The chiller was developed from an industrial perspective with a goal of overall compactness and use of commercially available components. Experimental tests were performed, providing adjustable power and temperature level for cooling or heating on the ports of the chiller. The experimental tests were developed on optimum control strategy to maximize the performance of the chiller in various real operating condition, the control strategy showed results close to the numerically expected one.

Evangelos *et al*., (2016), study the effect of absorption chiller operating with H_2O–LiBr solution as a refrigerant coupled with a collector field. The cooling demand was 100 kW at 10^{o}C for Athens

(Greece) in summer. Flat plate collectors, evacuated tube collectors, compound parabolic collectors, and parabolic trough collectors were investigated under the same conditions. An exergetic optimization of every system gives the optimum solution of every case, which leads to the minimum collecting area. A financial comparison between the four optimized systems proves that evacuated tube collectors were the most beneficial technology. On the other hand, the system with parabolic trough collectors was the energetic and optimum one, but its high capital cost render as an unprofitable solution.

2.5. Case study areas

Bekas chemical PLC and Ah-Wan food complex industry is the selected industry for the study. These two industries are preferred, as open systems is developed for the chiller in the case of the Ah-Wan food complex, so that, temperature measurement is easily conducted. And, annual data is found for the Ah-Wan food complex as the system is automated and data is taken regularly for each day of the year. Evaporator load and the required chilled water temperature is collected for both of the selected industries.

2.5.1. Beckas chemical PLC

Bekas chemical private limited company is engaged in the manufacturing of soaps, synthetic detergents, cosmetic products, packing materials, industrial surfactants, and putty. It also deals with import and wholesales of chemicals and related products. Chiller is needed on the bottle and cup making section of the industry, this section needs chilled water to cool the hydraulic oil of blow molding and injection machines. The capacity of the chiller is around 186.66 kW that measured by multiplying the pump flow rate in the evaporator side, which is around 80 m^3/hr, and the temperature of the cooling water to and from the chiller, which is 12 ^oC and 10 ^oC, respectively. The chiller layout of the industry is shown in Figure 2.11

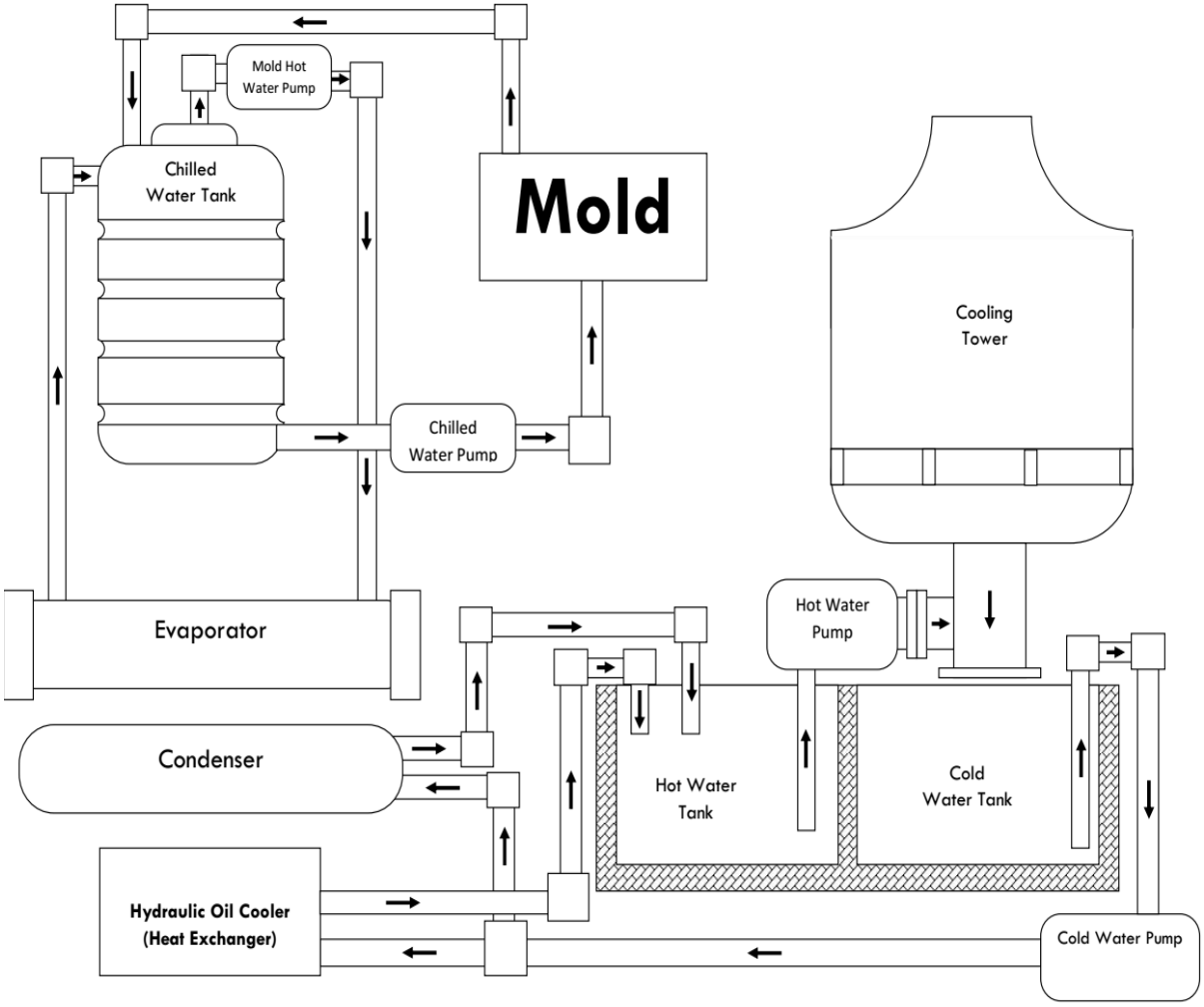

Figure 2.11: Chiller layout of Beckas chemical PLC

2.5.2. Ah-Wan Food Complex

Ah-Wan Food Complex is a Pasta/Macaroni manufacturing facility based in Adama region with professional working environment owned by the Group Ah-Wan Brothers Industry group. The plant automation minimizes the Pasta/Macaroni manufacturing supervision. The pasta production line is normally made up of flour conveying systems carrying semolina and various mixtures to semolina dozer which is placed over the press. Semolina and water dosing units feed the centrifugal mixer with properly dosed raw materials, which then mix and sprinkled. Then, the dough is passed into the vacuum mixer. The pasta production line of Ah-Wan food comlex is shown in Figure 2.12

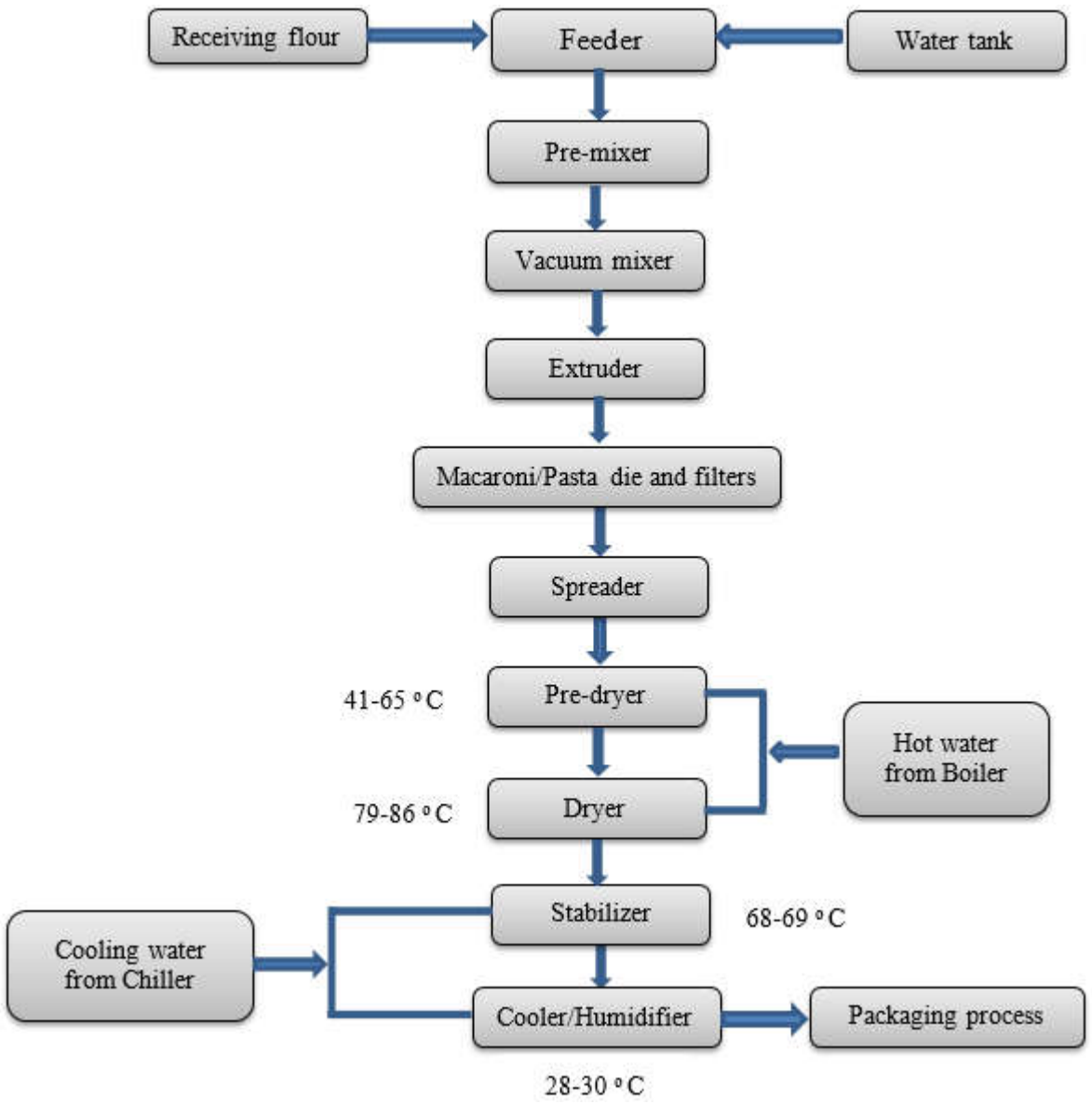

Figure 2. 12: The pasta production line for Ah-Wan Food Complex

Worm screw press dough against extrusion dies, which mold products to different shapes and sizes. The product (pasta) is then in the pasta holding sticks by spreader. The stick enter into pre-dryer where it is rapidly burnt on surface in order to make it mechanically resistant to stretching and prevent it from lengthening too much. When coming out from pre-dryer it conveyed into drying section by means of elevator where it stays for 4 minutes. From dryer section, the pasta sticks conveyed to the stabilizer section where the product stable for the next process to achieve better drying conditions, in this section the pasta stick lasts for 40 sec. The still-hot dry Pasta/macaroni is cooled by blowing cold air produced by circulating cold water coming from the utility house or

the chiller.

The capacity of the chiller is around 245 kW that measured by multiplying the pump flow rate in the evaporator side, which is around 60 m^3/hr, and the temperature of the cooling water to and from the chiller, which is 21.5 ^oC and 18 ^oC, respectively.

2.6. Conclusion from Literature review and Research gap

A literature review about the existing solar vapor absorption refrigeration system integrated with PCM has been studied briefly so far. From the works of literatures, it can be concluded that solar energy can be utilized and harnessed by installing the vapor absorption system. But contrary, the incorporation of solar energy in VARS may affect the process stability, which results from the daily fluctuate and unpredictable nature of solar energy. Thermal energy storage is a key issue to be addressed toward the intermittency of solar energy. Packed bed solar thermal energy storage with phase change material has a higher energy storage density with small temperature fluctuation. Therefore, integrating VARS with PCM based packed bed solar thermal energy storage is a promising technology to create a sustainable operation of VARS.

The cooling rate of VARS is affected by the operating temperature of the system. The non-tracking solar collectors that can be applicable for medium temperature requirement is studied in detail with special attention to the evacuated tube collector. From those studied ETC the heat pipe evacuated tube collector has been favored over the other candidate as it has great efficiency in transferring heat, requires no maintenance, cheap and readily available with a suitable phase-transition temperature. In the second portion, the thermal storage system for both sensible and latent heat storage is studied with advertence is given to the PCM storage system. From the PCM list to be used in a single effect vapor absorption refrigeration system, Erythritol is preferred as a storage material for this study. Due to its suitable phase transition temperature, high latent heat storage density, and cheap and readily available. In the last lesson of this chapter, a detailed review on the current commercial VARS is studied. comparing the NH_3-H_2O and H_2O-LiBr absorber-refrigerant mixture, the water LiBr solution is favored due to the following main reasons: No volatility (fulfill boiling requirement), eliminating the need for rectifiers, and no toxicity and flammability.

Numerical and experimental study on solar VARS has been conducted by some researchers (François *et al*., 2012; Vikas and Dinesh 2017; Ponshanmugakumar *et al*., 2015; Amir and M

Khalaji, 2011 … etc) on the base of a specific geographical location. But, there is a little study on the PCM integrated solar vapor absorption refrigeration system is developed and almost zero effort has been developed to make the system versatile which can be applicable for any industrial cooling capacity.

In this thesis, the thermal performance of a single effect H_2O-LiBr solar vapor absorption refrigeration system with a packed bed thermal energy storage system that uses Erythritol as a phase change material was investigated. Application of the design for Bekas chemical PLC and Ah-wan food complex at Adama weather condition is studied in the last chapter of this thesis.

CHAPTER 3: Design of Vapor Absorption Refrigeration System

3.1. Introduction

Solar VARS is conventional in thermal-driven refrigeration systems and has too many benefits in comparison with another cooling system as their performance is good and cost is low (Falahatkar and Assadi, 2011). Several studies investigate the effect of different parameters on the performance of VARS. Different mathematical models of various complexity have been developed for performance analysis, optimization, and design of VARS. In this chapter performance analysis and design of single effect VARS are studied briefly.

The line diagram of a single effect H_2O-LiBr VARS is shown in Figure 3.1, the operation takes place by the interaction of the four independent circuits: hot water, water-LiBr solution, cooling water and chilled water circuit.

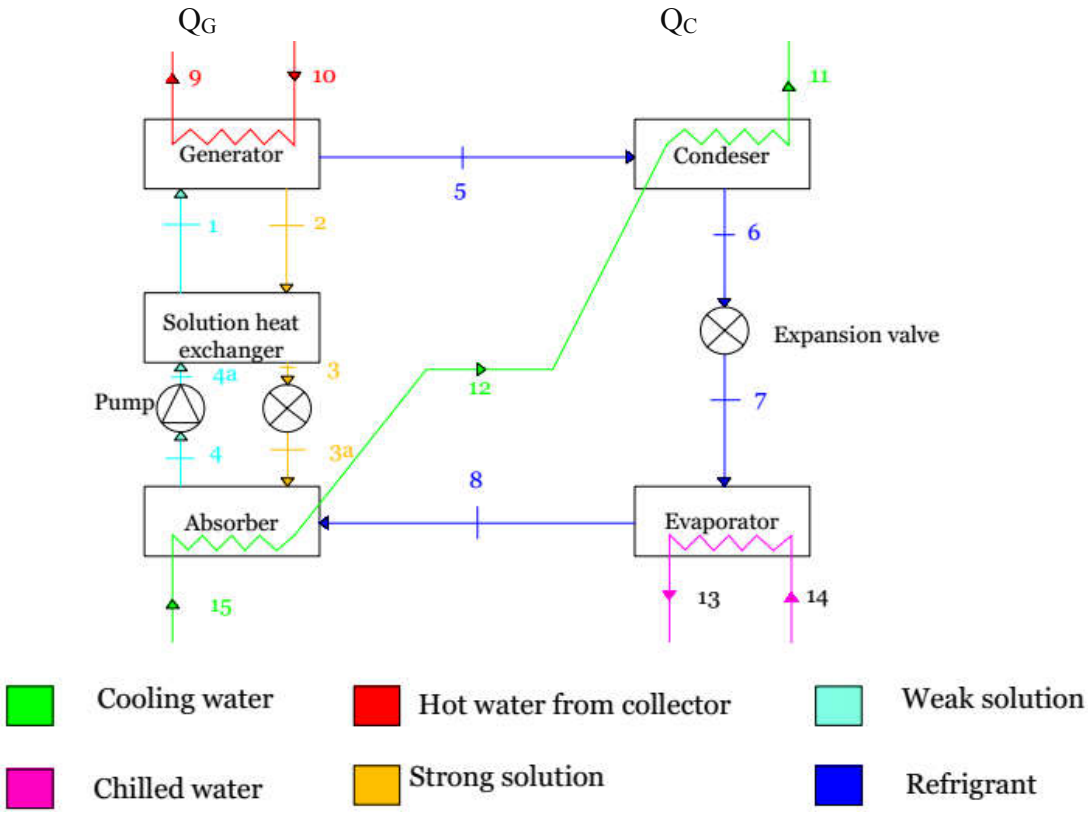

Figure 3. 1: Schematic diagram of single effect VARS

From state 4 to 1, the weak solution from absorber is pumped to the generator through solution heat exchanger (SHX) to desorb the refrigerant water from absorbent (LiBr). A heat source (Q_G) supply heat to the generator, and the heat supplied evaporates the refrigerant H_2O at high pressure from state 1-5. Once the refrigerant evaporate it is directed to the condenser and the condenser dissipates heat to the environment while the refrigerant changes its phase from vapor to liquid state from state 5-6.

Then, the refrigerant flows through the expansion valve from state 6-7, to reduce its pressure and subsequently leads to the evaporator. From state 7-8, the cooling process takes place inside the evaporator by absorbing heat from the utility. Finally, the water vapor from evaporator flow to the absorber from state 8-4 where it mixes with the strong solution from state 8-2, which comes from generator through the heat exchanger. The heat exchanger between generator and absorber, improves the efficiency of the chiller, by preheating the weak solution that returns to the generator.

3.2. Modeling of VARS

Before modeling, it is worthy to mention some of the critical terms and their respective mathematical expressions which are frequently encountered during the analysis.

Concentration: The concentration of water-lithium bromide solutions based on the mass fraction(x) can be expressed as (Kharagpur, 2008):

$$X = \frac{m_L}{m_L + m_w} \quad \text{..... (3.1)}$$

Where m_L and m_w are the mass of anhydrous lithium bromide and water in the solution, respectively.

Circulation ratio: The quantity of rich solution handled by the pump per unit mass of the vapor distilled called circulation ratio is given by (Kharagpur, 2008):

$$f = \frac{m_g}{D} = \frac{x_r}{x_r - x_w} \quad \text{..... (3.2)}$$

Where x_r = concentration of rich solution from generator

D = mass flow rate of distilled vapor

x_w =concentration of weak solution from absorber

$x_r - x_w$= degassing range

And, specific weak solution circulation will be (f – 1)

Cut-off temperature: Cut of temperature can be defined as the minimum generator temperature at which the system can operate. Cut off temperature is function of generator pressure and weak solution concentration (Pandya *et al*., 2017). Whenever the generator pressure and week solution concentration increase the cut-off temperature will increase.

Entropy: The second law of thermodynamics leads to the definition of a new property called entropy, which is a quantitative measure of microscopic disorder for a system. Entropy change is caused by heat transfer, mass flow, and irreversibility such as mixing and friction (Çengel and Boles, 2006). Clausius realized in 1865 that he had discovered a new thermodynamic property called entropy. It is designated as s and is defined as:

$$ds \geq \left(\frac{\partial Q}{T}\right) \quad \text{..... (3.3)}$$

Which is called the Clausius inequality. Where ∂Q the heat load of the internally reversible process, T is temperature, ds is the change in entropy of the system.

Exergy: the work potential of a source, that is, the amount of energy that can be extracted as useful work.

Molality: is normally defend as the number of moles of a solute per kg of a solvent. The molality can be calculated for the LiBr mass fraction (X_{LiBr}) as shown by the following equation (Kim and Ferreira, 2005):

$$m = \frac{X_{LiBr}}{(1-X_{LiBr})\, M_{LiBr}} \quad \text{..... (3.4)}$$

Where, X_{LiBr} and M_{LiBr} is the mole fraction and molar mass of LiBr respectively.

Modeling of the single effect VARS is studied by applying the energy, mass, material and exergy balance for the components of an absorption chiller. Some simplifying assumptions as shown below, are considered to design and simulate the system:

- The entire system is in a thermodynamic equilibrium.
- The analysis is made under steady-state condition
- Heat gain by solution pump is negligible as compared with the primary energy input to the generators.
- No pressure drop due to friction in the pipe

- The solution is at a saturated state when leaving generator and absorber, the same way refrigerant is at saturated state when leaving condenser and evaporator.
- Heat loss from the system to the environment is neglected.
- Flow through the valve is isenthalpic.
- The variation in potential and kinetic energy is negligible

The empirical equations of enthalpies, temperatures, concentrations and vapor pressures of the H_2O-LiBr solution as given by ASHRAE are presented in Appendix A (Ashrae handbook, 2009). And, prompting functional python code is developed in Appendix B to determine the respective thermo-physical property of water/LiBr solution.

An iterative approach is developed in the code to determine the concentration of a solution from the available refrigerant saturation and solution temperature for both the low and high-pressure states. Appendix B depict a function def x_libr (Ta,Te) that calculate concentration of the solution. Where, Ta represents solution temperature and Te is the temperature of saturated refrigerant. And, the entropy of H_2O-LiBr solution is discussed below:

3.2.1. Entropy of water/LiBr solution

Entropy, unlike energy, has a one-directional flow. That is entropy of a given process is always increasing called the principle of increasing entropy. From Equation 3.3, the equality holds for an internally reversible process and the inequality for an irreversible process.

Entropy is a property, and thus the value of entropy of a system is fixed once the state of the system is fixed (Çengel and Boles, 2006). However, unlike entropy of a pure substance, the entropy of a mixture is somehow complicated due to the variation with both concentration and the state of the system. The molar entropy of a binary mixture 1 and 2 is given by (Kim and Ferreira, 2005):

$$\bar{S} = y_1.\bar{S}_{1(T,P)} + (1- y_1).\bar{S}_{2(T,P)} - y_1.v.\bar{R}\left[\ln\left(\frac{m}{m_o}\right) - 1\right] + \bar{S}^{E}_{(T,P,m)} \quad \text{..... (3.5)}$$

Where $\bar{s}_{1(T,P)}$ is the molar entropy of fluid 1 and $\bar{s}_{2(T,P)}$ is the molar entropy of fluid 2. The third term is the entropy generation in an ideal mixture (m_o is the standard molality: $m_o = 0.001$ kmol kg^{-1} of solvent) and the last term $\bar{s}^{E}_{(T,P,m)}$ is the additional entropy generation for a real mixture process. y_1 is the mole fraction of the solute. v and $\bar{R}$ represent the dissociation number and the universal gas constant, respectively. The first two terms at the right side of Equation 3.5 can be

calculated as given by (Reynaldo et al., 2010):

$$\overline{S} = \overline{S}^{\infty}_{0,(T,P)} + \int_{T_0}^{T} \frac{Cp}{\partial T}\, dT - \int_{P_0}^{P} \frac{\partial V}{\partial T}\, dP \quad \text{..... (3.6)}$$

Where, $\overline{s}^{\infty}_{0,(T,P)}$ is entropy of a substance at the standard temperature and pressure. T, P, and V are temperature, pressure, and volume, respectively.

Considering Equation 3.5 and 3.6, to determine the entropy of water/LiBr solution, the correlation proposed by (Kim and Ferreira, 2005) is somewhat satisfactory regression results, given by:

$$\overline{S} = y_{LiBr}.\ \overline{S}^{\infty}_{LiBr} + (1- y_{LiBr}).\ \overline{S}^{1}_{H_2O(T,P)} - y_{LiBr}.v.\ \overline{R}\left[\ln\left(\frac{m}{m_o}\right) - 1\right] + \overline{S}^{E}_{(T,P,m)} \quad \text{..... (3.7)}$$

Where, the term $\overline{s}^{\infty}_{LiBr}$ is the molar entropy of the ideal LiBr fluid, and $\overline{s}^{1}_{H_2O(T,P)}$ is the molar entropy of pure water. And each respective values are given below as stated by Kim and Ferreira, (2005):

$$\overline{S}^{\infty}_{LiBr} = .\ \overline{S}^{\infty}_{LiBr;0} - R.\left[\frac{c_0}{2}\left(\frac{1}{T^2} - \frac{1}{T_0^2}\right)\right] + \left[\frac{c_1}{3}\left(\frac{1}{T^3} - \frac{1}{T_0^3}\right)\right] + \left[\frac{c_2}{4}\left(\frac{1}{T^4} - \frac{1}{T_0^4}\right)\right] - R.\left(b_{00} - \frac{b_{02}}{T^2}\right).\ (P - P_0^*)$$

..... (3.8)

$$\overline{S}^{1}_{H_2O} = \overline{S}^{1}_{H_2O;0} + R.\left(d_o\left(ln\frac{T}{T_O}\right) + d_1(T - T_0) + \frac{d_2}{2}(T^2 - T_0^2) - R.(e_1 + 2e_2.T).\ (P - P_0^*)\right) \quad \text{.....(3.9)}$$

$$^{-E}_{(T,P,m)} = y_{LiBr}.v.R\sum_{i=1}^{6}\left[a_i + \frac{i.b_i}{2.v}P + T.\left(\frac{\partial a_i}{\partial T} + \frac{i}{2.v}\frac{\partial b_i}{\partial T}p\right)\right].m^{i/2} \quad \text{..... (3.10)}$$

Where: $a_i = \sum_{j=0}^{2} a_{ij}T^{-j}$ ..... (3.11)

$b_i = \sum_{j=0}^{2} b_{ij}T^{-j}$ ..... (3.12)

In Equation 3.8 to 3.12, R represent the universal gas constant in kJ/km.K and v is dissociation number for the solute (2 for LiBr). The regression constant is given in Table 3.1 (Bereche *et al*., 2010):

Table 3. 1: Constants in Equation 3.8 to 3.11, (Bereche *et al*., 2010):

J	0	1	2
a_{1j}	-2.196 x 10^{1}	4.93723 x 10^{3}	-6.55480 x 10^{5}
a_{2j}	-3.810475 x 10^{3}	2.611535 x 10^{6}	-3.6699691 x 10^{8}
a_{3j}	1.22808 x 10^{5}	-7.7187923 x 10^{7}	1.039856 x 10^{10}
a_{4j}	-1.471674 x 10^{6}	9.1952848 x 10^{8}	-1.1894502 x 10^{11}
a_{5j}	7.765821 x 10^{6}	-4.937566 x 10^{9}	6.317554 x 10^{11}
a_{6j}	-1.5118920 x 10^{7}	9.839997 x 10^{9}	-1.273789 x 10^{12}
b_{0j}	-4.41786 x 10^{-5}	3.115 x 10^{-2}	-4.3611
b_{1j}	3.074 x 10^{-4}	-1.863 x 10^{-1}	2.738 x 10^{1}
b_{2j}	-4.08 x 10^{-4}	2.16 x 10^{-1}	-2.517 x 10^{1}
c_j	-9.44 x 10^{5}	-5.8423 x 10^{8}	0
d_j	1.197 x 10^{1}	-1.83 x 10^{-2}	2.87 x 10^{-5}
e_j	2.66 x 10^{-3}	-3.865 x 10^{-6}	7.4648 x 10^{-9}
$\bar{s}^{\infty}_{\mathrm{LiBr};0}$	47.5562 (kJ kmol^{-1})	$\bar{s}^{1}_{H_2O;0}$	0
T_o	273.15 K	P_o	0.6108 kPa

To determine the entropy of the H_2O-LiBr solution an iterative analysis as a function of entropy(x,T) is developed in Appendix B that take the concentration and temperature of the solution at a given state point.

3.2.2. Exergy of a control volume

Exergy is defined as the maximum useful work attainable from an energy carrier at a given state in any process that brings the energy carrier into equilibrium with its environment. If a large reference environment is at temperature T_o then the exergy of a material stream can be defined as (Lee and Sherif, 2001):

$e = (h- h_o) –T_o(s-s_o)$ …….……...…… (3.13)

Where e is exergy of the fluid, h is enthalpy, and s is the entropy of the fluid at temperature T, respectively. The subscript o refers to the reference state. Exergy balance for the steady-state process of a control volume can be expressed as (Lee and Sherif, 2001):

$\Delta Є = \sum(me)_{in} - \sum(me)_{out} + [\sum(Q(1 - \frac{T_o}{T}))_{in} - \sum(Q(1 - \frac{T_o}{T}))_{out}] + \sum W$……..……... (3.14)

$\Delta Є$ is the lost exergy or the irreversibility that occurred in the process. Where the first and second term on the right side represents the exergy at inlet and outlet of the control volume transfer by mass. The third term represents the exergy transfer in the control volume by heat and the last one depicts the exergy transfer by work.

Exergy transfer by heat is considered negligible as the system is considered to be insulated from its environment, and the temperature difference between the pool solution and the tubes is very small to give rise to exergy destruction. And, exergy transfer by work is also not included for absorption systems unless the work by solution pump is considered. This implies the Equation 3.14 becomes:

$\Delta Є = \sum (me)_{in} - \sum (me)_{out}$……..…….…….. (3.15)

For the exergy calculation of water/LiBr solution, the thermodynamic properties are essential. Mainly, enthalpy and entropy are indispensable to calculate the physical exergy. Assuming each component of VARS as control volume, energy and exergy balance lead to the set of heat transfer equations discussed in the following sections.

3.2.3. Performance of VARS

Performance analysis for VARS is based on the analysis of the first and the second law of thermodynamics. These two analyses depend on the heat and exergy transfer of the system, respectively. The mathematical model that can be applicable for a heat transfer phenomena of any refrigerant-absorber combinations is taken from (Arora, 2010). For the exergy analysis a mathematical model by Pandya *et al.,* (2017) is used. Two main circuits in the VARS control both this interaction the solution, and the refrigerant circuit.

3.2.3.1. Solution circuit energy and exergy balance

The general mathematical model for an absorption system for mass, energy and exergy balance is

given below:

Mass balance

Let's say the amount of distilled water from generator is D so that the strong and weak solution mass flow rate is (D*f) and (D*(f-1)), respectively. Where f is the circulation ratio. Energy and exergy balance per unit mass of distilled water for each control volume is presented below:

Generator

In the generator, the external hot fluid provides the heat to boil the solution and super-heated vapor is generated, and flows to the condenser. Energy and exergy balance of the generator is given by Equation 3.16 and 3.17, respectively.

$Q_g + f*h_1 = h_5 + (f-1)\, h_2$ …..……..……..…. (3.16)

$\Delta Є_g = f*(h_1 - T_o s_1) - (f-1)[h_2 - T_o s_2] - (h_5 - T_o s_5) + \frac{m_g}{D}[h_9 - T_0 s_9) - (h_{10} - T_o s_{10})]$……(3.17)

Where, Q_g and $\Delta Є_g$ is heat transfer and exergy gain in the generator. m_g is the hot water mass flow rate, and h,s and T are specific enthalpy, specific entropy, and temperature, respectively.

Solution heat exchanger (SHX)

In the solution heat exchanger the strong LiBr solution which comes from the generator exchanges heat with the weak LiBr solution from the absorber.

The energy and exergy balance of SHX is given by Equation 3.18 and 3.19, respectively.

$Q_{SHX} = f(h_1 - h_4) = (f-1)(h_2 - h_3)$ ……..……..……..…. (3.18)

$\Delta Є_{SHX} = f[h_4 - h_1 - T_o(s_4 - s_1)] + (f-1)[h_3 - h_2 - T_o(s_3 - s_2)]$……..……..…….. (3.19)

Where, Q_{SHX} and $\Delta Є_{SHX}$ is heat transfer and exergy destruction in SHX, respectively.

Absorber

In the absorber, the water vapor from evaporator, is absorbed by the strong LiBr solution which comes from the solution heat exchanger, the heat generated during absorption is rejected to water flow. The weak LiBr solution is pumped through the solution heat exchanger.

Energy and exergy balance of absorber is given by Equation 3.20and 3.21, respectively.

$Q_a + f*h_4 = h_8 + (f-1)\, h_3$ ……..……..……. (3.20)

$\Delta Є_a = (h_8 - T_o s_8) + (f-1)(h_3 - T_o s_3) - f(h_4 - T_o s_4) + \frac{m_a}{D}[(h_{15} - T_0 s_{15}) - (h_{16} - T_o s_{16})]$…..…(3.21)

Where, Q_a and $\Delta Є_a$ is heat transfer and exergy destruction in the absorber, respectively.

3.2.3.2. Refrigerant circuit energy and exergy balance

The mass flow rate, as well as the composition, is the same at all sections for the refrigerant circuit.

Condenser

In the condenser, the superheated vapor is cooled down and condensed to saturated liquid by the cooling water which comes through absorber. Energy and exergy balance of condenser is given by Equation 3.22and 3.23, respectively.

$$Q_c = h_6 - h_5 \quad \text{(3.22)}$$

$$\Delta \epsilon_c = (h_6 - T_o s_6) - (h_7 - T_o s_7) + \frac{m_c}{D}[(h_{11} - T_0 s_{11}) - (h_{12} - T_o s_{12})] \quad \text{(3.23)}$$

Where, Q_c and $\Delta \epsilon_c$ are heat transfer and exergy destruction in the condenser, respectively.

Expansion valve

Inside the metering device, the saturated refrigerant which comes from condenser is throttled to drop its pressure. It is assumed that the process occurs in an isenthalpic manner.

$$h_6 = h_7 \quad \text{(3.24)}$$

$$\Delta \epsilon_{exp} = (h_7 - h_6) - T_o (s_7 - s_6) \quad \text{(3.25)}$$

$\Delta \epsilon_{exp}$ is exergy destruction in the metering device.

Evaporator

In the evaporator, the refrigerant evaporates by absorbing heat from the utility and the vapor is absorbed by the absorber. Energy and exergy balance of evaporator is given by Equation 3.26 and 3.27, respectively.

$$Q_e = h_8 - h_7 \quad \text{(3.26)}$$

$$\Delta \epsilon_e = (h_7 - T_o s_7) - (h_8 - T_o s_8) + \frac{m_c}{D}((h_{13} - T_0 s_{13}) - (h_{14} - T_o s_{14})) \quad \text{(3.27)}$$

Where, Q_e and $\Delta \epsilon_e$ is heat transfer and exergy destruction in the evaporator, respectively. The overall energy and exergy balance which is absorbed and rejected by the system gives:

Overall energy balance

$$Q_{recived} = Q_{absorbed} \quad \text{(3.28)}$$

$$Q_G + Q_e = Q_C + Q_a \quad \text{(3.29)}$$

The total rate of exergy destruction of the absorption system is the sum of exergy destruction in

each component and can be written as (Pandya *et al.,* 2017):

$\Delta Є_{sys} = \Delta Є_g + \Delta Є_a + \Delta Є_c + \Delta Є_e + \Delta Є_{SHX}$ ……..……..(3.30)

The coefficient of performance and exergetic efficiency of the VARS is given in Equation 3.31 and 3.32, respectively.

$$COP = \frac{Q_e}{Q_g + W_p} \text{……...……...……} \quad (3.31)$$

Where, W_p is the pump work.

Exergetic efficnecy of a vapor absorption refrigeration system is (Antonio *et al.,* 2014):

$$COPex = \frac{\Delta Є e}{\Delta Є g + W_p} \text{ ……...……} \quad (3.32)$$

3.3. Energy and exergy efficiency of the absorption system for variable input parameters

3.3.1. Effect of generator temperature on COP and COPex

Variation of COP and total exergy destruction rate of a system with the variation of generator temperature is shown in Figure 3.2. It is observed that generator temperature has a significant effect on COP up to a certain value and then after a negligible variation is observed. But, one can see the effect clearly from the second law efficiency for the effect of increasing generator temperature. As the generator temperature increase the exergy destruction at the absorber will increase so that a lot of energy will be lost without any significant effect. That is why one has to see the second law efficiency to signify his design is optimum.

From the Figure it can also be dictated that analysis of COP and COPex have done by varying generator temperature for each different condenser temperatures. Assuming the industrial Generator temperature (Tg) varying from 86 to 102 ^oC a positive effect for some condenser temperature (Tc) has been observed, a temperature that reaches the cut of temperature for the generator, up to a certain range. Then, the COP of the system is constant while exergy destruction will increase significantly.

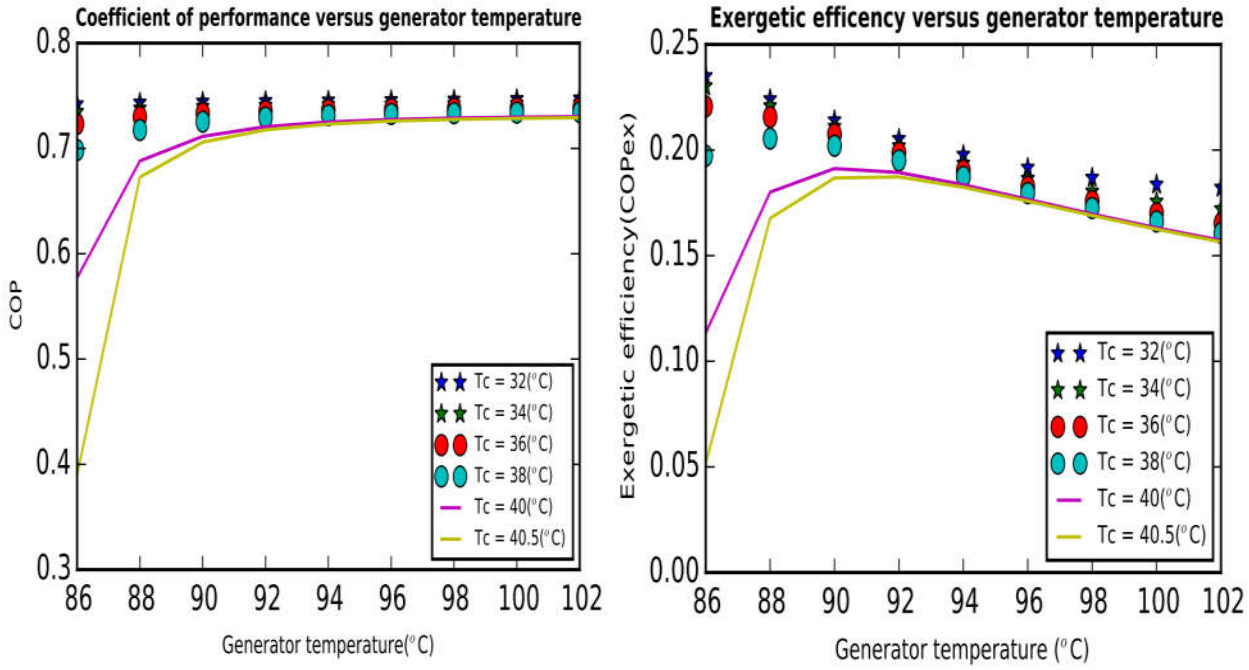

Figure 3. 2: Variation of COP and COPex with generator and condenser temperature

3.3.2. Effect of evaporator temperature on COP and COPex

It is observed from Figure 3.3 that increasing the temperature of evaporator has a positive effect on the COP and COPex of the system, as increasing the temperature of evaporator tends to

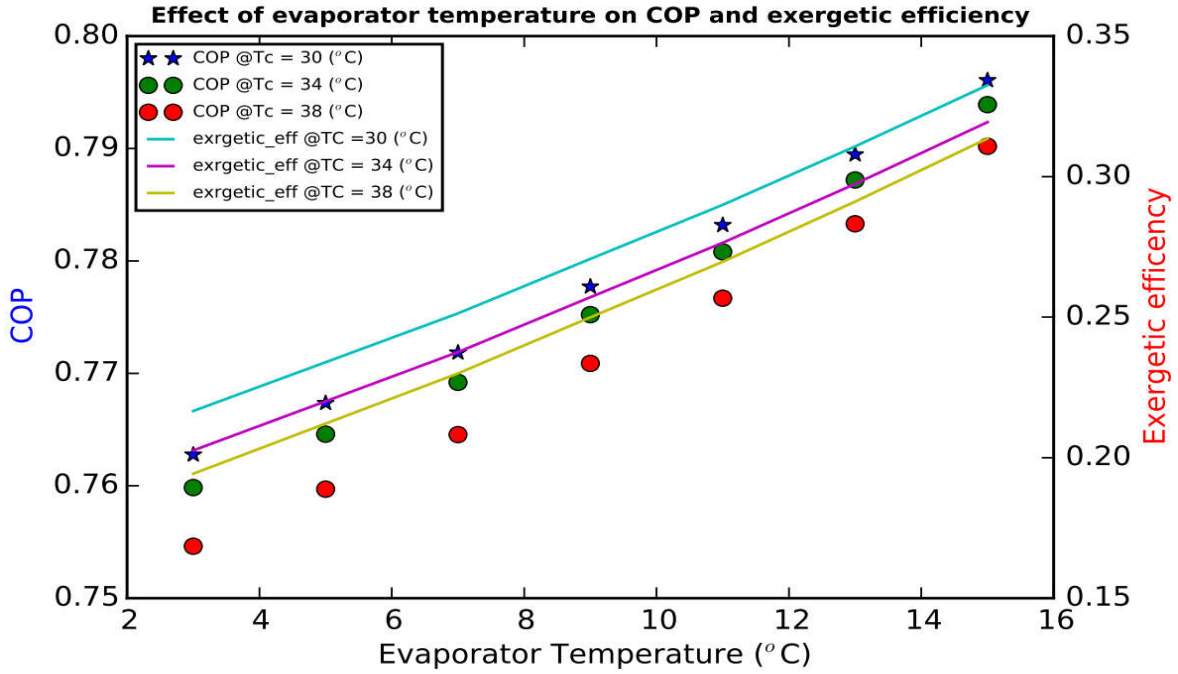

Figure 3. 3: Variation of COP and COPex with evaporator and condenser temperature

decrease the required optimum temperature of the generator. In other word, increasing evaporator temperature give rise to decreasing the amount of heat required on the generator side. The Figure shows the variation of COP and COPex for different condenser temperature (Tc) value.

3.3.3. Effect of absorber temperature on COP and COPex of the system

Increasing the absorber and condenser temperature for constant generator temperature have a negative impact on the COP and COPex of the system as shown in Figure 3.4. This is due to the increase in circulation ratio. As condenser and absorber temperature increase amount of degassing in the generator will decrease.

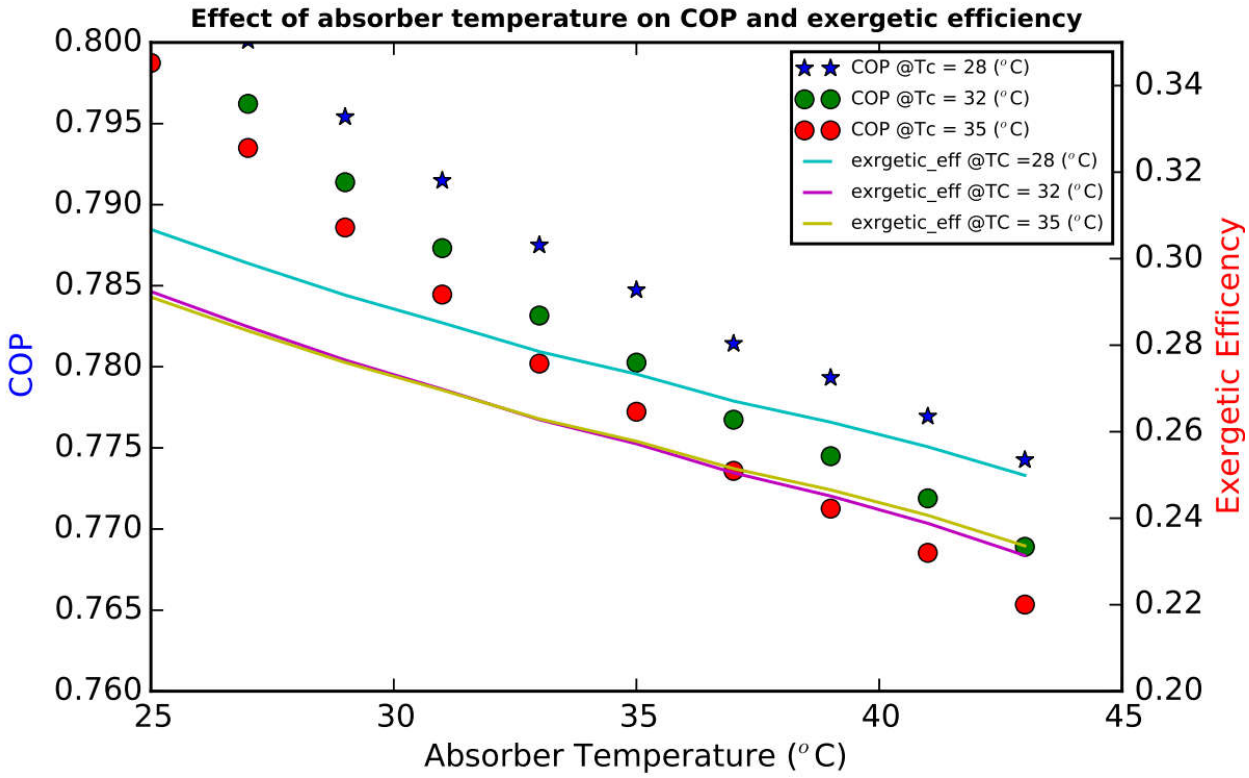

Figure 3. 4: Variation of COP and COPex with absorber and condenser temperature

3.3.4. Circulation ratio versus generator temperature

From Figure 3.5, one can see that the circulation ratio depends on the generator temperature. Whenever the system reaches its cut of temperature, the circulation ratio or the ratio of strong solution mass flow rate to weak solution mass flow rate, is abruptly increased. This is due to low vapor distilled from the generator. Far from the cut of temperature increasing generator

temperature have a negligible impact on the circulation ratio.

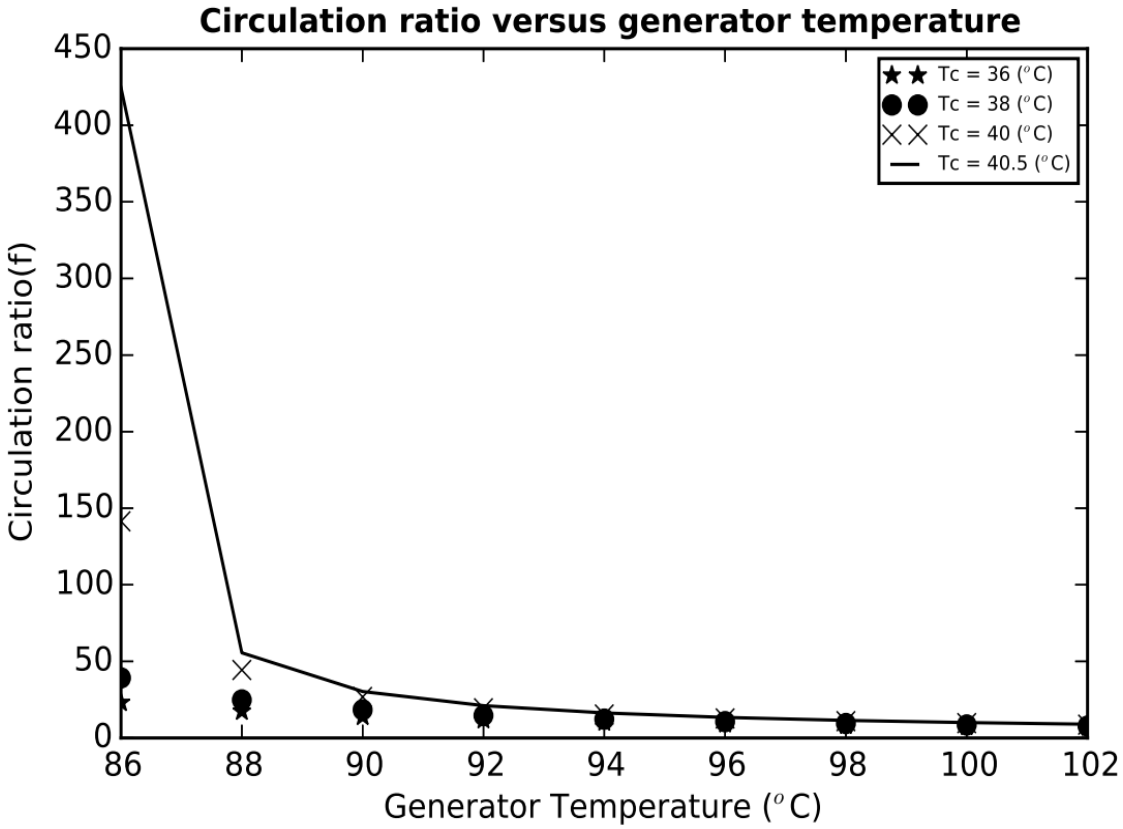

Figure 3. 5: Effect of generator temperature on circulation ratio

3.4. Heat load and exergy destruction per kW of evaporator load

Whenever the study of the performance of VARS is considered, it is very important to analyze the heat load and exergy destruction on each components of VARS for variable input parameters. The response of the system, in heat load and exergy destruction, to the variation of the generator and evaporator temperature per kW of evaporator load is studied in this section.

3.4.1. Heat Load and exergy destruction versus evaporator temperature

Figure 3.6 (a) shows that assuming the industrial evaporator temperature (Te) varying from 2 to 14 ^{o}C makes the generator and absorber load to decrease. As Te increase the concentration of rich solution increase and the circulation ratio (f) decrease. The decrease f, decrease the amount of heat provided to the generator. Figure 3.7 (b) describe that whenever Te increases exergy destruction in evaporator, absorber and generator will decrease. This is because of the decrease in

irreversibility due to mixing and temperature deference.

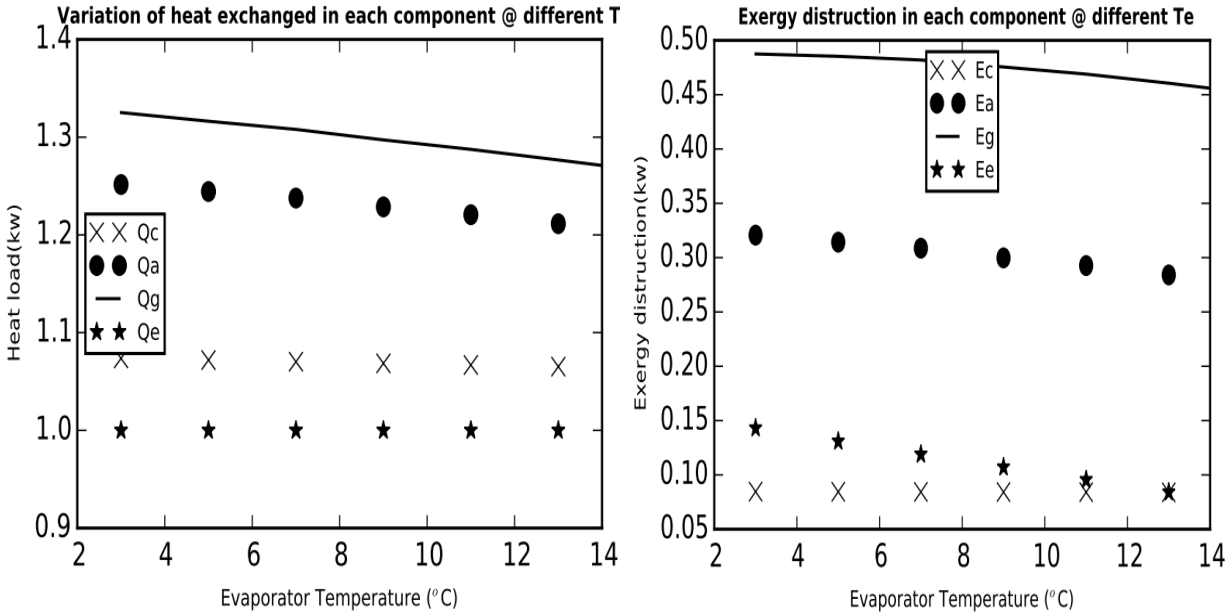

Figure 3. 6: Effect of evaporator temperature on a) heat load b) exergy destruction

3.4.2. Heat Load and exergy destruction versus generator temperature

Figure 3.7 (a) shows that increasing generator temperature from 86 to 102 ºC makes the generator and absorber load to decrease. As Tg increase the concentration of rich solution increase and

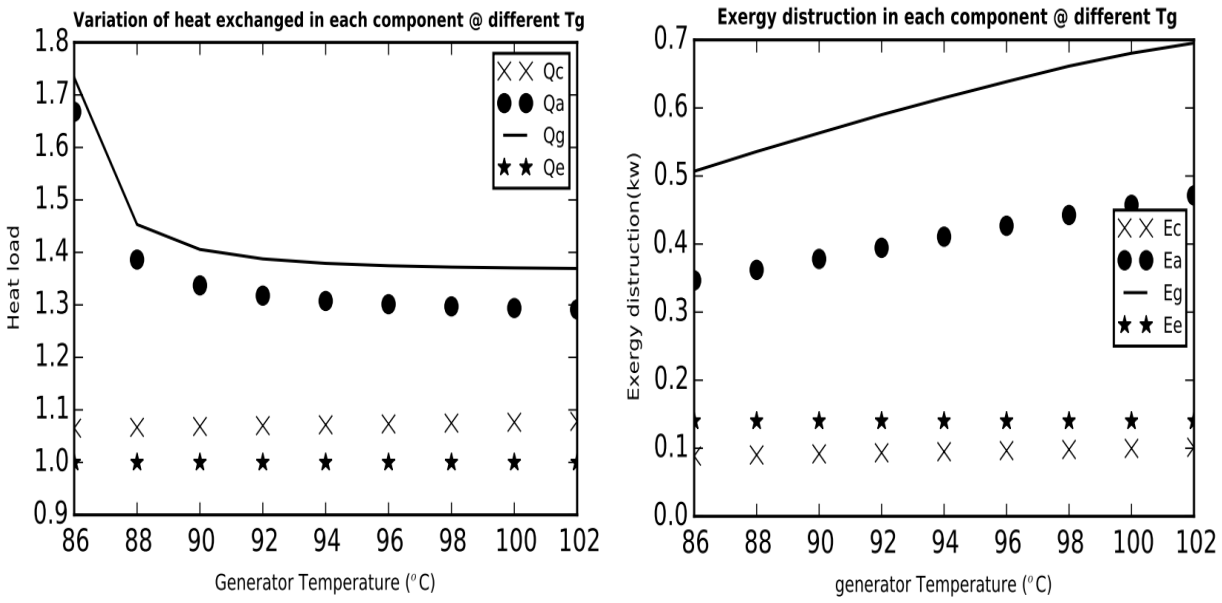

Figure 3. 7: Effect of generator temperature on a) heat load b) exergy destruction

circulation ratio decrease too. This makes, with a constant mass flow rate a large amount of heat will be transferred. But, Figure 3.7 (b) depict that whenever Tg increase exergy destruction in absorber and generator will increase. This is because of the increase in irreversibility due to mixing and temperature difference.

3.2.4. Model validation

Experimental investigation at different point of installation was carried out for single effect water/LiBr absorption chiller in an industrial manufacturing of detergent by Lamine and Said, (2014). The experiment shows the effect of a change in temperature of generator and evaporator, on the COP and heat load on the component. Figure 3.8 shows, elevation of Tg for different Tc value. Typically the graph shows increase of COP for temperatures Tg lower than 90 ° C, above this value COP begins to decline and it becomes constant for temperature of Tg relatively high (over 95 ° C). This result is comparable with the result obtained in Figure 3.2 (a), except a little variation may be considered as the pressure loss and environmental effect is not dealt.

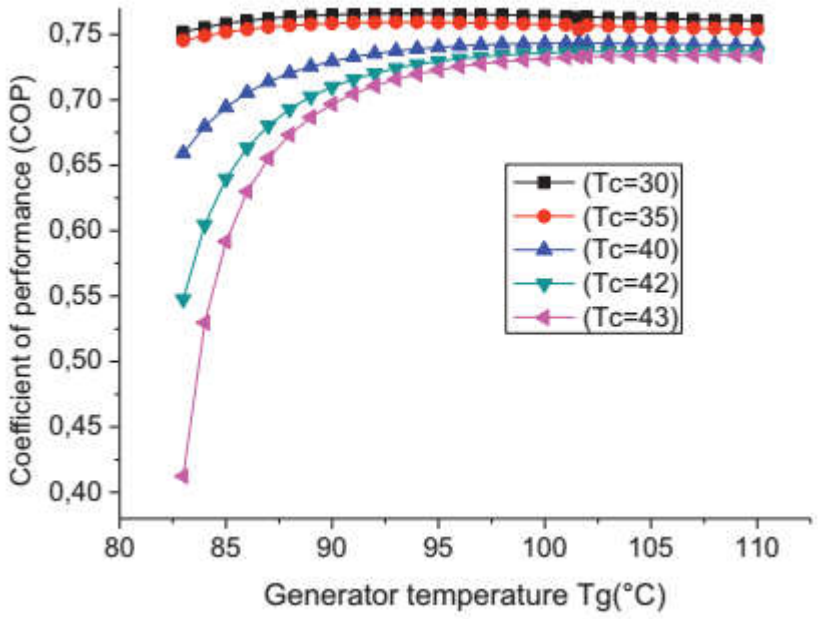

Figure 3. 8: Effect of temperature on COP of single effect VARS (Lamine and Said, 2014).

3.6. Design of VARS

As described in the literature the commercial water-LiBr VARS system can be:

1. Single-stage or single-effect system, and
2. Multi-stage or multi-effect system

Single-stage systems operate under two pressures: one corresponding to the condenser-generator (high-pressure side) and the evaporator-absorber (low-pressure side). Single-stage systems can be either (Kharagpur, 2008):

1. Twin drum type, or
2. Single drum type

In a twin drum single effect VARS, evaporator and absorber operate at the same pressure, so that, it can be housed on the same vessel, and the same is true for condenser and generator. The twin drum consists of two vessels operating under different pressure as it is demonstrated in Figure 3.9. Whereas, in a single drum single effect VARS the whole components are housed on the same vessel by separating the high and low-pressure house using a diaphragm. The single drum single effect VARS used for domestic application, as the components are housed using a diaphragm, the vessel can't withstand high pressure.

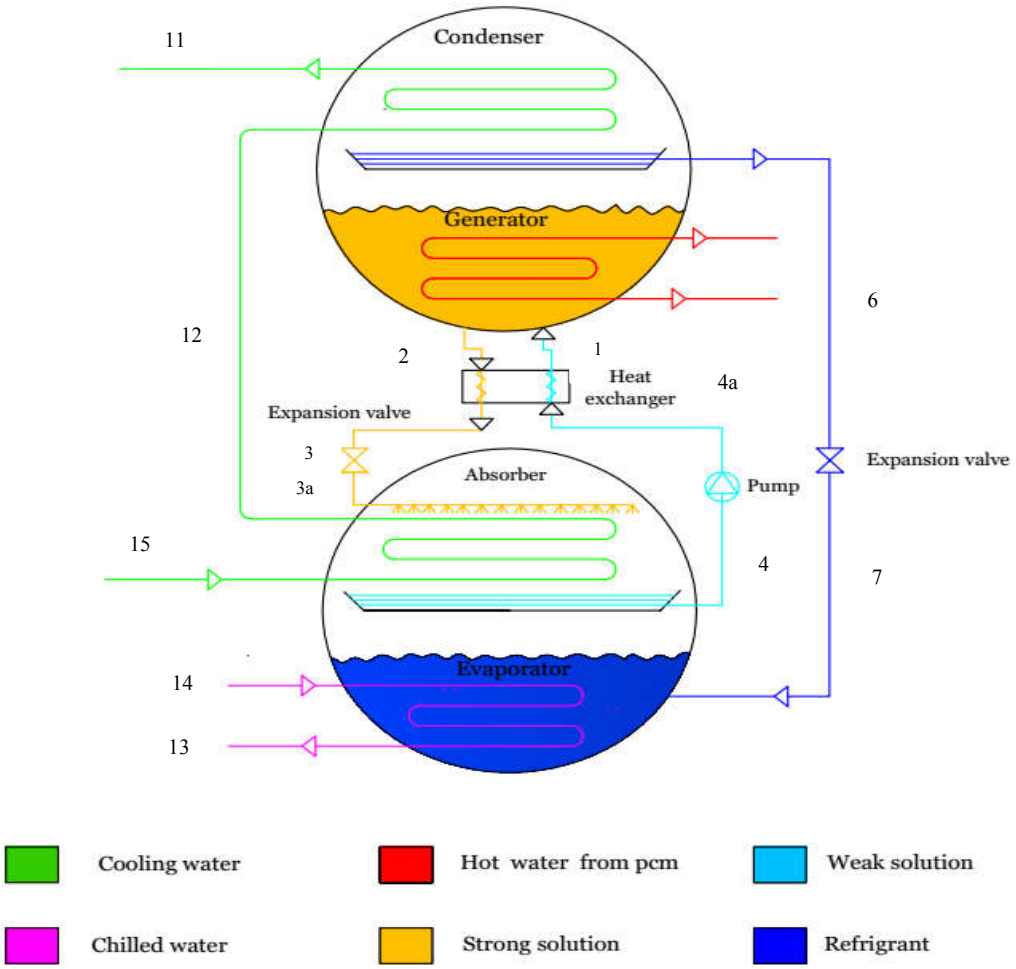

Figure 3. 9: Twin drum single effect VARS

As shown in the Figure, the cooling water acts as a heat sink in a series arrangement through the absorber and extract heat from both components. This type of arrangement has an advantage over the parallel arrangement by minimizing the required cooling water flow rate and prevent crystallization by increasing the condenser pressure. Heater tubes (hot water) are immersed in the strong solution pool of generator for vapor generation. Pressure drop between evaporator and absorber, and between generator and condenser are minimized, large-sized vapor lines are eliminated and air leakages can also be reduced due to less number of joints.

3.6.1. Design of single effect VARS

The general suggested order of calculation to design the components of the VARS is discussed below. To perform equipment sizing of a twin drum singe effect VARS some basic assumption and input values must be considered (Ashrae handbook, 2009).

- Generator and condenser, as well as evaporator and absorber, are under the same pressure
- The refrigerant vapor leaving the evaporator is saturated pure water
- Liquid refrigerant leaving the condenser is saturated
- Strong solution leaving the generator is boiling
- The refrigerant vapor leaving the generator has the equilibrium temperature of the strong solution at generator pressure
- Weak solution leaving the absorber is saturated
- Flow restrictors are adiabatic
- Pump is isentropic
- The log mean temperature difference (LMTD) expression adequately estimates the latent changes

3.6.2. System heat exchangers design

From energy balance, it can be dictated that the consecutive heat transfer on the cooling and heating medium is equal with the latent heat transfer on the refrigerant side. In the two-phase heat exchanger, the temperature difference ΔT is zero on the refrigerant side as the phase change process occur, whereas ΔT has none zero value for the heating and cooling medium (Kalogirou *et al*., 2001). In this design, an outer diameter (D_o) of 16 mm and inner diameter (D_i) of 14 mm is used as a base to size the exchanger. The refrigerant flow through the vessel while cooling and chilling water flow through the tubes in single to four tube passes (Kharagpur, 2008), and four tube pass is taken for this study to size the tube.

3.6.2.1. Generator design

Distillation of the vapor from rich solution leaving the strong solution behind for recycling will occur in the generator. Hot pressurized water from collector or PCM supplies the load to the generator. A Python code that evaluates the heat transfer area, tube length, and the number of tube is presented in Appendix B. To determine the thermophysical properties for water/LiBr solution, a correlation is given by the Ashrae handbook, (2009) is used, as depicted in Appendix A. To find the tube side heat transfer coefficient the following procedure is used.

The mean temperature of the hot pressurized water form collector or PCM is,

$$T_{mean,g} = \frac{T_{g\_in} + T_{g\_out}}{2} \quad \text{.....(3.34)}$$

The code evaluate by taking the property of the hot pressurized water from Iapws library, at an average of the hot inlet (T_{g_in}) and hot outlet (T_{g_out}) temperature. The hot water is supplied from the collector to the generator through a tube, the hot water Reynolds number is given by:

$$Re_g = \frac{\rho_g v_g D_i}{\mu_g} \quad \text{..... (3.35)}$$

Where, ρ_g, v_g and μ_g represents the density, velocity and dynamic viscosity of the pressurized hot water, respectively. Where: $v_g = \frac{\dot{m}_w}{\rho_g A}$, and, $\dot{m}_w$ is the mass flow rate and *A* is the flow area of water.

The flow area of water is (Kakac and Liu, 2002),

$$A = \frac{N_t}{N_p}\frac{\pi}{4}D_i^2 \quad \text{..... (3.36)}$$

Where, N_t is the total number of tube and N_p is the number of pass.

The mass flow rate of water through the tube is,

$$\dot{m}_w = \frac{Q_g}{C_p \Delta T} \quad \text{.....(3.37)}$$

Where, Q_g is the latent heat of vaporization in the generator as given in Equation 3.16 and ΔT is the change in temperature between the hot inlet and hot outlet.

Assuming fully developed flow, the flow can be laminar or turbulent, one can use the general derived equation for laminar or Dittus-Boelter equation if it is turbulent flow (Kakac and Liu, 2002).

If Re <2300, Laminar

$$Nu = \frac{h_i D_i}{K} = 3.66 \quad \text{..... (3.38)}$$

Else, turbulent

$$Nu = \frac{hD_i}{K} = 0.023\ Re^{0.8}\ Pr^{0.4} \quad \text{..... (3.39)}$$

Where, Re =Reynold's number

Pr = Prandtl number, and

Nu = Nusselt number

For the shell side, the pool boiling Rohsenow Correlation (Dewitt *et al*., 2010) predicts somewhat satisfactory relation for nucleate boiling.

$$h_o = \frac{\mu_f h_{fg}}{\Delta T}\left[\frac{g(\rho_f - \rho_g)}{\sigma}\right]^{\frac{1}{2}}\left[\frac{C_f \Delta T}{C_{s,f} h_{fg} Pr_f^{1.7}}\right]^3 \quad \text{..... (3.40)}$$

Where, h_{fg} = latent heat of evaporation (kJ/kg)

ρ = density of solution (kg/m^3)

ΔT = degree of super heat (^{o}C)

σ = surface tension of solution (J/m^2)

h_o = heat transfer coefficient (W/m^2 K)

Equation 3.40 is the first and the most widely used equation for nucleate boiling. In this expression, all the properties of liquid and vapor refrigerant are evaluated at the saturated temperature of evaporation. The coefficient $C_{s,f}$ and the exponent n depends on the solid-liquid combination, 0.0068 and 1 for water with copper tube, respectively (Dewitt *et al*., 2010).

Calculating h_i and h_o values and putting these in Equation 3.41 give the overall heat transfer coefficient (U_o) as depicted below.

$$\frac{1}{U_o} = \frac{A_o}{A_i h_i} + \frac{\ln(\frac{Do}{Di})}{2k} + \frac{1}{h_i} \quad \text{(3.41)}$$

Where k is tube thermal conductivity.

The logarithmic mean temperature difference (LMTD) is given by:

$$\Delta T_{LMTD} = \frac{\Delta T_1 - \Delta T_2}{\ln(\frac{\Delta T_1}{\Delta T_2})} \quad \text{(3.42)}$$

Where, $\Delta T_1 = T_{g\_in} - T_g$

$\Delta T_2 = T_{g\_out} - T_g$

Where, T_g is the generator temperature. The correction factor for single-phase convection on one side and two-phase convection on the other side heat exchangers is unity, thus LMTD is determined on the usual fashion.

The heat transfer area of the generator is,

$$A_O = \frac{Q_g}{U_o * \Delta T_{LMTD}} \quad \text{(3.43)}$$

Finally, the length of the generator tube per pass is given by:

$$L_g = \frac{A_O}{\pi N_t D_O} \quad \text{(3.44)}$$

3.6.2.2. Absorber design

Inside the absorber, absorption of the refrigerant from the evaporator by strong solution from the generator while releasing heat to the cooling water is processed. Ambient cooling water is used as a cooler to reduce the parasitic load of the VARS. Taking this as inlet cooling water and a five-degree increment at the outlet, A Python code that evaluates the tube length and the number of

tubes is presented in Appendix B. For the water/LiBr solution, a correlation is given by Ashrae handbook is used to determine the thermophysical property. In this analysis a vertical falling film absorber is assumed. A heat transfer correlation which governs the heat transfer phenomena for both the shell and tube side is determined as follows:

Cooling water from the cooling tower is supplied to the absorber in a pipe. To find the heat transfer coefficient inside the tube, the same procedure as the generator design is used. The mean temperature of the cooling water from the cooling tower is,

$$T_{mean,a} = \frac{T_{a\_in} + T_{a\_out}}{2} \quad \text{..... (3.45)}$$

The code evaluates by taking the property of the cooling water from Iapws library, at an average of inlet (T_{a_in}) and outlet (T_{a_out}) temperature.

For the tube side heat transfer, the general derived equation for laminar or Dittus-Boelter equation for turbulent flow as given in Equation 3.38 and 3.39 is used, respectively. For the shell side heat transfer, as the absorber is a vertical falling film absorber, the correlation given by Miller, (2001) is used:

$$Nu = C_1 Re^{\alpha 1} Pr^{\alpha 2} Ka^{\alpha 3} Ja^{\alpha 4} \quad \text{..... (3.46)}$$

Where, Ka = Kapitaz number

Ja = Jakobs number

And, the regression constant is given by:

$C_1 = 0.8429$, $\alpha 1 = 0.145664$, $\alpha 2 = 0.048053$, $\alpha 3 = 0.330440$ and $\alpha 4 = -0.071242$

Ka and Ja are a correlational function for the regression heat transfer equation as per Miller, (2001) given by:

$$Ka = \frac{\sigma}{\rho(v^4 g)^{1/3}} \quad \text{..... (3.47)}$$

$$Ja = \frac{C_{p\Delta T}}{h_{fg}} \quad \text{..... (3.48)}$$

Where, σ and v are the surface tension and kinematic viscosity of the solution, respectively.

The shell side heat transfer equation for the absorber is determined by:

$$h_o = \frac{Nu * k}{D_o} \quad \text{..... (3.49)}$$

Where, D_o and k are tube outside diameter and thermal conductivity, respectively.

Then the overall heat transfer equation and the logarithmic mean temperature difference for the absorber can be evaluated using Equation 3.41 and 3.42, respectively.

The heat transfer area of the absorber is,

$$A_O = \frac{Q_a}{U_o * \Delta T_{LMTD}} \quad \text{..... (3.50)}$$

Where, Q_a is absorber heat load, finally, the length of the tube per pass is given by:

$$L_a = \frac{A_o}{\pi N_t D_o} \quad \text{..... (3.51)}$$

Where, N_t is the total number of tube in the absorber, and D_o is the outer diameter of absorber tube.

3.6.2.3. Evaporator design

Liquid refrigerant from condenser evaporates by the chilled water inside the evaporator. For the shell side heat transfer as the boiling is assumed nucleate, the Rohsenow pool boiling correlation (Dewitt *et al*., 2010) as given in Equation 3.40 predict somewhat satisfactory relation for nucleate boiling. The code evaluates at an average temperature of chilled water (Tchill_in) and (Tchill_out) by taking thermo-physical property from Iapws library.

The mean temperature of the chilled water form utility is,

$$T_{mean,chill} = \frac{T_{chill\_in} + T_{chill\_out}}{2} \quad \text{..... (3.52)}$$

For the tube side heat transfer assuming fully develop a flow for laminar or turbulent, one can use the general derived equation for laminar flow or Dittus-Boelter equation if it is turbulent (Kakac and Liu, 2002) as given in Equation 3.38 and 3.39, respectively. Then the overall heat transfer equation and the logarithmic mean temperature difference for the evaporator can be evaluated using Equation 3.41 and 3.42, respectively.

Using the same procedure as the generator design, the heat transfer area and the length of the absorber tube can be evaluated. The heat transfer area of the evaporator is,

$$A_O = \frac{Q_e}{U_o * \Delta T_{LMTD}} \quad \text{..... (3.53)}$$

Where, Q_e is evaporator heat load, finally, the length of the tube per pass is given by:

$$L_e = \frac{A_o}{\pi N_t D_o} \quad \text{..... (3.54)}$$

Where, N_t is the total number of tube in the evaporator, and D_o is outer diameter of evaporator tube.

As the evaporator and absorber are on the same vessel, their tube length has to be the same ($L_e = L_a$). An iterative calculation is developed to determine the number of tube from the available

absorber length, as depicted in Appendix B.

3.6.2.4. Condenser design

Distilled vapor from the generator is condensed by cooling water from absorber inside the condenser. In most of the case, film-wise condensation outside a bank of horizontal tubes is assumed in the condenser design. As a series arrangement is considered through the absorber and condenser, cooling water leaving absorber is taken as inlet cooling water to condenser and assuming a five-degree increment at the outlet, A Python code evaluate the tube length and number of tubes is presented in Appendix B. A heat transfer correlation which governs the heat transfer phenomena for both the shell and tube side is determined as follows:

Cooling water from absorber is supplied to the condenser in a pipe. The mean temperature of the cooling water from absorber is,

$$T_{mean,a} = \frac{T_{a\_out} + T_{c\_out}}{2} \quad \text{..... (3.55)}$$

The code evaluates by taking the property of the cooling water from Iapws library, at an average of absorber outlet (T_{a_out}) and condenser outlet (T_{c_out}) temperature.

To find the heat transfer coefficient inside the tube, the same procedure as the generator design is used. The general derived equation for laminar or Dittus-Boelter equation for turbulent flow as given in Equation 3.38 and 3.39 is used, respectively.

For the shell side heat transfer, a typical correlation known as Nusselt's correlation for film-wise condensation outside a bank of horizontal tubes is used (Kharagpur, 2008):

$$h_0 = 0.729\left(\frac{k_f^3 \rho_f (\rho_f - \rho_g) g h_{fg}}{N D_0 \mu_f \Delta T}\right)^{0.25}$$, for single tube pass ..... (3.56)

$$H_o = N^{-0.25} h_0$$, for banks of tubes ..... (3.57)

Where, h_{fg} = latent heat of evaporation (kJ/kg)

ρ = density of solution (kg/m^3)

$\Delta T = T_{saturation} - T_{surface}$ (^{o}C)

N = number of tubes

K_f = thermal conductivity of the fluid (W/mK)

h_o = heat transfer coefficient for single tube pass (W/m^2 K)

H_o = heat transfer coefficient for bank of tubes (W/m^2 K)

Using the same procedure as the generator design, the heat transfer area and the length of the absorber tube can be evaluated. The heat transfer area of the condenser is,

$$A_O = \frac{Q_c}{U_o * \Delta T_{LMTD}} \quad \text{(3.58)}$$

Where, Q_c is condenser capacity, finally, the length of the tube per pass is given by:

$$L_c = \frac{A_o}{\pi N_t D_o} \quad \text{(3.59)}$$

Where, N_t is the total number of tube in the condenser, and D_o is an outer diameter of condenser tube.

As the condenser and generator are on the same vessel, their tube length has to be the same ($L_c = L_g$). An iterative calculation is developed to determine the number of tube from the available generator length, as depicted in Appendix B.

3.6.2.5. Solution heat exchanger (SHX) design

To improve the performance of VARS, SHX is incorporated between the low-pressure absorber and high-pressure generator. The heat exchanger for SHX is a double tube counter flow design. The inner tube contains the hot strong solution and the annular gas contains the cold weak solution. From the general energy and exergy balance equation the temperature of the weak and strong solution can be determined. In the inner tube high-temperature weak solution of H_2O-LiBr is flowing and in the annular region strong solution flow to the absorber. So, heat transfer takes place between the week and the strong solution. The procedure of the design is as follows:

To find the week and strong solution heat transfer coefficient the following procedure is used.

Mean temperature of the week solution form absorber is,

$$T_{mean,g} = \frac{T_1 + T_a}{2} \quad \text{(3.60)}$$

Where, T_1 is a weak solution leaving the SHX to the generator, and T_a is absorber temperature.

The mean temperature of the strong solution form generator is,

$$T_{mean,g} = \frac{T_1 + T_a}{2} \quad \text{(3.61)}$$

Where, T_3 is strong solution leaving the SHX to the absorber, and T_a is the generator temperature.

For the average temperature of the weak and strong solution, thermodynamic properties from Ashrae handbook, (2009) as depicted in Appendix A, are used to get the Reynolds number for both solutions. The velocity for both the weak and strong solution is calculated by:

$$V_{weak} = \frac{\dot{m}_w}{p_w * A_i} \quad \text{(3.62)}$$

Where, $\dot{m}_w$ and p_w is the mass flow rate and density of the weak solution, respectively. And, $A_i = \frac{\pi}{4} D_i^2$, is area of the inner pipe.

$$V_{strong} = \frac{\dot{m}_s}{p_s * A_o} \quad \text{(3.63)}$$

Where, $\dot{m}_s$ and p_s is the mass flow rate and density of the strong solution, respectively. And, $A_o = \frac{\pi}{4}(D_o^2 - D_i^2)$, is area of annulus.

Reynolds number for both the weak and strong solution is calculated by:

$$Re_{weak} = \frac{\rho_w v_{weak} D_i}{\mu_w} \quad \text{(3.64)}$$

Where, μ_w is dynamic viscosity of the weak solution

$$Re_{strong} = \frac{\rho_s v_s D_e}{\mu_s} \quad \text{(3.65)}$$

Where, μ_s is dynamic viscosity of the strong solution, and D_e is the hydraulic diameter of the annulus given by:

$$D_e = \frac{4 * A_o}{P_h} \quad \text{(3.66)}$$

Where, P_h is perimeter of annulus calculated by:

$$P_h = \pi D_o \quad \text{(3.67)}$$

For the tube side, if the flow is laminar, the generalized derived equation given in Equation 3.38 can be used. For the concentric annular smooth duct, if the flow is laminar, the modified Sieder-Tate equation is used (Kakac and Liu, 2002):

$$Nu = 1.86\left(\frac{D_e R_e Pr}{L}\right)^{\frac{1}{3}} \quad \text{(3.68)}$$

If the flow is turbulent, the heat transfer is governed by the Dittus-Boelter equation written for both the tube and annular side (Kakac and Liu, 2002):

$$Nu = 0.023 Re^{0.8} Pr^n \quad \text{(3.69)}$$

n = 0.4 and 0.3 for heating (weak solution) and cooling (strong solution), respectively.

After, calculating h_i and h_o values and putting them in Equation 3.41 gives the overall heat transfer coefficient (U). Putting U value to the LMTD in Equation 3.43 gives the heat exchanger area of the SHX. Form this area, the length of the tube required can be calculated by Equation 3.44.

3.6.2.6. Expansion valve

An expansion device in a refrigeration system normally serves two purposes. One is a thermodynamic function of expanding the liquid refrigerant from the condenser pressure to the evaporator pressure. And the other is the controlling function which may involve the supply of the liquid to the evaporator at the rate of its evaporation (Arora, 2010).

Basically, there are two types of expansion devices. These are:

1. Constant restriction type
2. Variable restriction type

The constant restriction type device is the capillary tube which is merely a long tube with a narrow diameter bore. This type of metering device cannot be used for large cooling capacity and fluctuating load conditions as it cannot adjust itself to the load fluctuation. In the variable restriction type, the extent of opening or area of flow keeps on changing depending on the type of control. These metering units could be automatic expansion valve, the thermostatic expansion valve or the float valve. Float type expansion valves are normally used with flooded evaporators in large capacity refrigeration systems as in the case of this study. Afloat type valve opens or closes depending upon the liquid level as sensed by a buoyant member, called as float (Kharagpur, 2008).This type of metering unit is normally used in large capacity system.

Thus the float valve always maintains a constant liquid level in a chamber called float chamber. Depending upon the location of the float chamber, a float type expansion valve can be either a low-side float valve or a high-side float valve (Kharagpur, 2008).either of the two ways can be used interchangeably.

CHAPTER 4: Thermal Performance Analysis of Heat Pipe Evacuated Tube Collector

4.1. Introduction

In this chapter, a heat pipe evacuated tube collector, used as a heat source to run the generator of VARS is studied. The HPETC is a device with very high thermal conductance. If any tube is broken, it is just replaced, which is considered as a cheaper option compared to a flat plate collector (FPC) which requires the replacement of the whole collector (Ghoneim, 2016). ETC is strong and long-lasting. The main components of the heat pipe collector are evaporator, condenser, and the contained working fluid (Jafarkazemi and Abdi, 2012).

The following assumptions is considered in the mathematical modeling of heat pipe evacuated tube collectors:

- The collector absorber area is always at a uniform temperature.
- The temperature gradient across the absorber thickness and over its perimeter is neglected.
- The temperature gradient along the longitudinal direction of absorber is negligible.
- The thermal contact resistance between the absorber area and the evaporator tube, and between the condenser section and the condenser manifold is neglected.
- The connection of the evaporator and condenser of the heat pipe is assumed to be adiabatic.
- The Heat exchanger (manifold) is well insulated to consider the heat loss negligible.
- Crossflow heat exchanger containing the working fluid flow perpendicularly to the condenser section of the heat pipe.
- Conduction through the heat pipe is so high that thermal resistance inside the heat pipe is considered negligible.

4.2. Collector specification

The design parameters from the manufacturer specification for the selected type of heat pipe evacuated tube collector is depicted in Table 4.1. The type of collector is Firebird TZ58-1800-20R which is manufactured by Sunrain in China. These collectors are favored over the other as it offers an extremely high efficiency and can deliver solar energy even in overcast weather conditions and have optimum performance to price ratio.

Table 4. 1: Collector specification

Collector Dimensions	Symbol	Value
Space Between Evacuated Tubes(m) (Center to Center)	Δx	0.075
Outer Diameter of Copper Heat Pipes(m)	D_{cuo}	0.008
Inner Diameter of Copper Heat Pipes(m)	D_{cui}	0.0068
Outer Diameter of condenser(m)	Dc	0.024
Diameter of manifold(m)	D_{mani}	0.042
Thickness of Glasses(m)	t_g	0.0018
Outer Diameter of Inner Glass Tube(m)	D_p	0.047
Outer Diameter of Outer Glass Tube(m)	D_g	0.058
contact sheet(Al) thickness	t	0.0002
Heat pipe length(m)	L	1.8
Length of Evaporation Section(m)	L_e	1.6
Length of Condensation Section(m)	L_c	0.1
Length of Adiabatic Section (m)	L_a	0.1
Number of Tubes	N	20
Volume of Heat Transfer fluid (Water) Per Heat Pipe (m^3)	V_f	0.0007
Filling Ratio of Heat Transferring Fluid	V_t	0.654
Aperture Area (m^2)	A_c	1.86
Absorber area(m^2)	A_b	3.377
Max. operating pressure	p_{max}	6bar
Stagnation temperature	T_{stag}	200
The angle of inclination permitted (deg)	B	15^o -75^o
Mass of Collector (kg)	M	73

4.3. Solar data collection and radiation analysis

The Ethiopian metrological service collects the average sunshine hour for some cities as solar radiation data. As a result, it is necessary to use some models and correlations to determine the

global daily and hourly radiation received by the solar collector. Figure 4.1 shows the average temperature and wind speed of Adama for an average climatic condition of five years.

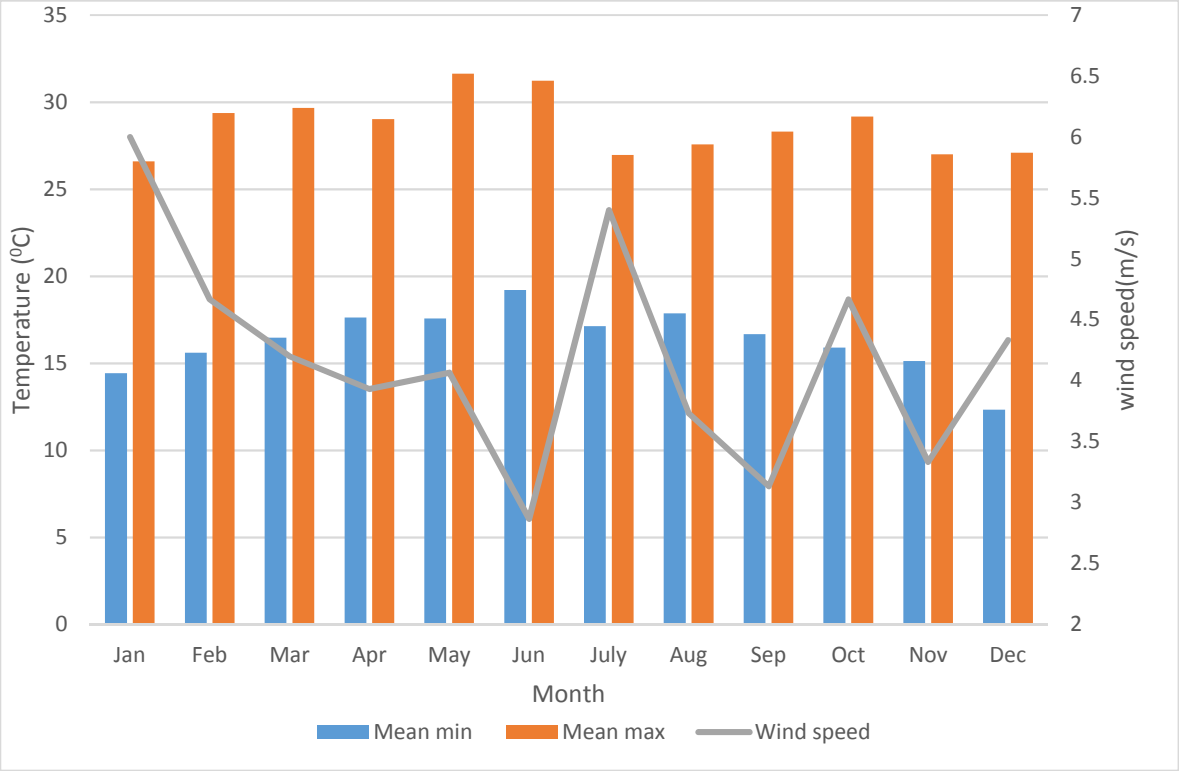

Figure 4. 1: Metrological data for temperature and wind speed of Adama, for an average climatic condition of five years.

4.3.1. Estimation of angular dimensions and solar geometry

To compute solar radiation analysis, it is crucial to know the variation of solar geometry and angular dimension thorough out the day and year**.** The respective model equations are given by (Duffie and Beckman, 2013):

4.3.1.1. Basic earth sun angles

Latitude (φ): the angular location north or south of the equator, north positive,$-90^{o} \leq \varphi \leq 90^{o}$. Adama is located on 8.54^{o} due north of the equator.

Slop (β): the angle between the plane of the surface and the horizontal. ,$-180^{o} \leq B \leq 180^{o}$. $\beta < 90^{0}$ means that the surface has a downward-facing component.

Declination angle (δ): the angular position of the sun at solar noon (i.e, when the sun is on the local meridian) to the plane of the equator, north positive, $-23.45^{o} \leq \delta \leq 23.45^{o}$:

$\delta = 23.45 \sin(\frac{360(284 + n)}{365})$ ……..…….. (4.1)

Hour angle(ω): the angular displacement of the sun east or west of the local meridian due to rotation of the earth on its axis at 15^0 per hour, morning negative, afternoon positive. Given by:

$\omega = 15(solar\ time - 12)$…… (4.2)

Zenith angle (θ_z): the angle between the vertical and the line to the sun or the angle of incidence of beam radiation on a horizontal surface:

$\theta z = cos\varphi cos\delta cos\omega + sin\varphi sin\delta$ ……. (4.3)

Angle of incidence (θ): the angle between the beam radiation on a surface and the normal to that surface.

$cos\theta = \cos\delta\cos\omega(\cos\varphi\cos\beta + \sin\varphi\sin\beta) + \sin\delta(\sin\varphi\cos\beta - \cos\varphi\sin\beta)$ ……. (4.4)

4.3.2. Radiation analysis

4.3.2.1. Extraterrestrial radiation

The extraterrestrial radiation on a surface normal to sun's rays kept at a distance of sun-earth (not the mean distance, but the actual distance on that day, that time), the I_{sc} will essentially be the solar constant, modified to take into account the varying distance between the sun and the earth extraterritorial radiation (I_o) is given by (Tiwari *et al*, 2016):

$I_o = \frac{24*3600}{\pi} Isc[1 + 0.033 \cos(\frac{360n}{365})]$……..……..…… (4.5)

Where I_{sc} = 1367 W/m^2, solar constant

n = day of the year, 1 for January 1st

4.3.2.2. Daily extraterrestrial radiation on a horizontal surface

Corresponding to I_{sc}, the solar radiation intensity under extraterrestrial conditions, the intensity on a horizontal plane I_o in W/m^2 is given by (Tiwari *et al*, 2016):

$I_o = \frac{24*3600}{\pi} Isc[1 + 0.033 \cos(\frac{360n}{365})]\ cos\theta z$ ……..…….…….... (4.6)

By integrating Equation 4.6 from sunrise to sunset we can obtain the daily extraterrestrial solar radiation on a horizontal surface as:

$H_o = \frac{24*3600}{\pi} Isc[1 + 0.033 \cos(\frac{360n}{365})] * [cos\varphi cos\delta sin\omega_{sr} + \pi \frac{\omega_{sr}}{180} sin\varphi sin\delta]$……...(4.7)

Where ω_{sr} is the sunset hour angle, which is

$(\omega_{sr}) = cos^{-1}(-\tan(\varphi)\tan(\delta))$……..……...……...…….. (4.8)

4.3.2.3. Prediction of monthly average daily global and diffuse radiation on a horizontal surface

Surface solar radiation on a ground level was suggested by Angstrom, who relate it with the amount of sunshine hour in the day, using some empirical constant obtained by regression analysis (Tiwari *et al*, 2016):

$\frac{H_G}{H_O} = a + b(\frac{ns}{Ns})$ ……..…….. (4.9)

Where a and b are regression constant given by:

$a = -0.110 + 0.235cos\varphi + 0.323(\frac{ns}{Ns})$ ……..…… (4.10)

$b = 1.449 - 0.533cos\varphi - 0.694(\frac{ns}{Ns})$ ……..…….. (4.11)

Where, H_G is global daily solar radiation on a horizontal surface, n_s is the daily hours of bright sunshine hour as shown in Figure 4.2 and N_s is the maximum possible daily hours of bright sunshine.

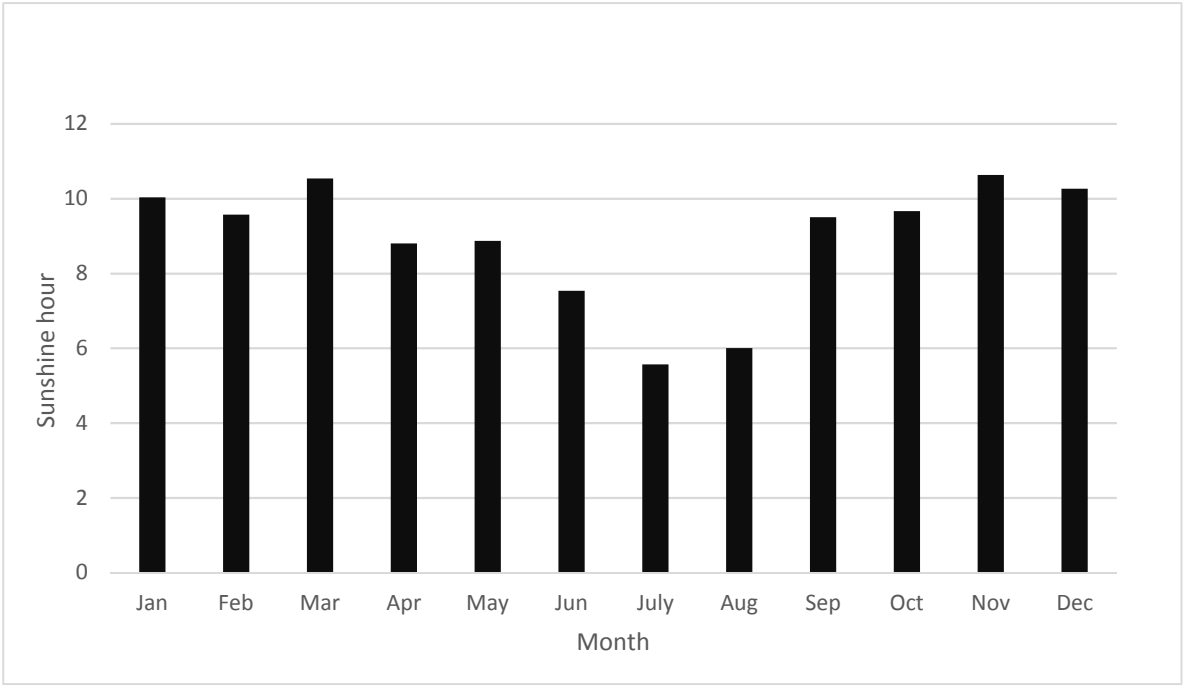

Figure 4. 2: Sunshine hour for the representative day of each month in Adama, for an average climatic condition of five years.

The monthly average daily diffuse solar radiation on a horizontal surface can be determined from the monthly average daily global radiation and the number of bright sunshine hours (Tiwari *et al*, 2016):

$\frac{H_D}{H_G} = 0.931 - 0.814(\frac{ns}{Ns})$ …….. (4.12)

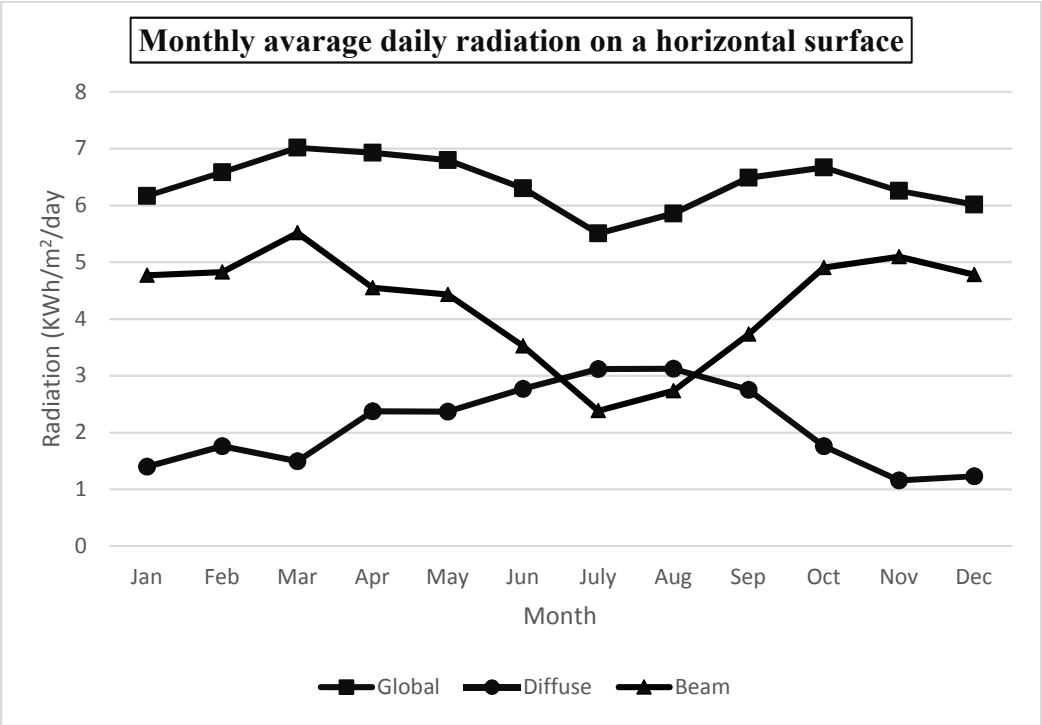

Figure 4. 3: Monthly average global, diffuse and beam radiation on a horizontal surface in Adama

4.3.2.5. Prediction of monthly average hourly Global radiation on a horizontal surface

The monthly average hourly global and diffuse radiation on a horizontal surface can be calculated from the knowledge of the monthly average daily global and diffuse radiation on a ground level (Tiwari *et al*, 2016).

Hourly global radiation:

$\frac{I_G}{H_G} = \frac{\pi}{24*3600}[a_1 + b_1 \cos\omega] * (\frac{\cos\omega - \cos\omega_{sr}}{\cos\omega_{sr} - \frac{\pi\omega_{sr}}{18\ \theta \cos\omega_{sr} * D_H}})$ …….. (4.13)

Hourly diffuse radiation:

$$\frac{I_D}{H_D} = \frac{\pi}{24*3600} * \left(\frac{\cos\omega - \cos\omega_{sr}}{\cos\omega_{sr} - \frac{\pi\omega_{sr}}{18\ 0*\cos\omega_{sr}*D_H}}\right) \quad \ldots\ldots (4.14)$$

Where a_1 and b_1 are regression constant given by:

$a_1 = 0.409 + 0.502\sin(\omega_{sr} - 60)$ ..... (4.15)

$b_1 = 0.661 + 0.477\sin(\omega_{sr} - 60)$..... (4.16)

Hourly Beam radiation:

$I_B = I_G - I_D$ ..... (4.17)

The average hourly global, diffuse and beam radiation on a horizontal surface is depicted in Figure 4.4 for the representative day of each season of the first month:

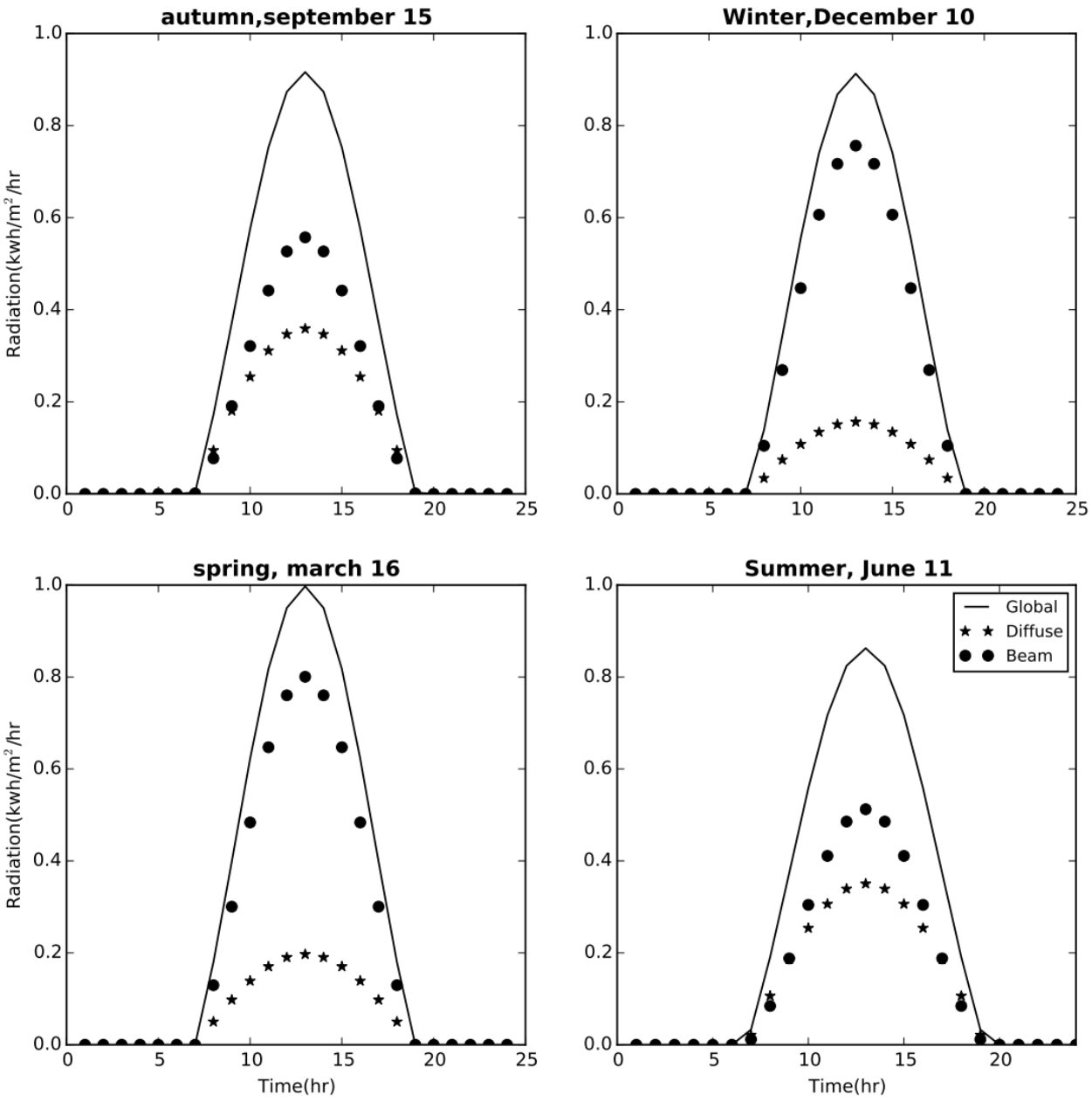

Figure 4. 4: Hourly global, diffuse and beam radiation on a horizontal surface for the representative day of each season of the first month

4.3.2.6. Incident solar radiation on the collector surface

The solar radiation incident on the collector surface depends on the tilt angle of the collector with the horizontal. An experimental measuring to determine the power output related to the title angle of HPETC is done by quality assurance in solar heating and cooling technology (Fischer, 2012). The study is conducted for a tilt angle in the range from 0 to 90^{o} and concludes that the power

increases significantly in the range of 10 to 15 degrees and reaches its maximum at approximately 30°. At higher angles of incidence the power decreases slightly again, this is due to the gravity effect on the evaporation of fluid inside the heat pipe.

The solar radiation energy incident on the collector surface which is inclined at an angle of β to the horizontal surface is defined in terms of global, diffuse, beam and reflected radiation. Total solar radiation incident on a surface consists of beam, diffuse and reflected solar radiation from the ground and surrounding. Total radiation on a surface can be evaluated by arbitrary orientation from knowledge of beam, diffuse and global radiation on a horizontal surface as shown below (Duffie and Beckman, 2013):

$$I_T = H_B R_b + H_D \left(\frac{1+\cos\beta}{2}\right) + H_G \rho_g \left(\frac{1-\cos\beta}{2}\right) \quad \text{(4.18)}$$

Where, R_b is the beam radiation factor and ρ_g ground reflectivity, the value of the reflection coefficient is 0.2 for ordinary ground. Beam radiation factor (R_b) is defined as the ratio of beam radiation incident on an inclined surface to that on a horizontal surface defined by:

$$R_b = \frac{\cos\theta}{\cos\theta_z} \quad \text{(4.19)}$$

Where, θ is the angle of incidence and θ_z is the zenith angle. The radiation on the collector for the representative day of each month is shown in Figure 4.5.

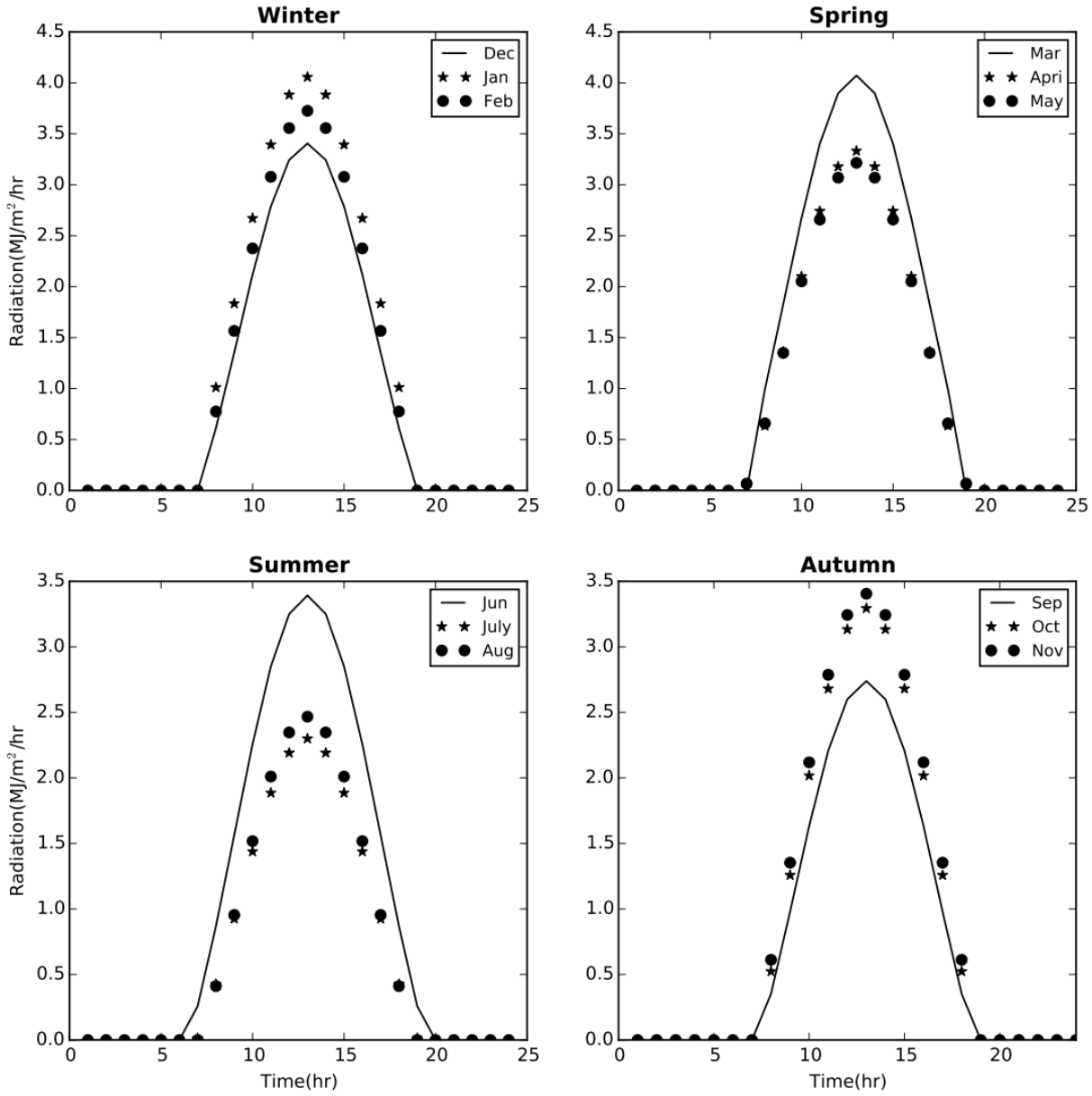

Figure 4. 5: Hourly incidence solar radiation on a tilted surface at an angle of 30^o degree for the representative day of each month at Adama

4.3.3. Prediction of hourly variation of atmospheric temperature

Estimation of hourly variation of atmospheric temperature is a critical data to study the thermal performance analysis of HPEC. However, in Ethiopia it is difficult to get hourly data for most cities. Hence estimation of hourly dry-bulb temperature from the daily mean maximum and daily mean minimum temperatures will give as an approximate value. A sinusoidal variation of the dry-

bulb temperature through the day and maximum temperature occurs at 15:00 hr sun time is assumed. T(t) represent the temperature variation at any time t, as given by (Jones., 1994).

$$T(t) = T_{max} - \frac{(Tmax - Tmin)}{2}\left[1 - \sin\frac{(\pi t - 9\pi)}{2}\right] \quad (4.20)$$

Where, Tmax = mean daily maximum temperature at 15:00 h sun time

Tmin = mean daily minimum temperature

t = Time of the day

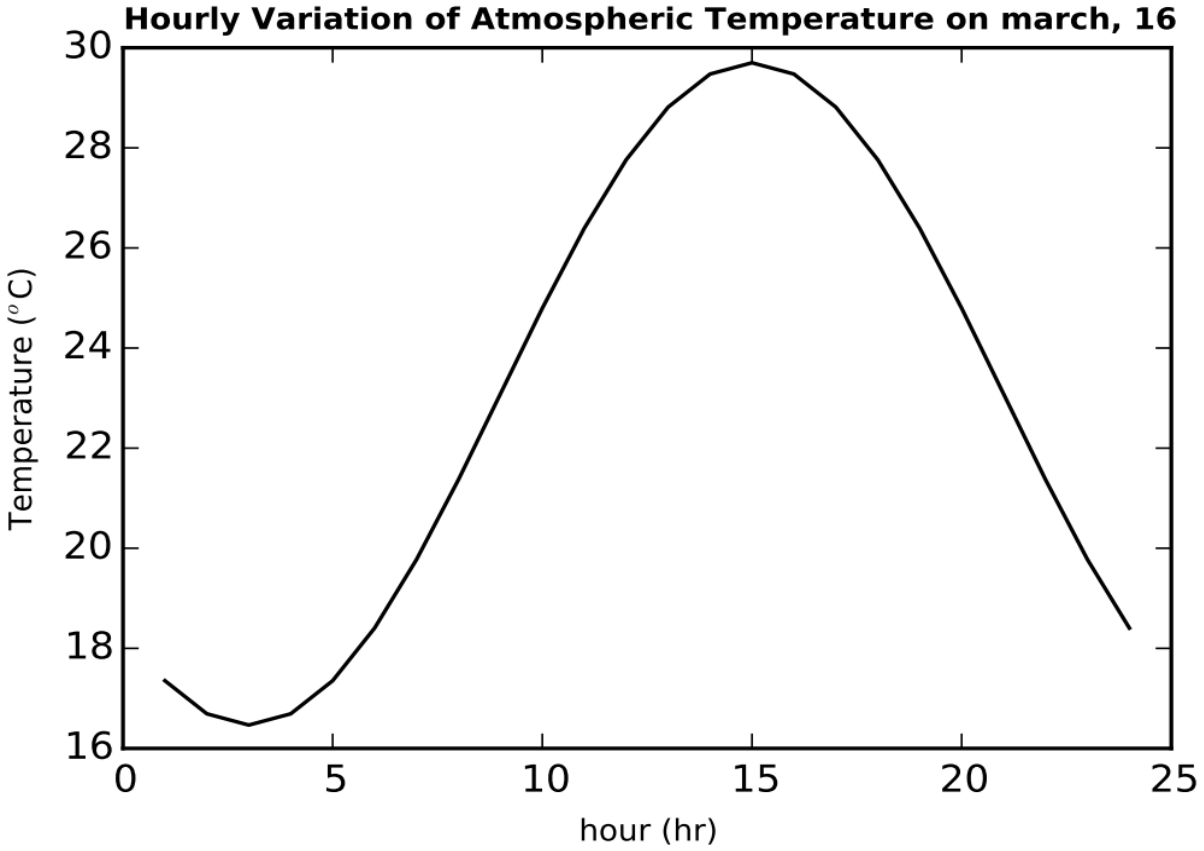

Figure 4. 6: Atmospheric temperature variation of Adama on March, 16

4.4. Modeling HPETC

4.4.1. Heat loss of the system

Thermal energy in heat pipe evacuated tubes solar collector is transferred in each component in the form of radiation, convection, and conduction. The majority of the incident solar energy transferred in the system is converted to useful thermal energy. However, some parts of the thermal energy are released into the atmosphere. The number of thermal energy losses is highly dependent

on the heat loss coefficient, heat transferring surface area and temperature difference between components.

4.4.1.1. Heat loss from the outer glass tube

First, heat is transferred by a combination of radiation and wind convection to the ambient environment, from the outer tube. The wind convection flows around a single-cylinder profile can be the heat transfer coefficient for natural convection that can be obtained as (Duffie and Beckman, 2013).

$h_w = 5.7 + 3.8v$ …… (4.21)

Where, v is the average wind speed for the day. The radiation heat transfer coefficient between the outer glass tube and the environment is given by (Duffie and Beckman, 2013).

$h_{r,g-a} = \varepsilon_g \sigma (T_g^2 + T_a^2)(T_g + T_a)$ …… (4.22)

Where, T_g and T_a is the temperature of the outer glass and the environment, respectively. The total heat transfer resistance between the outer surface and the environment is:

$R_{g-a} = \frac{1}{A_g * (h_w + h_{r,g-a})}$ …… (4.23)

4.4.1.2. Heat transfer between the two concentric cylinder

Heat is transfer by radiation between the two concentrically placed cylinders in an evacuated pocket, the heat transfer coefficient (h_{w-g}) and the heat transfer resistance is given by (Dewitt *et al*., 2010):

$h_{r,w-g} = \frac{\sigma * (T_{abs}^2 + T_g^2) * (T_{abs} + T_g)}{\frac{1}{\varepsilon_{abs}} + \frac{A_{abs}}{A_g}(\frac{1}{\varepsilon_g} - 1)}$ …… (4.24)

Where σ is the Stefan Boltzmann constant, T_{abs} is absorber temperature, ε_{abs} and ε_g are emissivity of the absorber and the outer glass cover respectively and A_{abs} and A_g are inner and outer glass cover respectively. The resistance between the two concentric classes is expressed as:

$R_{w-g} = \frac{1}{A_{DW} * h_{w-g}}$ …… (4.25)

4.4.1.3. Heat transfer through the HPETC

Heat transfer through heat pipe consists of three sections evaporation section condenser section and adiabatic section.

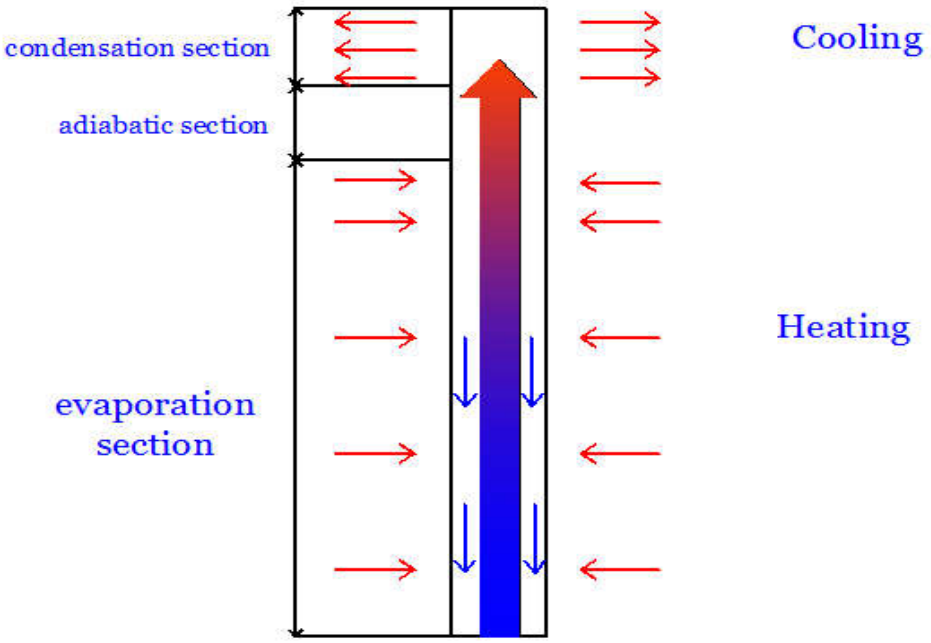

Figure 4. 7: Heat pipe schematic

The evaporator thermal resistance is a combination of three resistances. Circular fin resistance, the copper pipe resistance, and the boiling film evaporation resistance inside the evaporator pipe, which can be expressed as (Jafarkazemi and Abdi, 2012):

$R_{hp} = R_{fin} + R_{evap} + R_{b,film}$ .....(4.26)

$$R_{hp} = \frac{\ln(\frac{D_{0,fin}}{D_{i,fin}})}{2\pi k_{fin} L_{evap}} + \frac{\ln(\frac{D_{0,evap}}{D_{i,evap}})}{2\pi k_{evap} L_{evap}} + \frac{1}{h_{hp} A_{evap}} \quad \text{.....(4.27)}$$

Where, $D_{0,fin}$, $D_{0,evap}$= outer diameter of aluminum fin and heat pipe, respectively (m).

$D_{i,fin}$, $D_{i,evap}$= inner diameter of aluminum fin and heat pipe respectively (m).

k_{fin} = thermal conductivity of aluminum fin

k_{evap} = thermal conductivity of evaporator tube

Where(h_{hp}) represent the boiling film evaporation resistance which is given by (Jafarkazemi and Abdi, 2012):

$$h_{hp} = 0.555*\left(\frac{g\rho_l(\rho_l-\rho_v)k_l^3 h_{fg}^*}{\mu_l(T_w-T_s)D_{evap}}\right)^{1/4} \quad (4.28)$$

Where, T_w is heat pipe wall temperature, T_s the fluid temperature inside the heat pipe, k_l thermal conductivity of the fluid. h_{fg}^* is the modified latent heat of vaporization considering the excess temperature of the wall which is given by (Dewitt *et al*., 2010):

$$h_{fg}^* = h_{fg} + \frac{3}{8}c_{pl}(T_w - T_s) \quad (4.29)$$

Where: h_{fg} is the latent heat of vaporization and c_{pl} is specific heat of the vapor

Similar to the evaporator stage, the condenser stage also has three thermal resistances, namely: the condensing film resistance, the condenser pipe conductance and contact conductance resistance at the dry manifold (Jafarkazemi and Abdi, 2012):

$$R_{cond} = R_{manifold} + R_{cond} + R_{c.film}$$

$$R_{cond,w} = \frac{\ln(\frac{D_{0,mani}}{D_{i,mani}})}{2\pi k_{c,mani}L_{evap}} + \frac{\ln(\frac{D_{0,cond}}{D_{i,cond}})}{2\pi k_{cond}L_{cond}} + \frac{1}{h_{cond.w}A_{cond}} \quad (4.30)$$

Removing the manifold resistance as the loss is negligibly small due to the insulation the equation will be:

$$R_{cond,w} = \frac{\ln(\frac{D_{0,cond}}{D_{i,cond}})}{2\pi k_{cond}L_{cond}} + \frac{1}{h_{cond.w}A_{cond}} \quad (4.31)$$

Where the condensing film heat transfer coefficient ($h_{cond.w}$) is evaluated as expressed in Equation 4.27 (Jafarkazemi and Abdi, 2012). The modified latent heat of condensation to take in to account the subcooled temperature of the condenser which is given by (Dewitt *et al*., 2010):

$$h_{fg}^* = h_{fg} + \frac{3}{8}c_{ps}(T_w - T_s) \quad (4.32)$$

Where: c_{ps} is the specific heat of the working fluid.

The total resistance of heat pipe in the form of convection from the evaporation section to condensation section is the sum of the resistance on the evaporator and condenser section which is given by:

$$R_{h,pipe} = R_{hp} + R_{cond,w} \quad (4.33)$$

Figure 4.8 shows the outlet temperature of hot pressurized water as a function of mass flow rate, from each tubes of the heat pipe collector inside the manifold. From the figure, the outlet temperature increase when the mass flow rate of the working fluid is decreased. A mass flow rate of 0.017 kg/sec which corresponds to an outlet temperature of 115 ^{o}C is selected as working mass follow rate for this study.

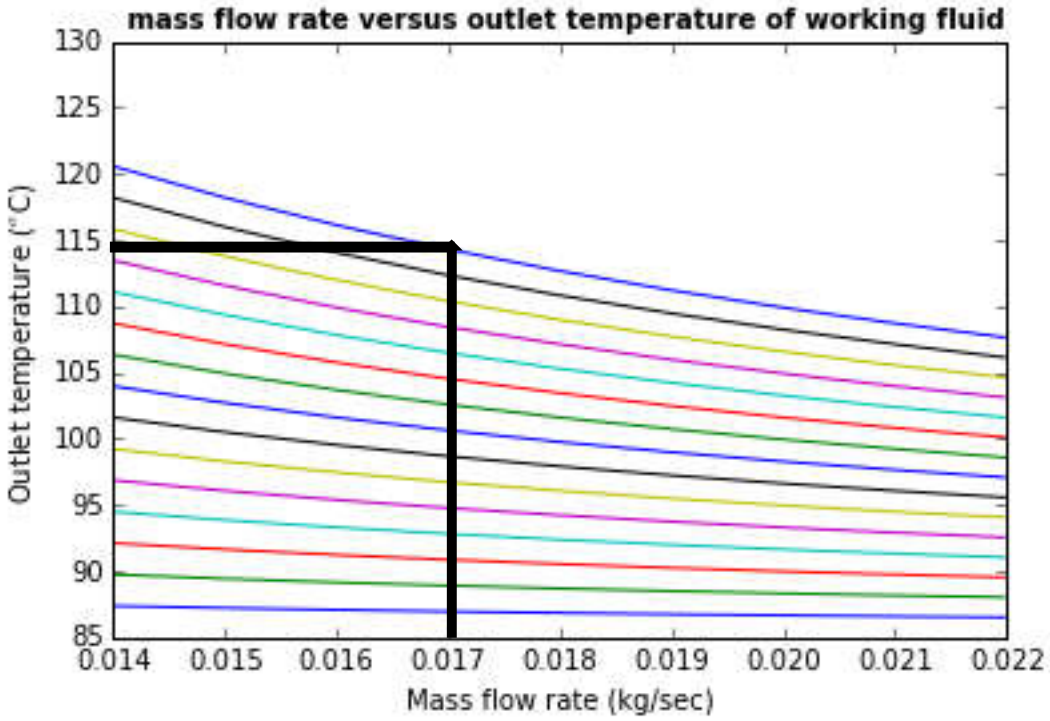

Figure 4. 8: Outlet temperature variation of the collector as a function of mass flow rate

4.4.2 Transient analysis of HPETC

Outer Glass Cover: the Transient heat balance equation of the outer glass cover is given by:

$$\frac{\rho_g V_g Cp_g \partial T_g}{\partial t} = I(t)A_g(1 - \tau) + \frac{(Tab - Tg)}{R_{w-g}} - \frac{(Tg - Ta)}{R_{g-a}} \quad \text{.....(4.34)}$$

Absorber Tube: the Transient heat energy balance equation of the absorber tube of HPETC is determined as:

$$\frac{\rho_{ab} V_{ab} Cp_{ab} \partial T_{ab}}{\partial t} = Ap * \tau\alpha * I(t) - \frac{(Tab - Tg)}{R_{w-g}} - \frac{(Tab - Tev)}{R_{hp}} \quad \text{.....(4.35)}$$

Evaporation Section: the Transient heat energy balance equation of saturated liquid of the

evacuated tubes heat pipe is determined as:

$$\frac{\rho_{ev} V_{ev} Cp_{ev}\, \partial T_{ev}}{\partial t} = \frac{(Tab - Tev)}{R_{evap+}\, R_{fin}} - \frac{(Tev - Tcond)}{R_{h,pipe}} \quad \text{(4.36)}$$

Condensation Section: the Transient heat energy balance equation of condensed liquid of evacuated tubes heat pipe is written as:

$$\frac{\rho_{cond} V_{cond} Cp_{cond}\, \partial T_{cond}}{\partial t} = \frac{(Tev - Tcond)}{R_{h,pipe}} - \frac{(Tc - Tw)}{R_{cond}} \quad \text{(4.37)}$$

Working fluid: The outlet temperature of the pressurized water in the manifold is calculated by:

$$\frac{\rho_w V_w Cp_w\, \partial T_w}{\partial t} = \frac{(Tc - Tw)}{R_{cond}} - \frac{\dot{m} Cp_w\, \partial T_w}{\partial x} \quad \text{(4.38)}$$

The explicit finite-difference method is proposed to solve the system of these equations. For each equation both the time and dimensional derivatives are replaced by a forward finite differencing scheme.

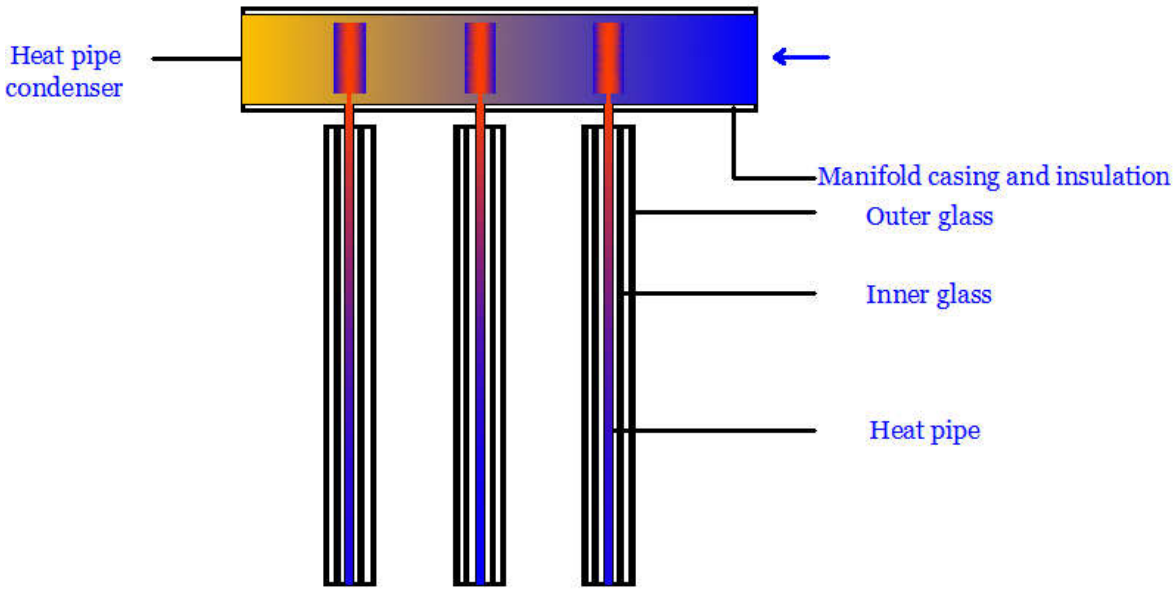

Figure 4.9: Evacuated heat pipe collector schematic

Based on the transient analysis of the energy balance equation, the outlet temperature of each element of the HPETC is obtained using discretization of Equation 4.34 to 4.38 with a one-second time step.

Outer glass cover:

$$\rho_g V_g Cp_g \frac{T_{g,i}^{k+1} - T_{g,i}^{k}}{\Delta t} = I(t)A_g(1 - \tau) + \frac{(T_{ab,i}^{k} - T_{g,i}^{k})}{R_{w-g}} - \frac{(T_{g,i}^{k} - Ta)}{R_{g-a}} \quad \text{(4.39)}$$

After some rearrangements

$$T_{g,i}^{k+1} = \left(A * I(t) + \left(\frac{1}{\Delta t} - (B + C)\right) T_{g,i}^{k} + B * T_{ab,i}^{k} + C * Ta\right) \Delta t \quad \text{(4.40)}$$

With the same principle as the outer glass cover the rest of the discretized equation can be evaluated as:

Absorber Tube:

$$T_{ab,i}^{k+1} = \left(D * I(t) + \left(\frac{1}{\Delta t} - (E + F)\right) T_{ab,i}^{k} + E * T_{g,i}^{k} + F * T_{eva,i}^{k}\right) \Delta t \quad \text{(4.41)}$$

Evaporation Section:

$$T_{ev,i}^{k+1} = \left(\left(\frac{1}{\Delta t} - (G + H)\right) T_{ev,i}^{k} + G * T_{ab,i}^{k} + H * T_{cond,i}^{k}\right) \Delta t \quad \text{(4.42)}$$

Condensation section:

$$T_{cond,i}^{k+1} = \left(\left(\frac{1}{\Delta t} - (I + J)\right) T_{cond,i}^{k} + I * T_{eva,i}^{k} + J * T_{w,i}^{k}\right) \Delta t \quad \text{(4.43)}$$

Working fluid:

$$T_{w,i}^{k+1} = \left(\left(\frac{1}{\Delta t} - (L + K)\right) T_{w,i}^{k} + K * T_{cond,i}^{k} - L * T_{w,i+1}^{k}\right) \Delta t \quad \text{(4.44)}$$

Where T is for temperature, t is the time, Δt is the time increment, Cp is for the specific heat capacity, ρ is for the density, α is the thermal absorptivity of plate, τ is the thermal transmissivity of the glass, ṁ is for the mass flow rate, and V is for the volume. The abbreviations g, ab, ev, cond, mani, and w are for the glass, absorber, evaporator, condenser, manifold and working fluid, respectively.

The outlet temperature of the working fluid from the collector is directly guided to the PCM or the generator based on the temperature of the outlet fluid from the collector.

In Equation 4.39 to 4.44:

$$A = \frac{A_g(1-\tau)}{\rho_g V_g Cp_g} \quad \text{(4.45)}$$

$$B = \frac{1}{\rho_g V_g Cp_g R_{w-g}} \quad \text{(4.46)}$$

$$C = \frac{1}{\rho_g V_g Cp_g R_{g-a}} \quad \text{(4.47)}$$

$$D = \frac{A_p \tau \alpha}{\rho_{ab} V_{ab} Cp_{ab}} \quad \text{(4.48)}$$

$$E = \frac{1}{\rho_{ab} V_{ab} Cp_{ab} R_{w-g}} \quad \text{(4.49)}$$

$$F = \frac{1}{\rho_{ab} V_{ab} Cp_{ab} R_{hp}} \quad \text{(4.50)}$$

$$G = \frac{1}{\rho_{ev} V_{ev} Cp_{ev} (R_{fin} + R_{evap})} \quad \text{(4.51)}$$

$$H = \frac{1}{\rho_{ev} V_{ev} Cp_{ev} R_{h,pipe}} \quad \text{(4.52)}$$

$$I = \frac{1}{\rho_{cond} V_{cond} Cp_{cond} R_{c,pipe}} \quad \text{(4.53)}$$

$$J = \frac{1}{\rho_{cond} V_{cond} Cp_{cond} R_{cond}} \quad \text{(4.54)}$$

$$K = \frac{1}{\rho_w Cp_w A_{mani} R_{cond}} \quad \text{(4.55)}$$

$$L = \frac{\dot{m} Cp_w}{\rho_w Cp_w A_{mani} \Delta x} \quad \text{(4.56)}$$

The simultaneous Equations 4.45 to 4.56 need an initial guess value to start the iteration for the PYTHON script. The initial temperature values for all elements in the above equation are guessed as follows:

$$T_{g,o} = T_{amb,o} \quad \text{(4.57)}$$

$$T_{ev,o} = T_{amb,1} \quad \text{(4.58)}$$

$$T_{cond,o} = T_{amb,2} \quad \text{(4.59)}$$

$$T_{w,o} = T_{amb,3} \quad \text{(4.60)}$$

Where $T_{amb,o}$, $T_{amb,1}$, $T_{amb,2}$ and $T_{amb,3}$ represents ambient temperature after 0,1,2 and 3 hours, respectively.

4.5. Results of HPETC analysis

4.5.1. Instantaneous Outlet temperature for the representative days

The instantaneous outlet temperature indicates that the exit temperature from the manifold depends on the irradiance on the surface. Figure 4. 10 shows outlet water temperature at tube element of i = 5, 10 and 20 for the representative day of each season of the first month. The outlet temperature

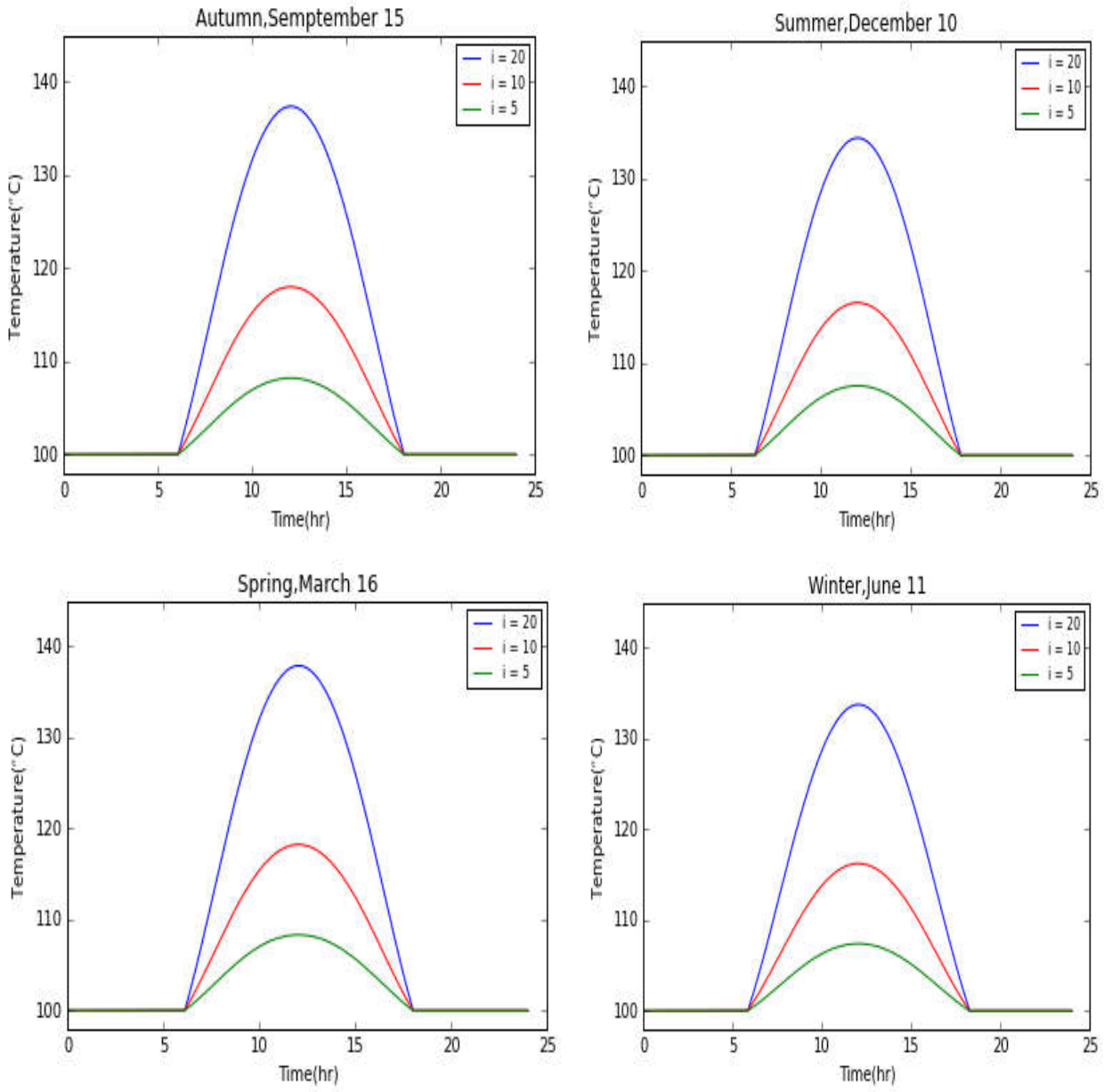

Figure 4. 10: Outlet temperature of HPETC for the representative day of each season of the first month

from the generator at 100°C is assumed for the instantaneous inlet water temperature to collector. The Figure shows that the outlet water temperature at the manifold has a downward parabolic shape for the day time, as the solar radiation incident to the surface has a parabolic with maximum at the noontime.

4.5.2. Instantaneous useful heat gained by HPETC

Instantaneous useful heat gained by a HPETC for each second interval from sunrise to sunset is calculated from the result found from outlet fluid temperature variation of HPETC, by multiplying the temperature rise of the heat transfer fluid to its mass flow rate, and specific heat capacity. The hourly average useful energy gain of a unit HPETC for the representative day of each season of the first month is presented in Figure 4.11.

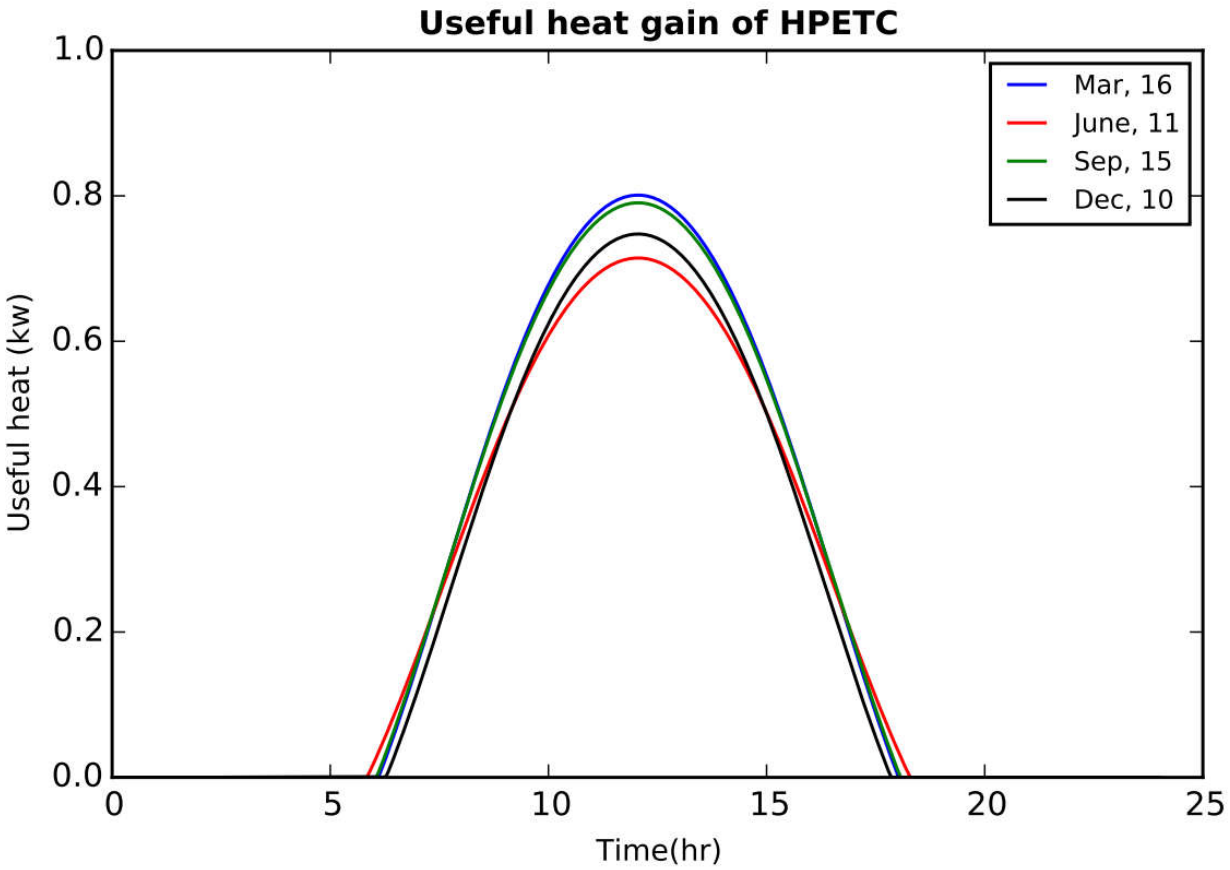

Figure 4.11: Instantaneous useful heat gained by a unit HPETC for the representative day of each season of the first month

4.5.2. Instantaneous Efficiency of HPETC

The instantaneous efficiency of HPETC depends on the amount of solar irradiance on the tilted surface .It is the ratio of useful heat gain of the collector to the instantaneous total amount of solar radiation incidence on the collector surface.

$$\eta_{ins} = \frac{Q_u}{I_T * A_b} \quad \text{..... (4.60)}$$

Where, Q_u is useful heat gain of the collector, I_T is radiation incident on the collector surface and A_b is absorber area of collector. Instantaneous efficiency for the representative day of each season of the first month is shown in Figure 4.12, from 8:00AM to 4:00PM. It can be easily understood from the graph that, whenever the incident radiation to the collector increases the efficiency of the collector will decrease, this is due to the increase in heat loss by radiation and convection from the collector.

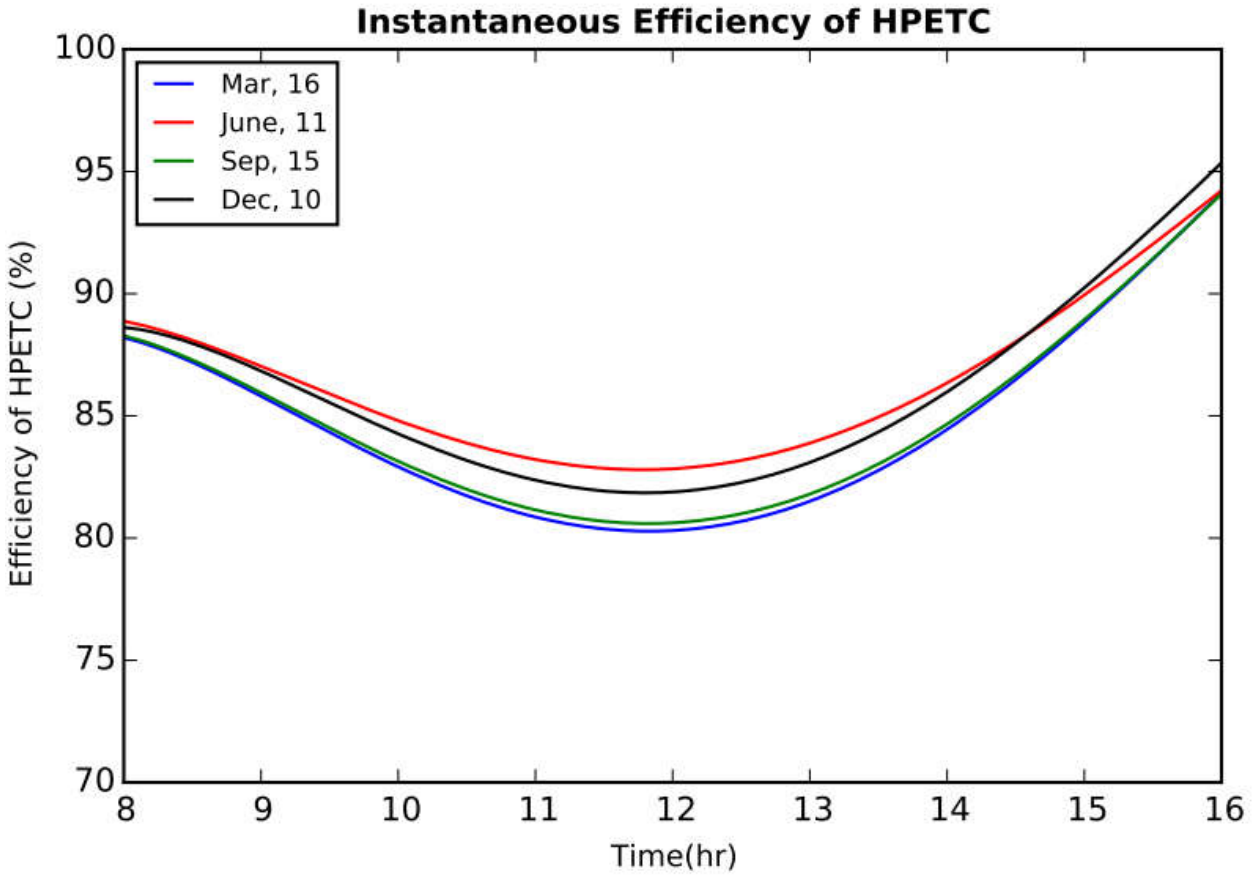

Figure 4. 12: Efficiency of HPETC for the representative day of each season of the first month

4.5.3. Collector arrangement and size determination

Collector arrangement

HPETC can be arranged in parallel, series, or series-parallel combination based on the required supply outlet temperature to the system, and mass flow rate through the manifold. In this study it is chosen to attain the maximum temperature with a single collector. So, all collectors for the respective application have to be arranged in parallel.

Size determination

The number of HPETC depend on the load requirement on the evaporator. Which is directly related to the heat load required on the generator and the amount of PCM required to store heat for night time use. The useful energy collected per day from a single HPETC is calculated by summing up the instantaneous heat gain of the collector for that day. Figure 4.13 is depict the total heat gain of a unit HPETC for the representative day of each season of the first month:

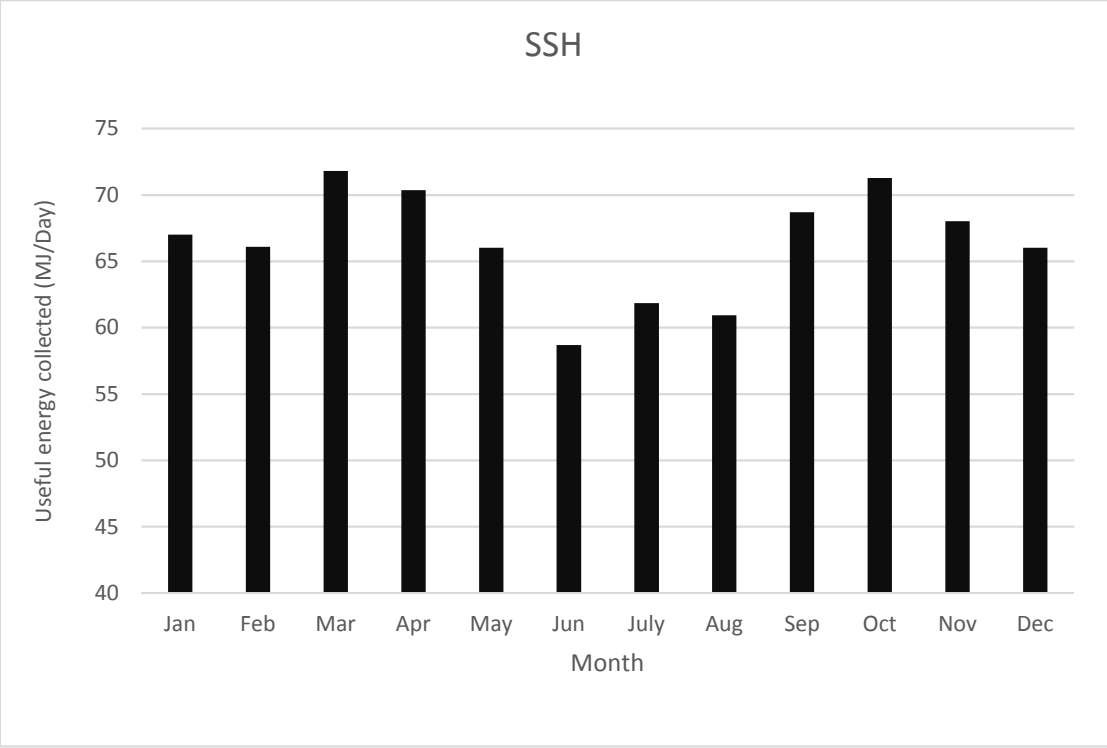

Figure 4. 13: Useful energy collected from a single HPETC for the representative day of each month

The average useful energy collected from a single HPETC throughout the year is 67.982 MJ/day. Thus the number of HPETC is calculated by knowing the heat load on the generator and the average useful energy collected per day, which is calculated by:

$$N = \frac{Q_g * 3600 * 24}{E_{ava}} \quad \text{..... (4.61)}$$

Where, Q_g heat load on generator and E_{ava} is average useful energy collected from a single HPETC.

CHAPTER 5: Thermal Performance Analysis of Thermal Storage System

5.1. Introduction

Thermal energy storage system is used to cater the time-dependent supply of solar energy, this is done by storing thermal energy during the sunshine hours. TES operates in three modes charging, discharging and standby mode. The charging and discharging mode occurs when there is a temperature difference between PCM and HTF. Whereas, the standby mode operation happen when both PCM and HTF are at the same temperature, during this time the hot water supply from the collector goes directly to the generator.

To analysis the unsteady one-dimensional heat transfer phenomena, the following assumption has been made:

- The flow is incompressible, laminar and axial.
- Average thermos-physical property of the PCM and HTF is taken.
- No heat loss to the environment so that the wall is perfectly insulated.
- PCM at the same layer have the same temperature and independent of radial position.
- PCM is packed orderly with the same shape.
- The tank is perfectly insulated
- No heat source due to radiation and internal heat generation considered.
- The temperature of the HTF at the entry of storage tank is equal to the exit temperature of HPETC

In this study, a phase change material (Erythritol) is encapsulated by spherical capsules. Erythritol is an organic PCM with a higher latent heat of fusion, from the list of material used in VARS. But, as Erythritol is organic PCM with low thermal conductivity a heat transfer enhancement is needed, to compensate the problem. Aspherical capsule with Aluminum as a capsule material is used to increase the heat transfer area. Encapsulated spherical phase change material is considered as identical and rectangular packed in a storage tank with porosity (ε), through which the heat transfer fluid (water) flows. The heat transfer fluid and the PCM are assumed to be initially at the same temperature. And, the packed bed column is divided into N elements with length to diameter ratio

of 1.5 (Regin et al., 2009), each containing phase-changing material capsules surrounded by heat transfer fluid. Thermo-physical property of Erythritol as per (Arefeh and Jinyue, 2011) is presented in Table 5.1:

Table 5. 1: Thermophysical property of Erythritol

Phase	Density (kg/m^3)	Thermal conductivity (W/m.K)	Specific heat capacity (kJ/kg.K)	Viscosity (kg/m s)	Latent heat of fusion kJ/kg.K
Solid	1480	0.326	1.38	0.02895	
Liquid	1300	0.733	2.76	0.01602	339.8

5.2. Thermodynamic analysis of PCM thermal storage system

The numerical modeling of PCM packed bed system can be divided into two groups: the single-phase model and the two-phase model. In the first group, the solid (the bed) and the fluid phase are considered as a single-phase, considering that the instantaneous temperature of both the solid and the fluid phases is the same. This model is useful in analyzing fixed beds of both high thermal conductivity and thermal capacity in comparison to the working fluid.

Regarding the two-phase models, solid and fluid phases are treated separately and the boundary between the solid-fluid interfaces is described by using Nusselt correlations (Gracia and Cabeza, 2012).

Three different typologies exist:

- The Schumann's model
- The continuous solid phase model
- The concentric dispersion model

The Schumann's model assumes one-dimensional heat transfer and considers heat conduction neither in the fluid nor in the solid phases. Whereas the concentric dispersion model considers conduction on both the fluid and the bed. In this study, the concentric dispersion model is used for the bed and the fluid. The coupled heat transfer concentric dispersion model for the fluid and the

bed are given in Equation 6.1, 6.2 and 6.3 by Gracia and Cabeza, (2012):

$$\varepsilon C_{pf}\rho_f\left(\frac{\partial T_f}{\partial t}+u\frac{\partial T_f}{\partial y}\right)=\varepsilon k_f\frac{\partial^2 T}{\partial y^2}+h_{PCM-HTF}(T_P-T_f)-U_L(T_f-T_{ENV}) \quad (5.1)$$

$$(1-\varepsilon)\rho_f\frac{\partial H}{\partial t}=(1-\varepsilon)k_{PCM}\frac{\partial^2 T}{\partial y^2}+h_{PCM-HTF}(T_f-T_{PCM}) \quad (5.2)$$

$$\rho_{PCM}\frac{\partial H}{\partial t}=\frac{1}{r^2}\frac{\partial}{\partial r}(k_{PCM}r^2\frac{\partial T}{\partial r}) \quad (5.3)$$

Where: ε is porosity of the tank given by $\varepsilon = V_{fluid}/V_{tank}$

C_{pf} = specific heat of the fluid (J/kgK)

ρ_f = density of the fluid (J/kgK)

T_f = fluid temperature (^oC)

T_P = PCM temperature (^oC)

H = Enthalpy of PCM (J/kg)

k_{PCM} = Thermal conductivity of PCM (W/mK)

k_{PCM} = Thermal conductivity of the PCM (W/mK)

$h_{PCM-HTF}$ = Overall heat transfer coefficient between the working fluid and PCM (W/mK)

U_L = heat loss coefficient from working fluid to the environment (W/mK)

The first and the second term to the left of Equation 5.1 represent the rate of stored energy in the control volume due to the variation in inlet temperature and the heat transfer due to the flow of the heat transfer fluid, respectively. Whereas, the three-terms to the right represents thermal conductivity of the fluid, the heat transfer between the PCM and the fluid, and the heat transfer between the bed and the environment, respectively.

The overall heat transfer coefficient between the fluid and PCM $h_{PCM-HTF}$ can be found after determining the Nusselt correlation (Nu) for the fluid-solid interface. One of the most used imperial correlation is the one provided by (Gracia and Cabeza, 2012):

$$Nu = 3.22 * R_e^{1/3} Pr^{1/3} + 117 \cdot Re^{0.8} Pr^{0.4} \quad (5.4)$$

Where, the Reynold's number is calculated using equation $Re = \frac{\rho_f d_p \varepsilon v_f}{\mu}$ and Pr is Prandtl number of HTF. Thus the overall heat transfer coefficient is given by:

$$h_{PCM-HTF} = \frac{Nu.\ k_f}{d_p} \quad (5.5)$$

Where, d_p is diameter of PCM.

The heat transfer in the axial direction of the layer is considered in the concentric dispersion model. Instead of using directly the thermal conductivity k_f of the fluid, some empirical correlation is suggested to determine the effective axial thermal conductivity of the fluid.

$$k_{eff,y} = 0.5 \cdot Re \cdot Pr \cdot k_f \quad (5.6)$$

Where, $k_{eff,y}$ is the axial effective thermal conductivity.

The low thermal conductivity of PCM affects the charging and discharging rate of the packed bed system. However, during the charging process natural convection in the liquid region enhance significantly the heat transfer rate. Thus, effective thermal conductivity value varies during the process as it does the Rayleigh number (Bellan *et al*., 2015). The effect of natural convection, when a phase change process from solid to liquid occurs, depend on the solid-liquid interface position which can be calculated by relating it to the effective thermal conductivity of PCM.

$$\frac{k_{eff,y}}{k_{liq.PCM}} = C\, Ra^m \quad (5.7)$$

Where, the coefficient C and m are 0.18 and 0.214, respectively.

The second part of the coupled concentric dispersion equations describe the governing equation of the PCM baked bed. The first term to the left of Equation 5.2 represent the stored enthalpy of the PCM, and the first and the second term to the write shows the axial conduction of the PCM and heat conduction between the fluid and the PCM, respectively. The last part of the coupled concentric dispersion equation represent enthalpy distribution inside the sphere due to the heat transfer by the working fluid, which is not the interest of this thesis.

Considering the two-equation, Equation 6.1 and 6.2, it can be fairly simplified by neglecting the axial thermal conduction of the PCM as a point to point contact is considered, and the heat loss to the environment by assuming the wall is insulated. The two equations will be reduced to:

$$\varepsilon C_{pf} \rho_f \left(\frac{\partial T_f}{\partial t} + u \frac{\partial T_f}{\partial y}\right) = \varepsilon k_f \frac{\partial^2 T}{\partial y^2} + h_{PCM-HTF}(T_{PCM} - T_f) \quad (5.8)$$

$$(1-\varepsilon)\rho_f \frac{\partial H}{\partial t} = h_{PCM-HTF}(T_f - T_{PCM}) \quad (5.9)$$

The energy equation for working fluid and the bed was discretized by applying the Finite Difference Method (FDM). The tank under consideration, filled with packed bed column, is

divided into a number of layers as shown in Figure 5.1, the square packing is assumed instead of rhombic to reduce the pressure drop.

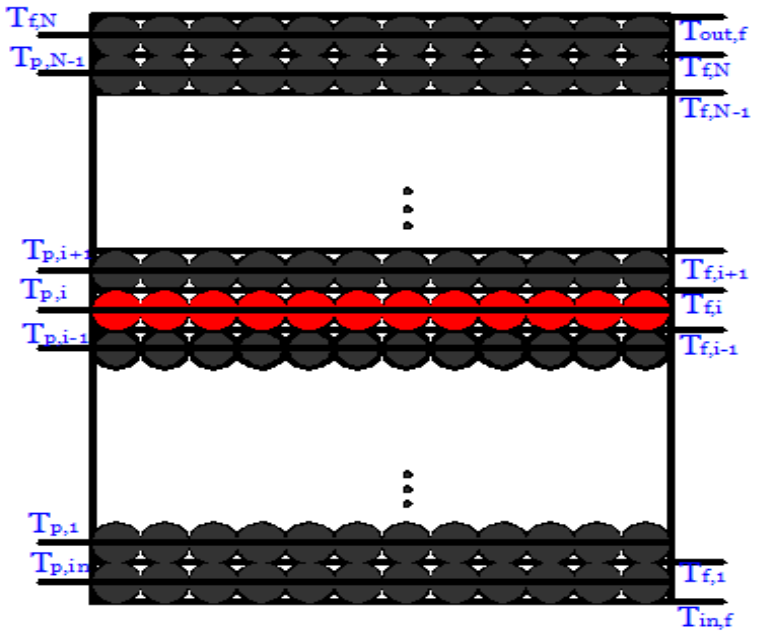

Figure 5. 1: PCM packed bed schematic

The time derivative is discretized using a fully explicit forward scheme. For the diffusion term second-order central differencing scheme is used, whereas for convection term the upwind differencing scheme is applied for the working fluid. The final discrete equation for HTF for all internal nodes gives:

$$\varepsilon C_{pf}\rho_f \frac{T_{f,i}^{k+1}-T_{f,i}^{k}}{\Delta t} + \varepsilon C_{pf}\rho_f v(T_{f,i+1}^{k} - T_{f,i}^{k}) = (\varepsilon k_f \frac{T_{f,i+1}^{k}-2T_{f,i}^{k}+T_{f,i-1}^{k}}{\Delta y}) + h_{PCM-HTF}(T_{i,P}^{k} - T_{f,i}^{k}) \quad \text{(5.10)}$$

Rearranging Equation 4.10 gives:

$$T_{f,i}^{k+1} = a_f(T_{f,i+1}^{k} - T_{f,i}^{k}) + b_f(T_{f,i+1}^{k} - 2T_{f,i}^{k} + T_{f,i-1}^{k}) + c_f(T_{i,PCM}^{k} - T_{f,i}^{k}) + T_{f,i}^{k} \quad \text{(5.11)}$$

In Equation 5.11,

$$a_f = \Delta t * v \quad \text{(5.12)}$$

$$b_f = \frac{k_f}{C_{pf}*\rho_f*\Delta y} \quad \text{(5.13)}$$

$$c_f = \frac{h_f}{\varepsilon C_{pf}\rho_f} \quad \text{..... (5.14)}$$

For the external nodes i = 1, and i = N of Equation 4.11, $T^k_{f,i-1}$ will be replaced by inlet fluid temperature T_{in} and $T^k_{f,i+1}$ will be replaced by exit fluid temperature (T_{ext}), respectively.

For the bed, the time derivative is discretized using a fully explicit forward difference scheme as shown below.

$$(1-\varepsilon)\rho_f \frac{H^{k+1}_{p,i} - H^k_{p,i}}{\Delta t} = h_{PCM-HTF}\left(T^k_P - T^k_f\right) \quad \text{..... (5.12)}$$

After some rearrangement

$$H^{k+1}_{p,i} = a_p\left(T^k_{i,PCM} - T^k_{i,f}\right) + H^k_{p,i} \quad \text{..... (5.13)}$$

Where, $a_p = h_f/(1-\varepsilon)\,\Delta\, t$

Using this equation, enthalpy of bed in the element at a particular time can be determined by using the known enthalpy values from the previous time. These equations are valid at all elements at a particular time.

Initial and boundary condition

Initial condition @ t = 0sec

$T_f = T_p = 100\ ^oC$, for $0 \le y \le H$

Boundary condition, t > 0sec

Axial coordinate (m)	Boundary condition
y = 0	$T_f = T_{in}$
y = 0	$\partial T_f/\partial y = 0$
y = 0	$\partial T_p/\partial y = 0$
y = H	$\partial T_f/\partial y = 0$
y = H	$\partial T_p/\partial y = 0$

5.3.1. Enthalpy- temperature relation of the packed bed unit

The enthalpy temperature relation for solid, solid-liquid and liquid state is coded on appendix B, an If –else statement is used to handle the relation. An algorism that shows the simulation is shown in Figure 5.2 below.

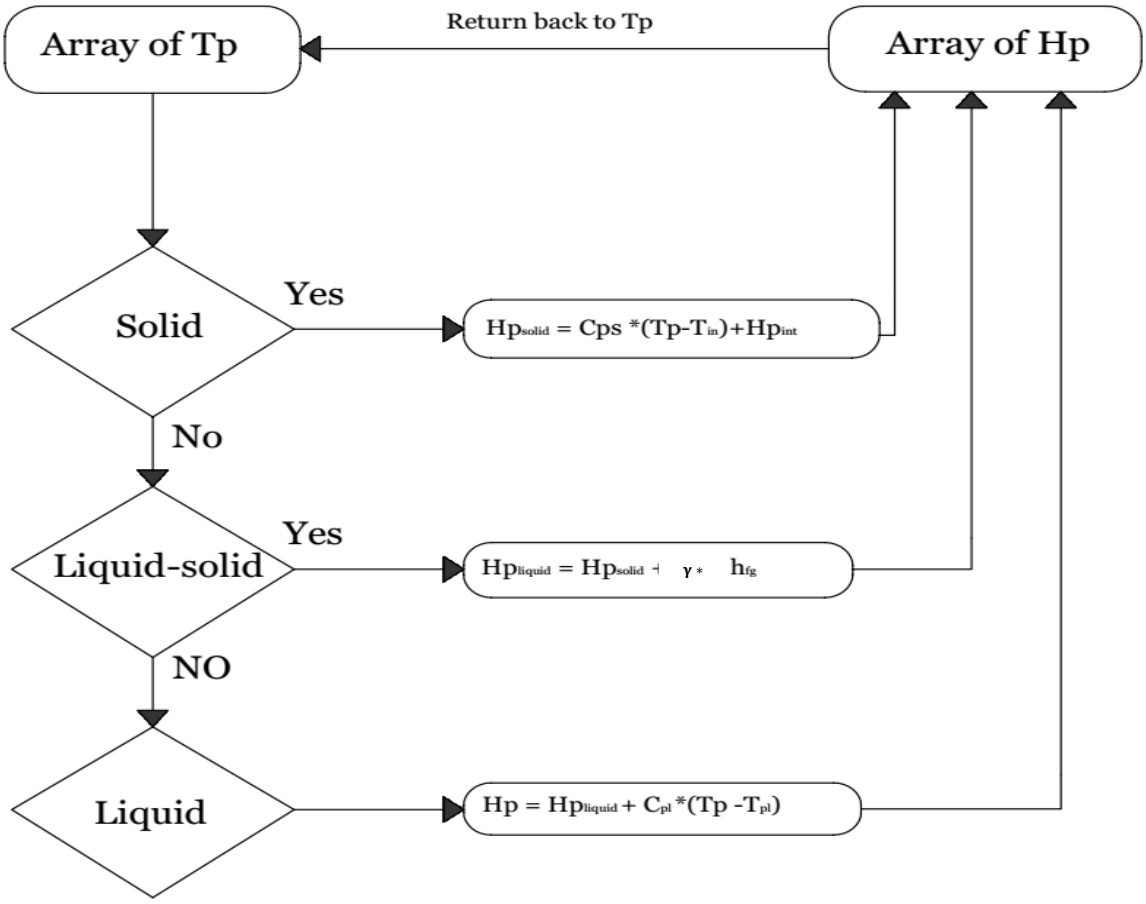

Figure 5. 1: Workflow of enthalpy- Temperature relation

Workflow for the relation of enthalpy and temperature

Where, Hp_{in} = enthalpy of PCM @ t = 0

Cps = specific enthalpy of the solid bed for $T_{in} < Tp < T_p$

Cpl = specific enthalpy for the working fluid, $T_p > T_{pl}$

Where, γ is the melt fraction of the phase changing material during the phase changing process, T_{pl} is liquid PCM temperature, and T_{ps} is solid PCM temperature. The melt fraction, at each element of the PCM domain is given by (Bellan *et al*., 2017):

$$\gamma = \begin{cases} 0 & \text{if } Tp < Tps \\ \frac{Tp-Tps}{Tpl-Tps} & \text{if } Tps \leq Tp \leq Tpl \\ 1 & \text{if } Tpl < Tp \end{cases} \quad \text{.....(5.14)}$$

Figure 5.3, shows the instantaneous temperature of the PCM layers for the full day round of March, 16 for the design of Bekas Chemical PLC. The figure shows, the charging and discharging time of the bed at 1, 10, 20 and N^{th} layer. The figure shows that the first layer of the bed is charged first and attain the maximum temperature from the other layers as the inlet temperature of the working fluid is higher. From the figure, one can see that the charging time of the bed is lower than the discharging time due to the natural convection heat transfer during the charging period as described in the model.

.

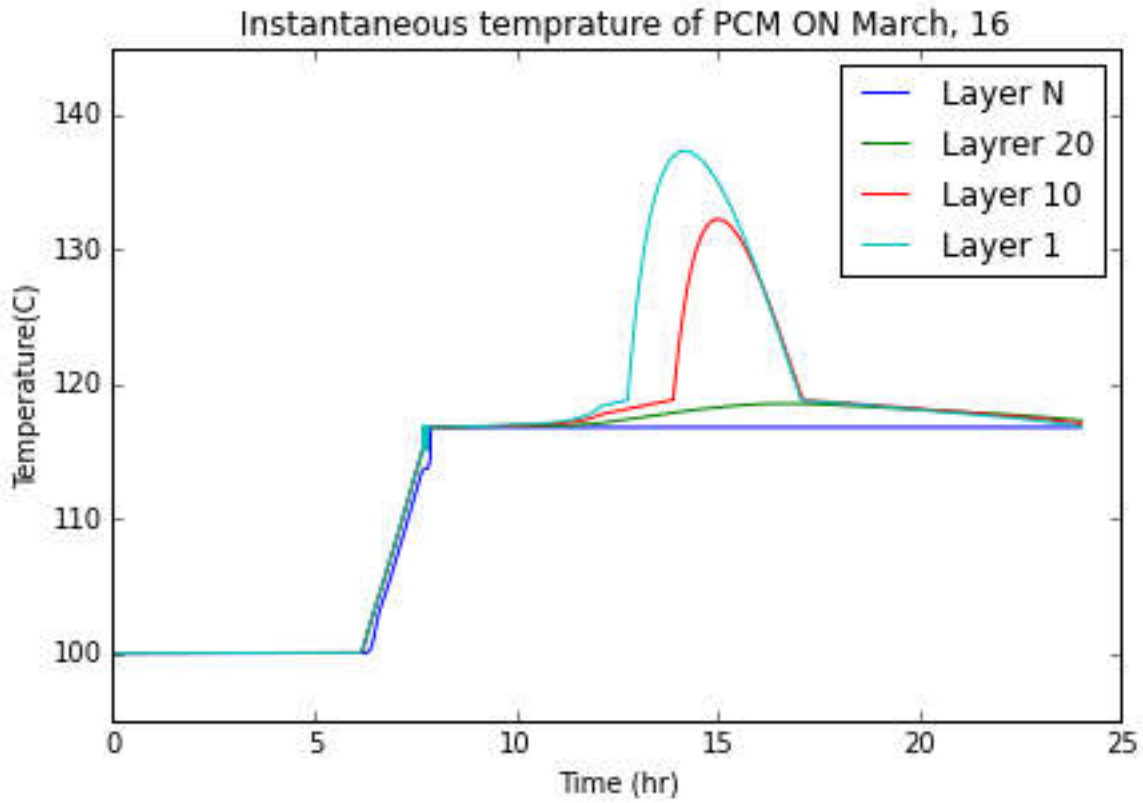

Figure 5. 2: Temperature variation of the PCM layer for the full day of March, 16

5.3. Model validation

The mentioned numerical method that has been solved using python computer code is validated against an experimental work done by Bellan *et al*., (2015). The authors studied the charging and discharging performance of spherically encapsulated phase change material (PCM, sodium nitrate) using high-temperature synthetic oil (Therminol 66) as a heat transfer fluid. In their investigation,

a cylindrical storage tank of length 1.5m and radius 0.352m is considered to study the charging and discharging performance of PCM for different scenarios. The case for capsule diameter of 0.03m and porosity 0.4694 with a HTF flow rate of $1m^3/h$ is used as a base to validate against the model.

For the charging mode, the initial temperature of HTF and PCM is considered as 256.8ºC and 365.8ºC, respectively. Whereas for the discharging mode, 256.8ºC and 365.8ºC temperature for PCM and HTF is taken. A unit second time step is used in the time range of 2 and 2.5 hr for the transient analysis of charging and discharging mode, respectively.

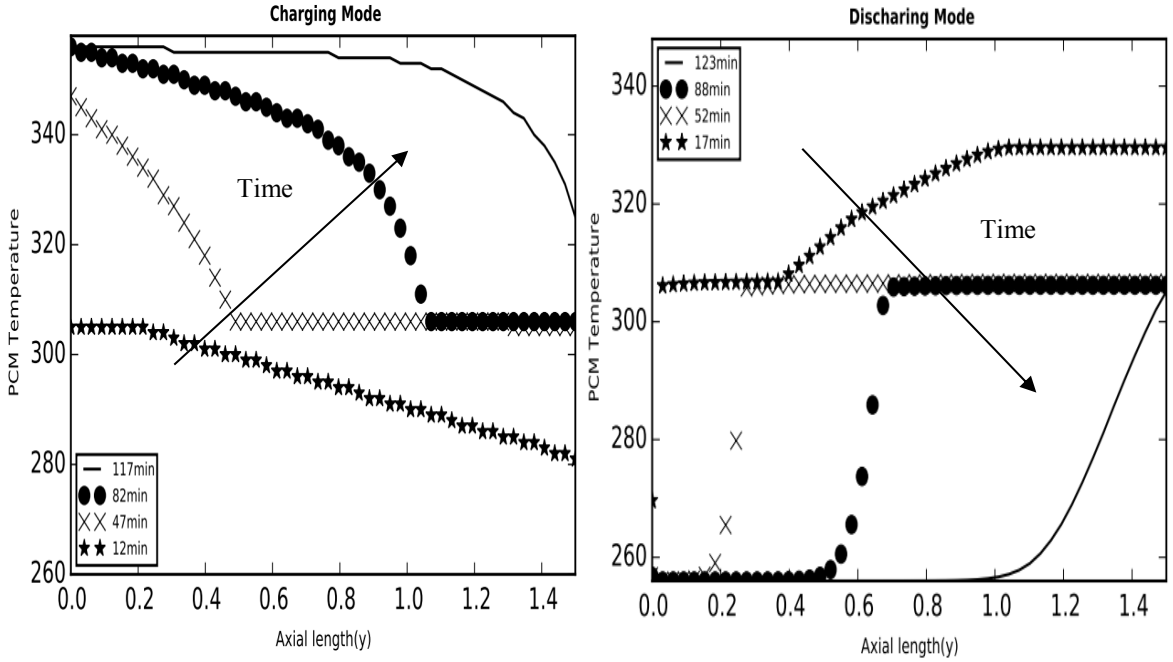

Figure 5. 3: Variation of PCM temperature for different time step and axial length (a) Charging mode and (b) Discharging mode

The abscissa in Figure 5.4 represent the axial length of the cylindrical shell. And, the two arrows on the graph show the charging and discharging time of the PCM. Figure 5.4 (a) represent the temperature distribution at each layer of PCM for charging mode. From the graph, at 117 min almost all layers are above the melting temperature of PCM. For the discharging process, one can see from Figure 5.4 (b) that at 17 min most of the PCM layers are in the liquid phase, after discharging for 123 min almost all of the layers are at HTF temperature.

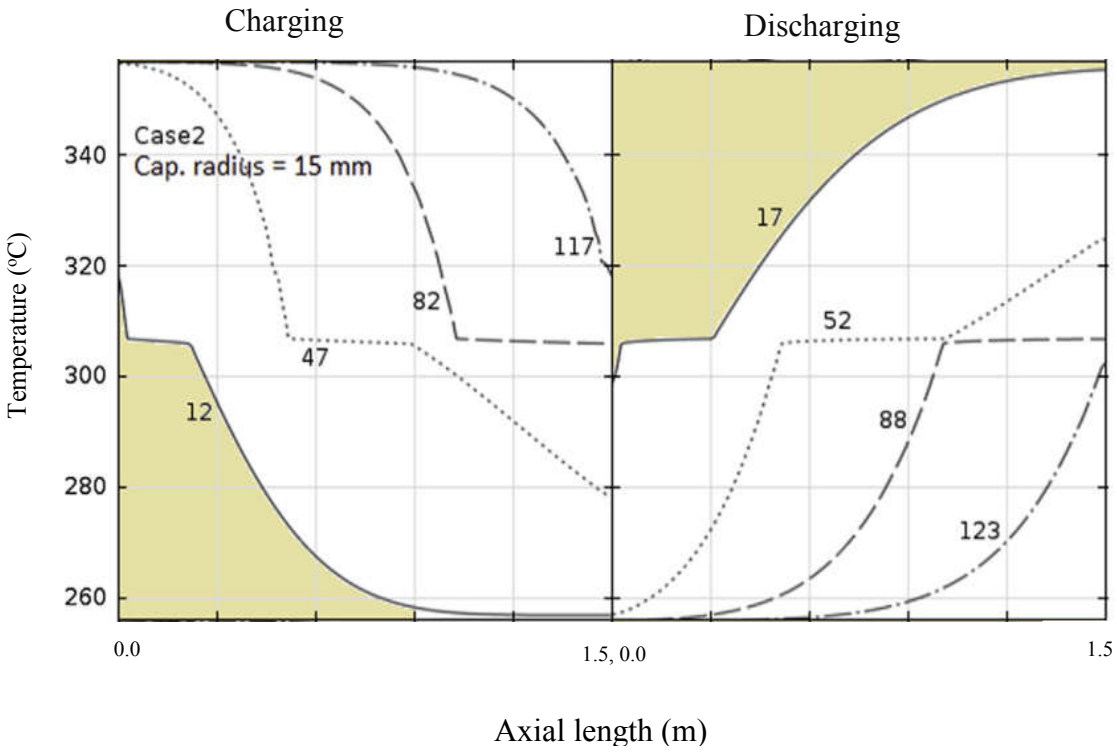

Figure 5. 4: PCM temperature distribution at the axial symmetry of the storage tank as a function of time (Bellan *et al*., 2015)

Comparing the model and the result of (Bellan *et al*., 2015) graph, there is a little variation on the charging and discharging time of PCM. This is due to a constant thermo-physical property is considered for the numerical model and neglecting the effect of heat loss to the atmosphere.

CHAPTER 6: Application on Bekas Chemical PLC and Ah-Wan Food Complex Industry

6.1. Introduction

In this chapter, the developed model on the previse chapters is applied for Bekas chemical PLC and Ah-Wan food complex industry. The selection of optimum generator temperature from the available evaporator, absorber and condenser temperature is done from the work of optimization by Pandya *et al.,* (2016). On their work, first and second law analysis, to determine the cut-off and optimum generator temperature required for the operating evaporator temperatures, is studied.

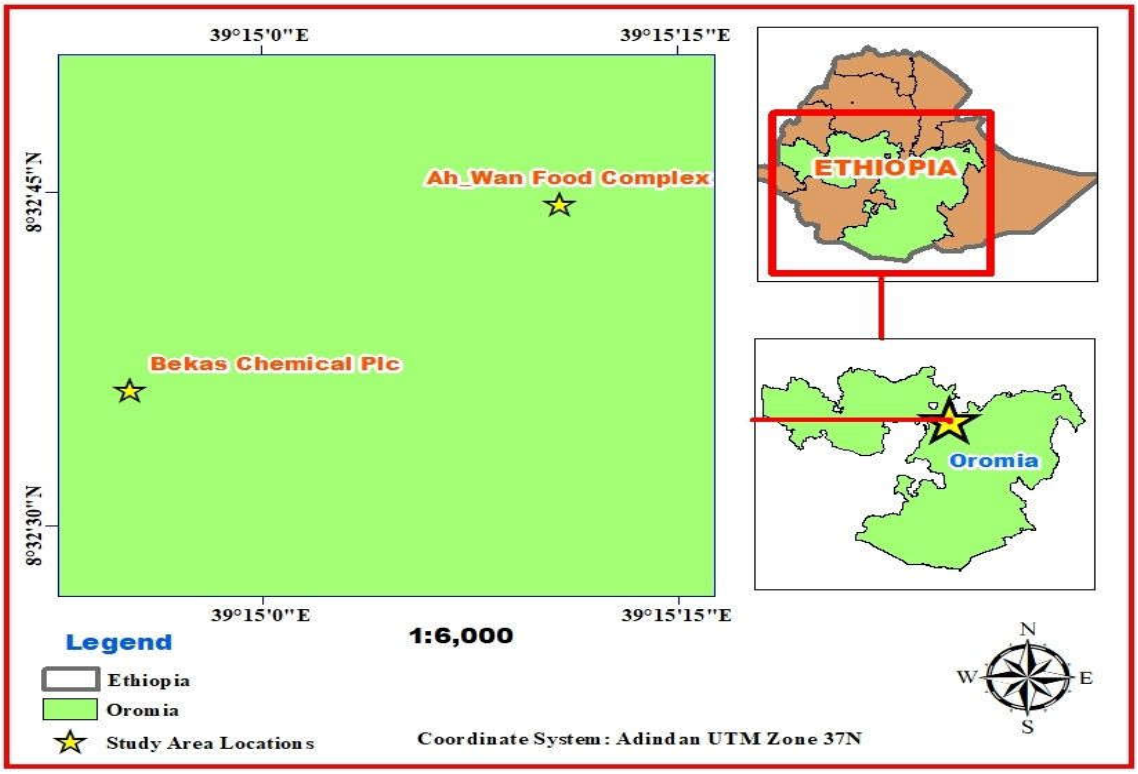

Figure 6. 1: Location of the study area

6.2. Bekas chemical PLC

Chiller is needed on the bottle and cup making section of the industry, this section needs chilled water to cool the hydraulic oil of blow molding and injection machines.

Figure 6. 2: Chiller temperature measurement in Bekas Chemical PLC

The chiller is comprised of the vapor compression machine, cooling tower, and the chilled water and cooling water tank. The working layout of the chiller is represented as shown in Figure 6.3 below. On the cooling water tank, hot water from hydraulic oil and cooled water from cooling tower will mixed. A part of the mixed water is poured to the condenser to exchange heat with the refrigerant, and some parts will return back to the hydraulic oil heat exchanger. Whereas, on the chilled water tank, chilled water from mold and evaporator mix. The temperature of each port is measured using a thermometer and the averaged results are:

Inlet chilled water to evaporator – 12 ^{o}C
Outlet chilled water from evaporator – 10 ^{o}C
Cooling water from Cooling Tower – 20 ^{o}C
Hot water from hydraulic oil – 30 ^{o}C
Hot water tank temperature – 23 ^{o}C

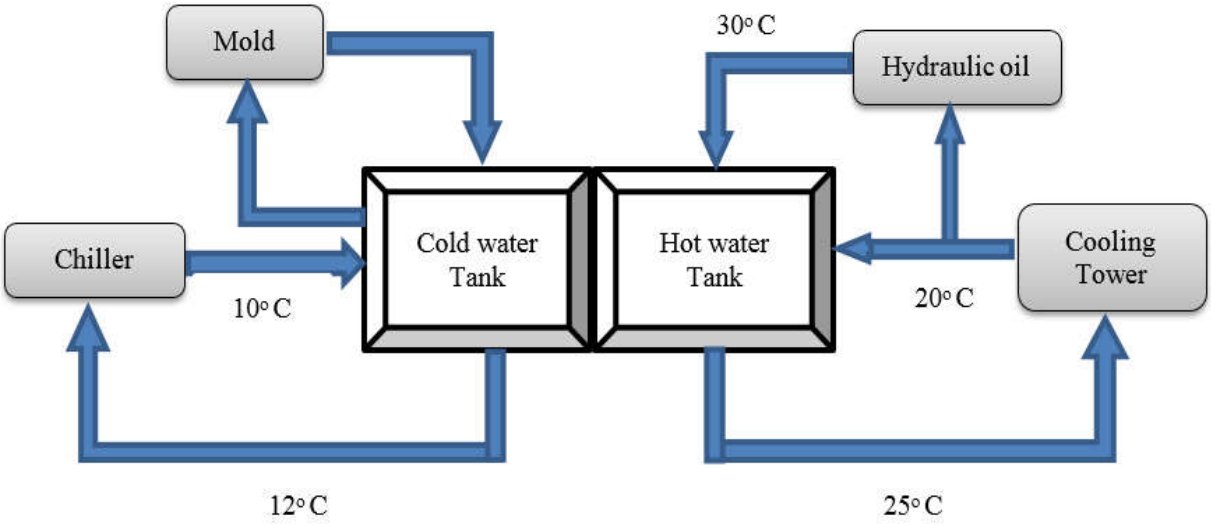

Figure 6. 3: Chilling process of Bekass Chemical PLC

6.3. Ah-Wan Food Complex

Average temperature, for the year 2018, of chilled water which cools the pasta product in the stabilizer and the cooling section is given in table 6.1:

Table 6. 1: Average chilled water temperature for the year 2018 of ahwan food complex inustry

Month	Jan	Feb	Mar	Apr	May	June	July	Aug	sep	Oct	Nov	Dec
Chilled water from chiller (°C)	17.5	17	18.7	17.4	19.7	18.7	17.4	19.3	18.4	17.4	18	18.3
Chilled water to chiller (°C)	21	20.7	21.6	22.6	22	21.3	22.3	20.6	21.3	22.3	22.4	20.3

From the data, the water temperature to the chiller is in the range of 20-23 °C and the water temperature from the chiller is in the range of 17-20 °C. The average temperature for the year, 2018 of the water temperature to and from the chiller is 18 and 21.5 °C, respectively. To remove the parasitic load of absorber and condenser, ambient temperature as a cooler is used for the modeled VARS.

6.4. Model implmentation

The intended purpose of this chapter is to develop a solar vapor absorption refrigeration system that can replace the existing conventional refrigeration system. To run the integrated simulation the following parameters have to be feed by the user as an input to the code.

Input ____(evaporator temperature)
Input ____(absorber temperature)
Input ____(condenser temperature)
Input ____(generator temperature)
Input ____(evaporator load)
Input ____(chilled water temperature from chiller)
Input ____(chilled water temperature to chiller)

The input parameters for Bekas chemical PLC and Ah-Wan food complex is depicted in Table 6.2:

Table 6. 2: Input values of Bekas chemical PLC and Ah-wan food complex

Input parameters	Bekas chemical PLC	Ah-Wan food complex
Evaporator temperature (°C)	6	10
Absorber temperature (°C)	33	33
Condenser temperature (°C)	38	38
Generator temperature (°C)	93	85
Chilled water temperature from chiller (°C)	10	18
Chilled water temperature to chiller (°C)	12	21.5
Evaporator load (kW)	186.66	245

Output simulated results from the single effect solar H_2O-LiBr vapor absorption refrigeration system are shown in the following Tables:

Table 6. 3: Mass flow rate, heat load and exergy destruction in each component

Description	Bekas chemical PLC	Ah-Wan food complex
Weak solution mass flow rate (kg/s)	0.427	0.571
Strong solution mass flow rate (kg/s)	0.348	0.467
Mass flow rate of cooling water (kg/sec)	3.628	4.638
Hot water mass flow rate to generator (kg/sec)	11.068	14.215
Evaporator load	186.66	245.00
Rate of heat rejected in the absorber (kW)	231.31	297.07
Rate of heat rejected in the Condenser (kW)	199.67	259.69
Rate of heat input in the Generator (kW)	244.33	311.76
Exergy of Evaporator (kW)	20.42	21.10
Exergy destruction in the Absorber (kW)	59.86	71.50
Condenser destruction in condenser (kW)	19.55	24.02
Exergy of Generator (kW)	105.64	102.491

Table 6. 4: Specifications for the component designs

Parameters	Bekas chemical PLC	Ah-Wan food complex
Specification of evaporator		
Overall heat transfer coefficient (W/m^2K)	9831.66	9271.68
Heat transfer area (m^2)	3.848	2.739
Length of tube per pass (m)	1.331	1.463
Specification of absorber		
Overall heat transfer coefficient (W/m^2K)	7488.67	8745.97
Heat transfer area (m^2)	4.282	4.708
Length of tube per pass (m)	1.331	1.463
Specification of condenser		
Overall heat transfer coefficient (W/m^2K)	1325.07	1360.10
Heat transfer area (m^2)	2.089	2.646
Length of tube per pass (m)	1.048	0.705
Specification of generator		
Overall heat transfer coefficient (W/m^2K)	8616.37	9968.93
Heat transfer area (m^2)	2.108	1.418
Length of tube per pass (m)	1.048	0.705
Specification of solution heat exchanger (SHX)		
Overall heat transfer coefficient (W/m^2K)	5070.86	6217.55
Heat transfer area (m^2)	0.219	0.255
Length of tube per pass (m)	1.048	0.705
Number of tubes	3	5
Specification of PCM and HPETC		
Number of HPETC required	242	310
PCM cylindrical shell height (m)	4.917	5.334
PCM cylindrical shell diameter (m)	3.278	3.556
Number of PCM Layers	98	106

CHAPTER 7: Conclusions and Recommendations

7.1. Conclusions

In this study, numerical Performance and design of single effect solar H_2O – LiBr VARS integrated with PCM (Erythritol) thermal storage system has been carried out. A mathematical model is developed based on mass, energy and exergetic equations, and the numerical results were validated by an experimental test against ET-480 absorption refrigeration system. The response of the system has been investigated by varying relevant parameters of the system.

From the results, it can be clearly dictated that with increasing generator temperature, strong solution concentration increase for constant refrigerant mass flow rate, cause to decrease circulation ratio. Therefore, COP of the system increase. Whereas, total second low-efficiency decrease due to the total exergy destruction increase as the generator temperature increase. In other case, increasing the evaporator temperature for a constant temperature input of generator has a positive effect on both the first and second law efficiency of the VARS as the load on the generator side decrease. From the result, it can also concluded that increasing condenser and absorber temperature have a negative impact on both COP and second law efficiency of the VARS.

For the latent heat storage, the coupled partial differential equations of the spherical PCM and the heat transfer fluid were numerically solved using the Finite Difference Method and the enthalpy approach. From the result, it is demonstrated that the time required to charge the PCM is lower than the discharging time. This is due to the natural convection inside the spherical capsule at phase transition state. The liquid part creates natural convection on the interface of the sphere, which is directly related to the amount of liquid phase inside the capsule.

From the transient analysis of HPETC, the outlet temperature and collector efficiency of heat pipe collector are somewhat higher than the competing flat plate collector. And, the result from the outlet temperature for each element shows that the failure of a single heat pipe element has a negligible effect on the performance of the whole collector. This is the advantage of HPETC over the others, as it is described in the literatures.

Lastly, the applicability of the model for Bekas Chemical PLC and Ah-Wan Food Complex is studied, with a chiller capacity of 186.66 kW and 245 kW, respectively. Each components of the absorption system is designed for both industries. The result show that 242 units of heat pipe evacuated tube collector with a storage tank size of 4.917m height and 3.278m diameter is demanded for Bekas Chemical PLC. Furthermore, on the same routine for Ah-Wan Food Complex, 310 units of evacuated tube collector with a storage tank size of 5.334m height and 3.556m diameter is needed to satisfy the heat demand with supply.

7.2. Recommendations

Solar-powered VARS offer a good opportunity to reduce electrical consumption, from the economic point of view. The system improve the application area of renewable energy resources, by increasing the scope of its utilization to combat the CO_2 emission. So, I urge that whenever new industries are installed, which are in need of a cooling process, to go for this refrigeration system. However, when this system is installed in the industry one have to consider the parasitic load in the absorber and condenser. To tackle this problem, I apprise the user to utilize the cooling water in a series arrangement from the environment. In this arrangement the cooling water acts as a heat sink through the absorber and condenser, and extract heat from both components. I also recommended that as solar energy is intermittent and unpredictable in nature, it is necessary to have an auxiliary heating source to sustain the operation of the system. This problem is getting worse during the summer season in Ethiopia, so a secondary heat source have to be a critical part of the design.

7.3. Future work

- Integrating PCM in another components other than generator such as evaporator, absorber, and condenser is a possible way to sustain the night time operation of solar VARS. The study by integrating in either of the three components or their combination is a possible future work.
- Thermo-physical property of PCM is taken as constant to simplify the study with the loss of some accuracy. The study by considering variable property is considered as another possible future work.

- The double and tipple effect absorption system is more efficient regarding both the first and second law efficiency. So, a study can be done on these two effects if a higher energy resource is available.
- Performance analysis and sizing of the vapor absorption refrigeration system are studied briefly in this thesis. But, Optimization of the VARS can be done for future work to have a better design.
- It is possible to pack PCM in a cylindrical manner, whenever the thermal conductance of the PCM is satisfactory, as such, a study can be done by packing the PCM in a cylindrical fashion.
- Effect of pump and expansion valve on thermodynamic analysis is neglected to simplify the study with a loss of some accuracy but, one can consider the effect for a better results for future work.
- The variation of temperature along the evaporation section of the heat pipe evacuated collector is neglected in this study, but it can also lead to some accuracy loss. Taking the temperature variation can lead to a better accuracy.

References

Abdalla, F., Tuohy, P., Evans, D. and Blackwell, P. (2018). A review of integrated phase change materials for the evacuated tube solar collector system. *International conference on energy research,* **1**: 340-365.

Abhishek, A. and Babu, M. (2015). Performance characteristics of single-effect lithium bromide/ water absorption chiller for small data. *The University of Texas at Arlington.*

Adel, A., Hany, M., Mohamed, S. and Adel, M. (2016). Performance analysis of evacuated tube collector in hot climate. *International Journal of science and technology,* **5**(3): 2304-9693.

Aman, S. and Pathak, A. (2016). Evacuated tube solar collector's importance and innovations in wide range applications. *International Journal of scientific and technical advancements,* **2**(4): 39-44.

Antonio, A., Carlos, J. and Recarte, J. (2014). Energy and exergy analysis of the performance of 10 TR lithium bromide/water absorption chiller. *A Review of technical engineering,* **37**(1): 38 - 47.

Arabkoohsar, A., Ismail, K., Machado, L. and Koury, R. (2016). Energy consumption minimization in an innovative hybrid power production station by employing PV and evacuated tube collector solar thermal systems. *Renewable energy*, **93**: 424-441.

Arefeh, H. and Jinyue, Y. (2011). CFD modeling of heat charging process in a direct-contact container for mobilized thermal energy storage.

Arora.C P. *Refrigeration and air conditioning*. Third edition.

Arun, K. and Shukla, S. (2015). A Review on thermal energy storage unit for solar thermal power plant Application. *Centre for energy and resources development***, 74**.

Ashutosh, S., Abhishek, G. and Gaurav, S. (2018). Performance investigation of evacuated tube solar Heating System. A review, *Journal of alternate energy sources and technologies*, **9**(3).

Ayompe, L. and Duffy, A. (2013). Thermal performance analysis of a solar water heating system with heat pipe evacuated tube collector using data from a field trial. *Solar energy*, **90**: 17-

28.

Bellan, S., Cordiviola, A., Barberis, S., Traverso, A., Aguila, J. and Romero, M. (2017). Numerical analysis of latent heat storage system with encapsulated phase change material in spherical capsules. *Renew. Energy Environ. Sustain*, **2**(3).

Bellan, S., Tanvir, E., Aguila, J., Romero, M., Rahman, M., Yogi, D. and Goswami, K. (2015). Numerical and experimental studies on heat transfer characteristics of thermal energy storage system packed with molten salt PCM capsules. *Applied thermal engineering*, 90: 970-979.

Bouzenadaa, S., McNevinb, C., Harrisonc, S., and Kaabid, A. (2016). "Performance of a liquid desiccant Air-conditioner driven by Evacuated- tube, Flat-plate, or Hybrid Solar thermal Arrays". *Energy and Buildings,* **4**: 256-267.

Castro, M., Vieira, R. and Biscaia, A. (2000). Automatic differentiation tools in the dynamic simulation of chemical engineering processes Braz.

Chow, T., Chan, L., Fong, K., Tan, R., and Dong, Z. (2011). Experimental study of evacuated-tube solar water heaters in Hong Kong. *Building energy and environmental technology research Unit*, **226**(1).

Dewitt, Bergman, and Lavine. *Fundamental of heat and mass transfer*. Six edition.

EE IIT, Kharagpur. *Refrigeration and Air conditioning*. Fourth edition.

Evangelos Bellos , Christos Tzivanidis, Kimon A. Antonopoulos exergetic, energetic and financial evaluation of a solar-driven absorption cooling system with various collector types. *Applied thermal engineering* (102) 2016: 749–759.

Falahatkar, A and M. KAssadi. (2011). Analysis of solar lithium bromide-water absorption cooling system with heat pipe solar collector. *World renewable energy Congress,* **1**: 25-40

Farzad, J., Emad, A and Hossein, A. (2016). Energy and exergy efficiency of heat pipe evacuated tube solar collectors. *Thermal Science*, **20**(1): 327-335.

François, B., Hélène, D., Joël, W., Xavier, J., David, C. and Philippe, P. (2012). Development of a 5 kW cooling capacity ammonia-water absorption chiller for solar cooling applications. *Energy Procedia,* **30**: 35 – 43.

Goswami, D., Elias, K. and David, C. (2014). Numerical analysis of charging and discharging performance of a thermal energy storage system with encapsulated phase change material. *Applied thermal engineering,* **71**: 481-500.

Gustavo. C., Karina, F., Macarena, M., Krzyszt., N. and Anna, D (2017). Encapsulated Nitrates phase change material selection for use as thermal storage and heat transfer materials at high temperature in concentrated solar power plants. A review*, Energies,* **10**.

Hosseini, A., Infante, F. and Engel, V. (2011). Design and Analysis of a solar assisted absorption cooling system integrated with latent heat storage.

http://en.sunrain.com/SolarCollector/Heat-pipe-collector-R1.shtml

http://www.mingyangsolar.com/en/index.php/index/show/id/48.html

https://www.buffalopumps.com/products/absorption-pumps/

Jafarkazemi, F and Abdi, H. (2012). Evacuated tube solar heat pipe collector model and associated tests. *Journal of renewable and sustainable energy*, **4**(2): 1941-7012.

Jerko, M., Joan, C. and Alberto, C (2012). Review on absorption technology with emphasis on small capacity absorption machines. *University of Belgrade, Serbia*.

Jones, W. *Air Conditioning Engineering.* Fourth Edition.

Josef B (2012). Modeling and design of a latent heat thermal storage system with reference to thermal solar absorption refrigeration.

Kakac, S. and Liu, H. Heat exchanger selection, rating, and thermal design. Second edition.

Kalogirou, S., Florides, G., Tassou, S. and Wrobel, L. (2001). Design and Construction of a Lithium Bromide Water Absorption Refrigerator. *World Congress*, **5**(3).

Kim, D. and Infante, F. (2006). A Gibbs energy equation for LiBr aqueous solutions. *International Journal of Refrigeration,* (**29**): 36–46.

Kondakkagari, D., Pathi, V. and Tupakula, R. (2014). Parametric Study on Phase Change Material Based Thermal Energy Storage System. *Energy and Power Engineering,* **6**.

Kunal, B., Sandip. K. and Saha. A. (2016). Numerical analysis of latent heat thermal energy storage using encapsulated phase change material for solar thermal power plant. *Journals of renewable energy,* **95**: 323-336.

Lee, S. and Sherif, S. (2001). Thermodynamic analysis of a lithium bromide/water absorption system for cooling and heating applications. *International journal of energy research*, **25**: 1019-1031.

Lingayat, B. and Suple, Y. (2013). Review on phase change material as thermal energy Storage Medium. *International Journal of science and technology,* **3**(4).

Meenakshi. R., Reddy, N., Nallusamy, A and Hemachandra, K. (2012). Experimental studies on phase change material-based thermal energy storage system for solar water heating. *Journal of fundamentals of renewable energy and applications*, **2**: 47 – 57.

Mohamed, H., Mohamed, E., Osama, S. and Wael. A (2017). An experimental evaluation of direct flow evacuated tube solar collector integrated with phase change material. Journals of science direct, **139**: 1111-1125.

Mohammed, M., Khana, R. and Fahad, A. (2017). A review for phase change materials (PCMs) in solar absorption Refrigeration systems. *Renewable and sustainable energy reviews*, **76**:105-137.

Muthukumar, P. and Hakeem, N (2018). Comparison of thermal characteristics of sensible and latent heat storage materials encapsulated in different capsule configurations. *Concentrated solar thermal energy technologies*, **1**: 978-981.

Nallusamy, N., Sampath, S. and Velraj, R. (2006). Study on performance of a packed bed latent heat thermal energy storage unit integrated with solar water heating system. *Zhejiang Univ Science*, **7** (8): 1422-1430.

Pandya, B., Patel, J. and Anurag Mudgal (2017). Thermodynamic Evaluation of Generator Temperature in LiBrWater Absorption System for Optimal Performance. *Renewable Energy,* **109**: 270 – 278.

Ponshanmugakumar, A., Deepak, P., Sivaraman, H. and Vignesh, K. (2015). Numerical investigation on vertical generator integrated with phase change materials in the vapor absorption refrigeration system. *Appl Mech Mater,* **1**: 468-473.

Qarnia, E. (2009). Numerical analysis of a coupled solar collector latent heat storage unit using various phase change materials for heating the water. *Energy conversion and management,*

50.

Raghurajsinh, B. and Kedar. B (2016). Performance of an evacuated tube collector with heat pipe technology. *International Journal of engineering research and general Science,* **4**(3): 114-135.

Raja, B., Srikanth, V. and Raju, V. (2016). Thermodynamic analysis of single effect LiBr- water vapor absorption refrigeration system. *International Journal of science, engineering and technology research,* **5**(11): 450-467.

Reynaldo, P., Gonzales, R. and Nebra, S. (2010). Exergy calculation of lithium bromide–water solution and its application in the exergetic evaluation of absorption refrigeration systems LiBr-H2O. *International Journal of energy research*, 1.

Sabiha. M., Saidur, R., Mekhilef, S. and Omid Mahian. (2015). Progress and latest developments of evacuated tube solar collectors. *Renewable and sustainable energy reviews,* **51**:1038-1054.

Shobo, A. and Mawire, A. (2015). Numerical investigation of a packed bed thermal energy storage system for solar cooking using encapsulated phase change material. *Third southern African solar energy Conference*.

Srikhirin, P., Aphornratana, S. and Chungpa, S. (2001). A review of absorption refrigeration technologies. *Renewable and sustainable energy reviews,* **5**: 343–372.

Tiwari, G., Arvind, T. and Shyam, A. Handbook of Solar Energy Theory, Analysis and Applications.

Tong, Y., Kim, H. and Cho, H. (2016). Theoretical investigation of the thermal performance of evacuated heat pipe solar collector with optimum tilt angle under various operating conditions. *Journal of Mechanical Science and technology* **30**(2): 903-913.

Vaclav, N., Vaclav, V., Jakub, M. and Michal, K. (2017). Possibilities of water-lithium bromide absorption power cycles for low temperature, low power, and combined power and cooling systems. *Energy Procedia* **1**: 000–000.

Yunus, A. Çengel. and Michael, A. Boles. *Thermodynamics: An Engineering Approach*. Fifth edition.

Zbysław, P. (2011). Evacuated tubular or classical flat plate solar collectors. *Journal of power technologies*, **19**(3): 158–164.

APPENDIX

ANNEX A: Thermophysical property of LiBr - H_2O solution

The empirical equation of density, specific heat, enthalpy, temperature, concentration and vapor pressure of the H_2O - LiBr solution is given by the ASHRAE handbook, (2009) are used.

I. Density of LiBr solution

Range 20 % < x < 60 %

T = solution temperature (^{0}c), 0 < T < 200 ^{0}C

ρ_x =LiBr solution density (kg/m^3)

x_0 =x/100

$\rho_x = 1145.36 + 470.84x_0 + 1374.79x_0^2 - (0.33339+0.571749x_0)(273+T)$

II. Specific heat of LiBr solution

x = %LiBr

C_p = specific heat of LiBr solution (J/kgk)

$C_p = 0.0976x^2 - 37.512x + 3825.4$

III. Saturated water vapour enthalpy

hg = vapor enthalpy (kJ/kg)

T = temperature (^{0}C)

$hg = -0.00125397T^2 + 1.88060937T + 2500.559$

IV. Latent heat of condensation of water vapour

hg = latent heat of condensation (kJ/kg)

T = saturation temperature (^{0}C)

$hg = -0.00132635T^2 + 2.29983657T + 2500.43063$

V. LiBr solution and refrigerant pressure and temperature

Range 45 %< x <70 %LiBr

T_{sol} = solution temperature (^{0}c).range $5<T_{sol}<175^0$c

T_{ref} = refrigerant saturated temperature (^{0}c).range $-15<T_{ref}<110^0$c

P = saturation pressure (kPa)

A_0 = -2.00755, A_1 = 0.16796, A_2 = -0.003133362, A_3 = 0.0000197668

B_0 = 124.937, B_1 = -7.71649, B_2 = 0.152286, B_3 = -0.0007959

$\sum A = A_0x^0 + A_1x^1 + A_2x^2 + A_3x^3$

$\sum B = B_0x^0 + B_1x^1 + B_2x^2 + B_3x^3$

C = 7.05, D = -1596.49, E = -104095.5

$LogP = C + D/(T_{ref} + 273) + E/(T_{ref} + 273)^2$

$T_{ref} = (-2E/(D + [D^2 - 4E(C - logP)]^{0.5})) - 273$

$T_{sol} = \sum B + T_{ref} \sum A$

VI. Enthalpy of LiBr solution

Range 45 %< x <70 %LiBr

T = solution temperature (^{0}c)

h = enthalpy (k/kg)

Solution temperature range 15 ^{0}C<T<165 ^{0}C

A_0 = -2024.33, A1 = 163.309, A2 = -4.88161, A_3 = 0.06302948, A_4 = -0.0002913704

B_0 = 18.2829, B_1 = -1.1691757, B_2 = 0.03248041, B_3 = -0.0004034181, B_4 = 0.0000018520569

C_0 = -0.037008214, C_2 = -0.000081313015, C_1 = 0.0028877666, C_3 = 0.00000099116628

C_4 = -0.0000000044441207

$\sum A = A_0x^0 + A_1x^1 + A_2x^2 + A_3x^3 + A_4x^4$

$\sum B = B_0x^0 + B_1x^1 + B_2x^2 + B_3x^3 + B_4x^4$

$\sum C = C_0x^0 + C_1x^1 + C_2x^2 + C_3x^3 + C_4x^4$

$h = \sum A + T\sum B + T^2\sum C$

ANNEX B: Python program of Single effect water/LiBr VARS

```
# -*- coding: utf-8 -*-
  """
Created on Tue Jun 18 12:19:55 2019

This code is developed to solve the thermal performance and design of a water/LiBr VARS for variable load requirement and temperature input of each component. As the study is mainly focused on single-effect water/LiBr VARS, the whole design is based in the limiting cause for a single effect LiBr solution. In this study the solution of refrigerant (water) and absorber (LiBr) stream flows through the shell side of the vessel and, the cooling water and hot pressurized water stream flow through the tube as per Twin drum type is considered.

@author: Natnale Sitotaw
"""
from scipy import *
from numpy import *
from pylab import *
from iapws import IAPWS95
Te = int(input('Enter evaporator temperature ')) # prompt users to enter evaporator temperature.
Tg = int(input('Enter generator temperature '))  # prompt users to enter generator temperature
Ta = int(input('Enter absorber temperature '))   # prompt users to enter absorber temperature
Tc = int(input('Enter condenser temperature '))  # prompt users to enter condenser temperature
Qe = int(input('Enter evaporator Load in kw '))  # prompt users to enter evaporator load
```

```
Tchill_in = int(input('Enter inlet chilled water temperature ')) #
prompt users to enter Tchill_in temperature
Tchill_out = int(input('Enter outlet chilled water temperature '))#
prompt users to enter Tchill_out temperature

if Te <3 or Te>20:
    print ('your input for evaporator temperature is wrong, please
input the correct value and run it again or')
    sys.exit(0)
else:
    Te = Te
if Tg <75 or Tg>110:
    print ('your input for generator temperature is wrong, please
input the correct value and run it again or')
    sys.exit(0)
else:
    Tg = Tg
if Ta <30 or Ta>40:
    print ('your input for absorber temperature is wrong, please input
the correct value and run it again or')
    sys.exit(0)
else:
    Ta = Ta
if Tc <35 or Tc>45:
    print ('your input for condenser temperature is wrong, please
input the correct value and run it again or')
    sys.exit(0)
else:
    Tc = Tc
if Qe <5 or Qe>200:
```

```
    print ('your input for heat load is wrong, please input the
correct value and run it again or')
    sys.exit(0)
else:
    Qe = Qe
evap=IAPWS95(T=Te+273.14, x=0)        #Take thermo-physical properties
of liquid water #@Te from iapws library
cond =IAPWS95(T=Tc+273.14, x=0)       #Take thermos-physical property
of Liquid water @Tc from iapws library
absor =IAPWS95(T=Ta+273.14, x=0)      #Take thermos-physical property
of liquid water @Ta from iapws library
gener =IAPWS95(T=Tg+273.14, x=0)      #Take thermos-physical property
of liquid water @Tg from iapws library
evap_v=IAPWS95(T=Te+273.14, x=1)      #Take thermos-physical property
of saturated vapor @Te from iapws library
cond_v =IAPWS95(T=Tc+273.14, x=1)     #Take thermos-physical property
of saturated @vapor @Tc from iapws library
absor_v =IAPWS95(T=Ta+273.14, x=1)    #Take thermos-physical property
of saturated vapor @Ta from iapws library
gener_v =IAPWS95(T=Tg+273.14, x=1)    #Take thermos-physical property
of saturated vapor @Tg from iapws library
##Density of water_LiBr solution as per Ashrae
def density(T,x):
    x = x/100
    Den  = 1145.36 + 470.84*x +1374.79*x**2 -
(0.33339 + 0.571749*x)*(273+T)
    return Den
##Entropy of water
def water(T):
    To  = 273.14
```

```
    T    = T+273.14
    d    = [11.97,-0.0183,2.87*10**(-5)]
    e    = [0.00266,-3.865*10**(-6),7.4648*10**(-9)]
    s_H2O =R*(d[0]*np.log(T/To)+d[1]*(T-To)+d[2]*(T**2-To**2)/2)-
R*(e[1]+2*e[2]*T)*(p-po)
    s_H2O =s_H2O/18.02
    return s_H2O
## Entropy of LiBr solution
def entropy(x,T):
    v = 2                       # dissociation number ( 2 for LiBr)
    R = 8.314                   # universal gas constant
    p = 7000                    #pressure
    po = 610.8                  # saturation pressure @ T =0C
    M_liBr = 86.85              # Molar mass of LiBr
    M_H20 = 18.02               # Molar mass of water
    To = 273.15
    Y_H20 =(1-x)*M_liBr/((1-x)*M_liBr+x*M_H20) #mole fraction of water
    Y_liBr = 1-Y_H20                           #mole fraction of LiBr
    Msol =Y_liBr*M_liBr+Y_H20*M_H20            #molar mass of
water_LiBr mixture
    m = x/((1-x)*M_liBr)                       #molality of solvent
    mo = 0.001                #standard molality of solvent @ standard
##Temperature and Pressure
   a = [[-21.96,4937.23,-655480],[-3810.475,2611535,-
3.6699691*10**8],[122808,-      77187923,1.039856*10**10],[-
1471674,9.1952848*10**8,-1.1894502*10**11],[7765821,-
4.937566*10**9,6.317554*10**11],[-15118920,9.839997*10**9,-
1.273789*10**12]]
    b = [[-4.41786*10**(-5),0.03115,-4.3611],[3.074*10**(-4),-
0.1863,27.38],[-4.08*10**(-4),0.216,-25.17]]
```

```
    c = [-9.44*10**5,-5.8423*10**8,0]
    d = [11.97,-0.0183,2.87*10**(-5)]
    e = [0.00266,-3.865*10**(-6),7.4648*10**(-9)]#regression constants
    def aa(i):
        x = a[i-1][0]+(a[i-1][1]/T)+(a[i-1][2]/T**2)
        return x
    def bb(i):
        if i<3:
            x = b[i][0]+(b[i-1][1]/T)+(b[i][2]/T**2)
        else:
            x = 0
        return x
    def aaa(i):
        x = -(a[i-1][1]/T**2)-2*(a[i-1][2]/T**3)
        return x
    def bbb(i):
        if i<3:
            x = -(b[i][1]/T**2)-2*(b[i][2]/T**3)
        else:
            x = 0
        return x
    sum = 0
    for i in range (1,7):
        sum = sum
+Y_liBr*v*R*(aa(i)+(i*bb(i)/(2*v))*p+T*(aaa(i)+(i*bbb(i)/(2*v))*p))*m*
*(0.5*i)
    T =T+273.14
    s_liBr = 47.556 - R*((c[0]*(1/T**2 -1/To**2))/2+(c[1]*(1/T**3 -
1/To**3))/3)+(c[2]*(1/T**4 -1/To**4))/4-R*(b[0][0]-(b[0][2])/T**2)*(p-
po)                              #Molar entropy of pure LiBr
```

```
    s_H2O = R*(d[0]*np.log(T/To)+d[1]*(T-To)+d[2]*(T**2-To**2)/2)-
R*(e[1]+2*e[2]*T)*(p-po)         #molar entropy of pure water
    s =(Y_liBr*s_liBr+(1-Y_liBr)*s_H2O - Y_liBr*v*R*(np.log(m/mo)-
1)+sum)                          # molar entropy of water LiBr solution
    s = s/Msol                   #Entropy of LiBr solution
    return s
```

Specific heat of LiBr solution as per Ashrae

```
def Cp_LiBr(T,x):
    Cp = 0.0976*x**2 -37.512*x + 3825.4
    return Cp
```

Latent heat of vaporization of water as per Ashrae

```
def hg_super(T):
    hg = 1.88*T + 2501
    return hg
```

##Saturated water vapor enthalpy as per Ashrae

```
def hg_vapor (T):
    hg  = (-0.00125397*T**2 + 1.88060937*T + 2500.559)
    return hg
```

##LiBr solution and refrigerant temperature as per Ashrae

```
def temp_libr (X,T):
    A0,A1,A2,A3 = -2.00755,0.16796,-0.003133362,0.0000197668
    B0,B1 ,B2,B3 = 124.937,-7.71649,0.152286,-0.0007959
    A = A0+ A1*X+ A2*X**2+ A3*X**3
    B = B0+ B1*X+ B2*X**2+ B3*X**3
    Tsol = B +T*A
    return Tsol
```

##Finding LiBr solution concentration iteratively from the available refrigerant saturation and solution temperature

```
def x_libr(Ta,Te):
    tolerance = 0.001 # limit of accuracy
```

```
    Differ = 1.0      # initializing error
    x = 46.0          #initial guess concentration value
    y =1
    for i in range(1,30000):
        if Differ>tolerance:
            x=x+0.001*i
            Differ = Ta - temp_libr (x,Te) # Calling temp_libr
function
        else:
            y = x
    return y
## Enthalpy of LiBr solution as per Ashrae
def enthalpy_libr (X,T):
    A0,A1,A2,A3,A4 = -2024.33,163.309 ,-4.88161 ,0.06302948 ,-
0.0002913704
    B0,B1,B2,B3,B4 = 18.2829,-1.1691757,0.03248041,-
0.0004034181,0.0000018520569
    C0,C1,C2,C3 = -0.037008214,0.0028877666,-
0.000081313015,0.00000099116628
    C4 = -0.0000000044441207
    A = A0+ A1*X+ A2*X**2+ A3*X**3+ A4*X**4
    B = B0+ B1*X+ B2*X**2+ B3*X**3+ B4*X**4
    C = C0+ C1*X+ C2*X**2+ C3*X**3+ C4*X**4
    h = A+T*B +T**2*C
    return h
## Solution method
Xstrong = x_libr(Tg,Tc)    # strong solution concentration
Xweak =x_libr(Ta,Te)       # weak solution concentration
Xr = 100-Xstrong           # weak solution concentration in water
Xa = 100-Xweak             # strong solution concentration in water
```

```
h4 = enthalpy_libr(Xweak,Ta)     #enthalpy of solution out from
absorber
h2 = enthalpy_libr(Xstrong,Tg)   #enthalpy of solution out form
generator
T1 = temp_libr(Xweak,Tc)         #saturation temperature of the LiBr
solution
h1 = enthalpy_libr(Xweak,T1)     #enthalpy of saturated LiBr
solution@genearator inlet
T3 = temp_libr(Xstrong,Te)       #saturation temperature of the LiBr
solution
h3 = enthalpy_libr(Xstrong,T3)   #enthalpy of saturated LiBr
solution@absorber inlet
h3a = h3                    #has the same enthalpy ,temperature and
composition as state 3.but with generator pressure
h4a = h4                    #subcooled state after pumping
f = (100-Xr)/(Xa-Xr)             #specific solution circulation rate
h1a = h4 +((f-1)/f)*(h2-h3)      #energy balance of the liquid heat
exchanger
h5 =hg_super(Tg)            # Latent heat of vaporization of water @ Tg
h6 = 4.1868*Tc              #saturated water at condenser outlet
h7 = h6                     #saturated water at evaporator pressure
h8 = hg_vapor (Te)               #saturated vapor at evaporator
qo = h8-h7                       #refrigerating effect
qh = h5 - h2 +f*(h2-h1a)         #heat added in the generator per unit
mass of vapor distilled
COP= qo/qh                  #coefficient of performance
D = Qe/qo                   #water vapor distilled per ton of
refrigeration
F = f*D                     #Mass flow rate of cold solution from the
absorber
```

```
G = F-D                    #Mass flow rate of hot solution from the
generator
Qc = D*(h5 - h6)                #heat rejected in the condenser
Qa =D*((h8-h3)+f*(h3 - h4))     #heat rejected in the condenser
Qh = D*qh                       #heat supplied in the generator
Eg = D*(qh- To*(gener_v.s-
entropy((Xstrong/100),Tg)+f*(entropy((Xstrong/100),Tg)-
entropy((Xweak/100),T1))))#rate of exergy gain @ generator
Ee = abs(D*(qo - To*(evap_v.s-evap.s)))   #rate of exergy gain @
evaporator, the value is negative as it is below To(Tamb)
Ec = Qc - D*(To*(cond_v.s-cond.s))         #rate of exergy destruction
@ condenser
Ea = Qa- D*(To*(evap_v.s-
entropy((Xstrong/100),T3)+f*(entropy((Xstrong/100),T3)-
entropy((Xweak/100),Ta))))#rate of exergy destruction @ absorber
COPex= Ee/Eg                    # second law efficiency
##checking the result
Qreceived = Qh+Qe               # net heat received
Qrejected = Qc+Qa               # net heat rejected
print ('the rate of heat input to generator is = ',Qh)
print ('the rate of heat rejected from condenser is = ',Qc)
print ('the rate of heat absorbed from absorber is = ',Qa)
print ('the net heat received = ',Qreceived,'the net heat rejected
=',Qrejected)
print ('the rate of exergy gain to generator is = ',Eg)
print ('the rate of exergy distruction from condenser is = ',Ec)
print ('the rate of exergy gain to evaporator is = ',Ee)
print ('the rate of exergy distruction from absorber is = ',Ea)
print('the coefficent of performance for your VARS is = ',COP)
print('the second law efficiency for your VARS is = ',COPex)
```

```
g = 9.81              #gravitational acceleration
cs_f = 0.0068         #for copper water
n = 1                 #for copper water
Dp = 0.016            #outside pipe diameter
IDp = 0.014           #inside pipe diameter
Np = 4                #number of pass
```

Component Design

##Generator design

```
Tg_in =116.0          #pressurized hot water to generator
Tg_out = 105.0        #pressurized hot water from generator
Tav = (Tg_in+Tg_out)/2# average hot water temperature
gen_liquid = IAPWS95(T=Tav+273.14, x=0)     #Take thermo_physical
propertys of hot water from iapws library
Mg= Qh/(gener.cp*(Tg_in-Tg_out))      # mass flow rate inside the pipe
Nt_G = Np*10                                # total number of tube
Ap = Nt*pi*Dp**2/(4*Np)                     # pipe area
Vp = Mg/(gen_liquid.rho*Ap)                 # velocity in the pipe
Rep = gen_liquid.rho*Vp *IDp/gen_liquid.mu  #tube side Reynolds number
Nup = 0.023*Rep**0.8*gen_liquid.Prandt**0.3 #tube side Nusselt number
hp = Nup*gen_liquid.k/IDp        #tube side heat transfer coefficient
dT = (Tg_in+Tg_out)/2-Tg         # degree of excess temperature
hs = (gener.mu*hg_vapor
(Tg)/dT)*(g*gener.rho/gener.sigma)**0.5*(1000*gener.cp*dT/(cs_f*hg_vap
or (Tg)*gener.Prandt))
U =((1/(IDp*hp) + 1/(Dp*hs))**(-1))/Dp      #over all heat transfer
coefficient
DT1 = Tg_in-Tg
DT2 = Tg_out-Tg
LMTD = (DT1 - DT2)/np.log(DT1/DT2)    #logarithmic mean temperature
```

```
difference
A = (Qh*1000)/(U*LMTD)                #heat transfer area
Lg = A/(Nt*pi*Dp)                     #tube length per pass
print ('Hot pressurized mass flow rate to generator  = ',Mg)
print ('heat transfer area of generator', A)
print ('number of tube required per pass for generator is = ',Nt_G)
print ('length per pass of gnererator is' ,Lg)
```

##absorber design

```
Ta_in =25.0                      #cooling water to absorber
Ta_out =30.0                     #cooling water from absorber
Tav = (Ta_in+Ta_out)/2           # average cooling water
abs_liquid = IAPWS95(T=Tav+273.14, x=0)#Take thermophysical properties
of cooling water from iapws library
Mp= Qa/(absor.cp*(Ta_out-Ta_in)) # mass flow rate inside the pipe
Nt_ab = Np*16                    # total number of tube
Ap = Nt*pi*Dp**2/(4*Np)                          #pipe area
Vp = Mp/(abs_liquid.rho*Ap)                      #velocity in the pipe
Rep = abs_liquid.rho*Vp *IDp/abs_liquid.mu       #Reynolds number
inside the pipe
Nup = 0.023*Rep**0.8*abs_liquid.Prandt**0.3      # tube side nusselt
number
hp = Nup*abs_liquid.k/IDp                        # tube side heat
transfer coefficient
dT = (Ta_in+Ta_out)/2-Tc
Ka =absor.sigma/(absor.rho**(-0.333)*(absor.mu**4*g)**0.33) #kapitza
number
Ja = absor.cp*(Tc-Tav)/hg_vapor (Tc)   #Jacobs number
Nup = 0.84298*Rep**0.145664 *absor.Prandt**0.048053*Ka**0.330440*Ja**-
0.071242                               # shell side nusselt number
U =((1/(IDp*hp) + 1/(Dp*hs))**(-1))/Dp           #over all heat
```

```
transfer coefficient
DT1 = Ta-Ta_in
DT2 = Ta-Ta_out
LMTD = abs(DT1 - DT2)/np.log(abs(DT1/DT2))       #Logarithmic mean
temperature
A = (Qa*1000)/(U*LMTD)                           #heat transfer area
La = A/(Nt*pi*Dp)                                #tube length per pass
print ('Mass flow rate of cooling water  = ',Mp)
print ('number of tube required per pass for absorber is = ',Nt)
print ('length per pass of absorber is = ',La)
print ('heat transfer area of absorber', A)
print ('Overall heat transfer coefficent of absorber', U)
## Evaporator design
Tolerance = 0.02
differ = 1
for i in range (1,1000):
    if differ > Tolerance:
        Tav = (Tchill_in + Tchill_out)/2    #chilled water avarage
temperature
        liquid = IAPWS95(T=Tav+273.14, x=0) #Take thermo_physical
propertys of chilled water from iapws library
        Mp= Qe/(liquid.cp*(Tchill_in-Tchill_out))# tube side mass flow
rate
        Nt = Np*i                            # total number of tube
        Ap = Nt*pi*Dp**2/(4*Np)             #pipe area
        Vp = Mp/(liquid.rho*Ap)             #velocity in the pipe
        Rep = liquid.rho*Vp *IDp/liquid.mu  #Reynolds number inside the
pipe
        Nup = 0.023*Rep**0.8*liquid.Prandt**0.3  #tube side nusselt
number
```

```
        hp = Nup*liquid.k/IDp            #tube side heat transfer
        dT = (Tchill_in+Tchill_out)/2-Te #degree of excess temperature
        hs= (evap.mu*hg_vapor(Te)/dT)*(g*evap.rho/evap.sigma)**0.5*(10
00*evap.cp*dT/(cs_f*hg_vapor(Te)*evap.Prandt))
        U =((1/(IDp*hp) + 1/(Dp*hs))**(-1))/Dp #over all heat transfer
coefficient
        DT1 = Tchill_in-Te
        DT2 = Tchill_out-Te
        LMTD = (DT1 - DT2)/np.log((DT1/DT2))   #logarithmic mean
temperature difference
        A = (Qe*10000)/(U*LMTD)                #heat transfer area
        Le = A/(Nt*pi*Dp)                      #tube length per pass
        differ = abs(Le-La)
    else:
        Nt = int(Nt)
print ('number of tube required per pass for evaporator is = ',Nt)
print ('heat transfer area of evaporator', A)
print ('overall heat transfer coefficient of evaporator',
U)
```

##Condenser design

```
Tci =30.0                      # inlet cooling water from  absorber
Tco =35.0                      # outlet cooling water from absorber
Tav = (Tci+Tco)/2              # average cooling water temperature
con_liquid=IAPWS95(T=Tav+273.14, x=0) #Take thermophysical properties
of cooling water from iapws library
Tolerance = 0.02
differ = 1
for i in range (1,1000):
    if differ > Tolerance:
        Mp= Qc/(con_liquid.cp*(Tco-Tci))
```

```
        Nt = Np*i                          #total number of tubes
        Ap = Nt*pi*Dp**2/(4*Np)            #pipe area
        Vp = Mp/(con_liquid.rho*Ap)        #velocity in the pipe
        Rep = con_liquid.rho*Vp *IDp/con_liquid.mu  # Pipe side
Reynolds number
        Nup = 0.023*Rep**0.8*con_liquid.Prandt**0.3 # Pipe side
nusselt number
        hp =Nup*con_liquid.k/IDp # pipe side heat transfer coefficient
        dT = (Tci+Tco)/2-Tc      # temperature difference
        hs=(Nt)**(-0.0833)*0.729*((cond.k**3* cond.rho**2*hg_vapor
(Tc)*9.81)/(Dp*cond.mu*(Tc -Tav)) )**0.25
        U =((Dp/(IDp*hp) + 1/(hs))**(-1))        #overall heat
transfer coefficient
        DT1 = abs(Tc-Tci)
        DT2 = abs(Tc-Tco)
        LMTD = (DT1 - DT2)/np.log((DT1/DT2))     #logarithmic
temperature difference
        A = (Qc*10000)/(U*LMTD)
        Lc = A/(Nt*pi*Dp)
     #Condenser length
        differ = abs(Lc-Lg)
    else:
        Nt = int(Nt)
print('number of tube required per pass for condenser is= ', Nt)
print ('heat transfer area of condenser', A)
print ('heat transfer area of condenser', U)
```

```
## Solution heat exchanger design
Dp = 0.0198
Tav_weak = (T1+Ta)/2             # average weak solution temperature
Tav_strong = (T3+Tg)/2           # average strong solution temperature
con_weak=IAPWS95(T=Tav_weak+273.14, x=0)         #Take thermo_physical
properties of weak solution from iapws library
con_strong=IAPWS95(T=Tav_strong+273.14, x=0)     #Take thermo_physical
properties of strong solution from iapws library
Ap = (pi*IDp**2/4)                                #pipe area
Vp = F/(density(Tav_weak,Xweak)*Ap)  #velocity in the pipe
Rep = density(Tav_weak,Xweak)*Vp *IDp/con_weak.mu# Pipe side Reynolds
number
Nup = 0.023*Rep**0.8*con_weak.Prandt**0.4   # Pipe side nusselt number
hp =Nup*con_weak.k/IDp           # pipe side heat transfer coefficient
Vs = F/(density(Tav_strong,Xstrong)*Ap)     #velocity in the annulus
Ph = pi*Dp
De = 4*Ap/Ph
Rep = density(Tav_strong,Xstrong)*Vs *De/con_strong.mu # annulus side
Reynolds number
Nup = 0.023*Rep**0.8*con_strong.Prandt**0.3            # annulus side
nusselt number
hs =Nup*con_strong.k/IDp
U =((Dp/(IDp*hp) + 1/(hs))**(-1))   #overall heat transfer coefficient
DT1   = abs(T1-T3)
DT2   = abs(Ta-Tg)
LMTD = (DT1 - DT2)/np.log((DT1/DT2))  #logarithmic temperature
difference
Qex   = F*Cp_LiBr(Tav_weak,Xweak)*(T1-Ta)
A     = (Qex)/(U*LMTD)
Lex   = A/(pi*Dp)                      #heat exchanger length
```

```
Nex   = Lex/Lg
Nex   = int(Nex)
print ('number of tube required per pass for solution heat exchanger
is = 'Nex)
print ('length per pass of solution heat exchanger is = ',Lg)
print ('heat transfer area of solution heat exchanger', A)
print ('heat transfer area of solution heat exchanger', U)
```

ANNEX C: Python program for Solar Radiation and Ambient Temperature

This code is developed to determine the daily and hourly global, diffuse and beam radiation for the representative day of each month. This code is present specifically for the average sunshine hour of Adama for five years, but one can easily change the location of its latitude and average sunshine hour to determine the radiation distribution at his own location.ho1, ho21, ho22, ho31,ho32, and ho3 are presented as an assignment for a variable to handle the lengthy daily extra-terrestrial radiation formula of Ho. The radiation distribution is presented for the representative day of each season of their respective first month. Also, the daily atmospheric temperature variation is coded here, but one can easily change the Tmax and Tmin value to determine the daily atmospheric temperature variation of interest.

```
@author: Natnale sitotaw
"""
from scipy import *
from numpy import *
from pylab import *
import matplotlib.pyplot as plt
from mpl_toolkits.axes_grid1 import host_subplot
import mpl_toolkits.axisartist as AA
import matplotlib.pyplot as plt
a = float(input('enter the latitude of your location ')) # User
prompting to input the latitude of his location.
Tmax = float(input('enter the maximum temperature of the day '))# User
prompting to input the maximum temperature of the day.
Tmix = float(input('enter the minimum temperature of the day '))# User
prompting to input the minimum temperature of the day.
```

```
arr = array([0.0]*12)
for i in range (1,13):
    if i == 1:
         data = float(input('enter januarys sunshin hour ')) # User
prompting to input sunshine hour of the representative day of the year
         arr[0] = data
    elif 1<i <12:
         data = float(input('please enter the next month sunshin hour
'))
         arr[i-1] = data
    else:
         data = float(input('enter the last month sunshin hour '))
         arr[i-1] = data
Isc = 1367                              # solar constant
A =array([[0.0]*(12)]*(12))
A[0][:]     = arr          #representative day of each months
A[1][:] = 23.45*sin((360*(284+A[0][:])/365)*pi/180)#declination angle
A[2][:] = arr                           #sun shine hours
A[3][:]    = np.arccos(-tan(a*pi/180)*tan((A[1][:])*pi/180))*180/pi
                                        # sunset hour angle
A[4][:] = 2*A[3][:]/15                  # number of daylight hours
A[5][:] = -
0.110 + 0.235*cos(a*pi/180) + 0.323*(np.divide(A[2][:],A[4][:]))#regre
ssion parameter
A[6][:] = 1.449 - 0.533*cos(a*pi/180) - 0.694*(np.divide(A[2][:],A[4][
:])) #regression parameter
A[7][:] = 0.409 + 0.5016*sin((A[3][:] - 60)*pi/180)  #regression
parameter
A[8][:] = 0.6609 - 0.4767*sin((A[3][:] - 60)*pi/180) #regression
parameter
```

```
ho1 = 1 + 0.033*cos((360*A[0][:]/365)*pi/180)
ho21 =cos(a*pi/180)*cos(A[1][:]*pi/180)
ho22 = sin(A[3][:]*pi/180)
ho2   =  np.multiply(ho21,ho22)
ho31 = sin(a*pi/180)*(pi*A[3][:]/180)
ho32 = sin(A[1][:]*pi/180)
ho3   = np.multiply(ho31,ho32)
A[9][:] = np.multiply((24*3600*(Isc/pi)*ho1),(ho2 + ho3))/3600000
#daily extraterrestrial radiation on a horizontal surface
A[10][:] =np.multiply(A[9][:],(A[5][:] +np.multiply(A[6][:],(np.divide
(A[2][:],A[4][:])))))
A[11][:] =np.multiply(A[10][:],(0.931 - 0.814*(np.divide(A[2][:],A[4][
:]))))
print A[3][:]
x = array([[0.0]*24]*12)
y = array([[0.0]*24]*12)
w =array([0.0]*24)
for t in range (1,25):
    if t == 1:
        w[t-1] = -180
    else:
        w[t-1]=w[t-2]+15
for i in range (1,12):
##Monthly average hourly global radiation on a horizontal surface
    for j in range (1,24):

         I =A[10][i-1]* pi/24*(A[7][i-1] + A[8][i-1]*cos(w[j-
1]*pi/180))*(cos(w[j-1]*pi/180) - cos(A[3][i-1]*pi/180))/(sin(A[3][i-
1]*pi/180) - pi/180*A[3][i-1]*cos(A[3][i-1]*pi/180));
         if I > 0:
```

```
            x[i-1][j-1] = I
```
##Monthly average hourly diffuse radiation on a horizontal surface
```
         else:
             x[i-1][j-1] = 0
    for j in range(1,24):
        Id =(A[11][i-1]* (pi)/24)*(cos(w[j-1]*pi/180) - cos(A[3][i-1]*pi/180))/(sin(A[3][i-1]*pi/180) - pi/180*A[3][i-1]*cos(A[3][i-1]*pi/180));
        if Id>0:
            y[i-1][j-1] = Id;

        else:
            y[i-1][j-1] = 0;
z = x-y  #monthly average beam  radiation on a horizontal surface
```
Hourly temperature variation for march, 16
```
zan=linspace(0,12,12)      #graduation of x axis
def hourly_temp(t):    T = Tmax - ((Tmax-Tmin)/2)*(1 - sin((pi*t-10*pi)/12))
    return T
T = array([0.0]*(24))
for i in range (1,25):
    T[i-1] = hourly_temp(i)
xan=linspace(1,24,24)
plt.subplots_adjust(right=1.25)
plt.subplots_adjust(top=1.25)
```
##Sunsine hour
```
plt.plot(zan,A[2][:])
plt.xlabel('month')
plt.ylabel('sunshine hour')
```

```
title('bright sunshine hour for representative day of each month' )
```
##Monthly average global, diffuse and beam radiation
```
plt.ylim([0,12])
WW = A[10][:]-A[11][:]
plt.plot(zan,A[10][:],label='Global')
plt.plot(zan,A[11][:],'*',label='Diffuse')
plt.plot(zan,WW,'o',label='Beam')
plt.xlabel('month')
plt.ylabel('Radiation(KWh/m2/day)')
plt.ylim([0,7])
legend(loc=0)
show()
```

##hourly average global, diffuse and beam radiation @ ground level on a horizontal surface
```
plt.subplots_adjust(right=0.75)
plt.figure(4,figsize = (10,10))
WW = x[8][:]-y[8][:]       # beam radiation of September, 15
Wx = x[10][:]-y[10][:]     # beam radiation of December, 10
Wy = x[2][:]-y[2][:]       # beam radiation of march, 16
Wz = x[5][:]-y[5][:]       # beam radiation of June, 11
plt.subplot(2,2,1)
plt.plot(xan,x[8][:])
plt.plot(xan,y[8][:],'*')
plt.plot(xan,WW,'o')
plt.title('autumn,september 15 ')
plt.subplot(2,2,2)
plt.plot(xan,x[10][:])
plt.plot(xan,y[10][:],'*')
```

```
plt.plot(xan,Wx,'o',)
plt.title('summer,December 10')
plt.subplot(2,2,3)
plt.plot(xan,x[2][:],)
plt.plot(xan,y[2][:],'*',)
plt.plot(xan,Wy,'o',)
plt.ylabel('Radiation(MJ/m2/hr')
plt.title('spring, march 16')
plt.subplot(2,2,4)
plt.plot(xan,x[5][:],label='Global')
plt.plot(xan,y[5][:],'*',label='Diffuse')
plt.plot(xan,Wz,'o',label='Beam')
plt.title('winter, June 11')
plt.xlabel('Time(hr)')
plt.ylim([0,1])
plt.xlim([0,24])
legend(loc='best')
show()
```

atmospheric temperature variation for march, 16 @Tmax = 29.7 and @Tmin = 16.466

```
plt.plot(xan,T,label='Hourly Variation of Atmospheric Temperature on, march 16')
plt.xlabel('hour')
plt.ylabel('Temperature')
plt.title('Hourly Variation of Atmospheric Temperature on march, 16')
```

ANNEX D: Python program for HPETC

This code is developed to determine the transient analysis of HPETC. The daily temperature extraction form collector is determined for the representative day of each month, as the code is intended to evaluate the transient response of the collector in each second. It is recommended to evaluate for each day separately to reduce the computational time cost. But, to evaluate for the next day one can easily change the global radiation input (x[0][:]) and the temperature variation on that day(Tmax and Tmin). The code needs radiation data called from the previse code. A two-dimensional array as a variable store is created to fill the data for the output of collector. The specification for the collector as per the manufacturer is used to evaluate the result. And, average property of fluid is used instead of using Ipaw library to take thermo-physical property for each time step, this is the limitation, because of the computational time it takes.

```
@author: Natnale sitotaw
"""
from scipy import *
from numpy import *
from pylab import *
import matplotlib.pyplot as plt  ##Estimation of Hourly Variation of
Atmospheric Temperature for March,16
def hourly_temp(t):
        T = Tmax - ((Tmax-Tmin)/2)*(1 - sin((pi*t-10*pi)/12))
    return T
T = array([0.0]*(24))
for i in range (1,25):
    T[i-1] = hourly_temp(i)+273.14
```

```
zan=linspace(1,24,24)           #graduation of x axis
I =x[0][:]
Vww    =4.2                     #wind speed
pl     = 937.207                #languid density@125
pv     = 1.367                  #vapor density@125
ul     =0.0002195               #liquid viscosity
kl    =0.688          # average thermal conductivity of liquid water
s_t    = 0.05385                #surface tension
Lt     = 1.8                    #heat pipe total length
Le     = 1.6                    #evaporator length
Lc     = 0.1                    #condenser length
La     = 0.1                    #adiabatic length
hr     =3600                    #seconds in one hour
n      =hr*24+1                 # number of second in a day
Dg,tg    = 0.058,0.0018         #glass diameter and thickness
Da,ta    = 0.047,0.0018         #glass diameter and thickness
Dc,IDc = 0.024,0.0228           #outer and inner condenser diameter
Di     = 0.0068                 #internal pipe diameter
w,t    = 0.1056,0.0002          #width and thickness of evaporator fin
De,IDe = 0.008,0.0068           #external and internal pipe diameter
Dmani  = 0.042                  #manifold diameter
K_hp    =401                    #thermal conductivity of evaporator
Ts     = 125+273.14             #Temperature of vaporization
hfg    = 2188.42                #latent heat of vaporization
cpl    = 4256                   #average specific heat of water
Khp    = 401                    #pipe thermal conductivity
g     = 9.81                    #gravitational acceleration
dx    =0.075          #distance between each tube, center to center
dt    =1              # time increment for transient response
m     = 0.008               #mass flow rate of working fluid
```

```
B     = 25                  #angle of inclination
Pres  = 600000              #working pressure
Dpgo   = 0.049              #outer glass diameter
Dgi    =0.058               #inner glass diameter
Tr_glas = 0.96              #emissivity of the glass
e_abso      = 0.1           #emissivity of the absorber
e_glass = 0.06              #emissivity of the absorber
a_abso      = 0.94          #absorptivity of absorber
sigma  = 5.67*10**(-8)      #Stefan Boltzmann constant
##Glass property
Cpg,pg,Vg = 835,2600,0.00027     #specific heat, density and volume of
the glass respectively
##Absorber property
Cpa,pa,Va = 835,2600,0.000221    #specific heat, density and volume of
the absorber respectively
##Evaporator property
Cpe,pe,Ve = 383,8933,0.0000352   #specific heat, density and volume of
the evaporator respectively
##Condenser property
Cpc,pc,Vc = 383,8933,0.00000441  #specific heat, density and volume of
the condenser respectively
##Working fluid property
Cpw,pw = 4203,967                #specific heat, density and volume of
the water respectively
Tg = array([[T[0]]*n]*20)             # array for glass temperature
Tp = array([[T[1]]*n]*20)             # array for absorber temperature
Te = array([[T[2]]*n]*20)             # array for evaporator
temperature
Tc = array([[T[3]]*n]*20)          # array for condenser temperature
Tw = array([[85+273.14]*n]*20) # array for working fluid temperature
```

```
Ag,Ap,Ac, Ae, A_mani = pi*Dg*Le ,
pi*Da*Le ,pi*Dc*Lc,pi*De*Le ,(pi*Dmani**2)/4 # area of glass,
absorber, condenser, evaporator, manifold
for i in range (1,25):
    for j in range (1,hr+1):
        for w in range (1,21):
            R_cond = (np.log(Dc/IDc))/(2*pi*K_hp* Lc) # resistance of
condenser
            Rwater = 1/(Ac*hc)
# convection resistance of water
            hga = 5.7 + 3.8*Vww         # convection heat transfer
coefficient from outer glass tube
            hr_g_a = Tr_glas*sigma*((Tg[w-1][j+hr*i-
(hr+1)])**2 + (T[i-1])**2)*(Tg[w-1][j+hr*i-(hr+1)] +T[i-1])# radiation
heat transfer coefficient between outer tube glass and the environment
            R_g_a = 1/(Ag*(hga+hr_g_a)) # thermal resistance between
outer glass and environment
            hr_w_g = (sigma*((Tp[w-1][j+hr*i-(hr+1)])**2+(Tg[w-
1][j+hr*i-(hr+1)])**2 )*(Tp[w-1][j+hr*i-(hr+1)]+Tg[w-1][j+hr*i-
(hr+1)]))/(1/e_abso +(Ap/Ag) *((1/e_glass) -1))  # radiation heat
transfer coefficient between outer and inner tube glass
            R_w_g = 1/(Ap*hr_w_g)               # thermal resistance
between inner and outer tube glass
            R_evap =(np.log(De/IDe))/(2*pi*K_hp* Le)   # thermal
resistance of evaporator tube
            A,B,C
= Ag*(1- Tr_glas)/(pg*Vg*Cpg) ,1/(R_w_g*pg*Vg*Cpg),1/(R_g_a*pg*Vg*Cpg)
            D,E,F=Ap**Tr_glas*a_abso/(pa*Va*Cpa),1/(pa*Va*Cpa*R_w_g),1
/(pa*Va*Cpa*Rwater)
            K,L =1/(pw*A_mani*Cpw*Rwater),m/(pw*A_mani*dx)
```

```
            Tg[w-1][j+hr*i-(hr)] = (A*I[j+hr*i-(hr+1)]*1000+((1/dt)-
(B+C))*Tg[w-1][j+hr*i-(hr+1)]+B*Tp[w-1][j+hr*i-(hr+1)]+C*T[i-1])*dt
            Tp[w-1][j+hr*i-(hr)] = (D*I[j+hr*i-(hr+1)]*1000+((1/dt)-
(E+F))*Tp[w-1][j+hr*i-(hr+1)]+E*Tg[w-1][j+hr*i-(hr+1)]+F*Tw[w-
1][j+hr*i-(hr+1)])*dt
            if Tp[w-1][j+hr*i-(hr)]<=(85+273.14):
                Tw[w-1][j+hr*i-(hr)] = 85+273.14
            else:
                if w==1:
                    Tw[w-1][j+hr*i-(hr)] = (((1/dt)-
(L+K))*(85+273.14)+K*Tp[w-1][j+hr*i-(hr)]+L*(85+273.14))*dt
                else:
                    Tw[w-1][j+hr*i-(hr)] = (((1/dt)-(L+K))*Tw[w-
1][j+hr*i-(hr+1)]+K*Tp[w-1][j+hr*i-(hr+1)]+L*Tw[w-2][j+hr*i-(hr)])*dt

xan=linspace(0,24,86401)        # graduation of x axis for temperature
outlet plot
X =Tw[19][:] - 273.14
y =Tw[9][:] - 273.14
Z =Tw[4][:] - 273.14            #change temperature to degree Celsius
plt.subplots_adjust(right=0.75)
plt.subplots_adjust(top=1)
plt.plot(xan,X,color ='blue',label='i = 20')     #outlet temperature @
20th element
plt.plot(xan,y,color ='red',label='i = 10')      #outlet temperature @
10th element
plt.plot(xan,Z,color ='green',label='i = 5')     #outlet temperature @
5th element
plt.title('winter, June 11')
plt.xlabel('Time(hr)')
```

```
plt.ylabel('Collector outlet temperature')
plt.ylim([80,180])
legend(loc='best')
show()
```

ANNEX E: Python program for PCM thermal storage system

This code is developed to evaluate the transient response of PCM-fluid heat exchange. A variable from the previse two codes is call (Qh and Tw[19][:]) to evaluate the size of cylindrical shell and the daily instantaneous temperature of PCM. An average thermophysical property of HTF and PCM is considered. Simultaneous numerical evaluation of both HTF and PCM equation is simulated through the code.

```
@author: Natnale sitotaw
"""
from scipy import *
from numpy import *
from pylab import *
import matplotlib.pyplot as plt
cps   = 1350                      #specific heat of PCM solid
cpl    = 2740                     #specific heat of PCM liquid
Ppcm    = 1450                    #density of PCM
Lfu    = 339000                   #latent heat of fusion of PCM
ee    = 0.608                     #porosity
QQ    = Qh*1000*3600*14           #total energy required to sustain the
operation for 14hr
Vp     = QQ/(Ppcm*Lfu)            #volume of PCM
Vs    = Vp/ee                     #volume of a cylindrical shell
Dp     = 0.05                     # PCM diameter
Ds     = (4*Vs/(1.5*pi))**0.334   #cylinder diameter
H      = Ds * 1.5                 #shell height
Nh     = int(H/Dp)                #number of PCM layer
Nd    = int(Ds/Dp)                #number of PCM in diameter of a shell
pf    =953.288                    #density of the fluid
```

```
cpf    = 4226                    #specific heat of the fluid
kf     = 0.683                   #thermal conductivity of the fluid
H_solid = (1000+cps*(116-85))    #total enthalpy gain up to saturated
solid
Cpcm_s = 1350                    #specific heat of PCM liquid
Cpcm_l = 2740                    #specific heat of PCM vapor
Kp_solid = 0.733                 #solid PCM thermal conductivity
Kp_liquid = 0.326                #thermal conductivity of PCM liquid
A = Nd*4*pi*Dp**2                # area of the layer
pr = 1.61                        #Prandtl number of working fluid
vf =Mg/(0.25*ee*pf*Ds**2)        #velocity of fluid
uf = 0.0026                      #Dynamic viscosity of the fluid
Re = pf*Dp*e*vf/uf               #Reynold's number
nn = 86401                       #Seconds in a day
Tf=array([[85]*nn]*Nh)           #array for temp of heat transfer fluid
Hp=array([[1000]*nn]*Nh)         #array of enthalpy for PCM
Tp=array([[84.5]*nn]*Nh)         #array for temp of PCM
Tx =Tw[19][:]-273.14             #collector outlet temperature of the
day
for i in range (1,nn):
##Charging mode
    if Tf[j-1][i-1] > Tp[j-1][i-1]:
        for j in range (1,Nh+1):
                Ra =(pr*(g/Tf[j-1][i-1])*abs(Tf[j-1][i-1]-Tp[j-1][i-
1])*R**3*pf**2)/(uf**2)
                keff = 0.18*Kp_solid*Ra**0.25    #effective thermal
conductivity @ interface
                Uv = 6*(1-ee)*(2+1.1*Re**0.6*pr**0.334)* keff/(Dp**2)
                Af,Bf,Cf = dt*vf,keff/(pf*cf*Dp) ,Uv/(e*pf*cf)
                #code for  HTF
```

```
                if j == 1:
                   Tf[j-1][i] = Af*(Tf[j-1][i-1]-T[i-1])+Bf*(Tf[j][i-
1]-2*Tf[j-1][i-1]+T[i-1])+Cf*(Tf[j-1][i-1]-Tp[j-1][i-1])+Tf[j-1][i-
1] #external nodes
                else:
                   Tf[j-1][i] = Af*(Tf[j-1][i-1]-Tf[j][i-
1])+Bf*(Tf[j][i-1]-2*Tf[j-1][i-1]+Tf[j-2][i-1])+Cf*(Tf[j-1][i-1]-Tp[j-
1][i-1])+Tf[j-1][i-1]           #internal nodes
        for x in range (1,Nh+1):
                Uv = 6*(1-ee)*(2+1.1*Re**0.6*pr**0.334)*keff/(Dp**2)
                keff = 0.18*Kp_solid*Ra**0.25  #effective thermal
conductivity @ interface
                Ntu = Uv*A*H/(Mg*cpf)
                y = (Mg*cpf)*Ntu/(Ppcm*(1-ee)*A*H)
                #code of PCM
                if Hp[x-1][i-1]<H_solid:#if PCM is in sloid state
                   if x==1:
                      Hp[x-1][i] =y*(Tx[i-1]-Tp[x-1][i-1])+Hp[x-1][i-
1]                              # external nodes
                   else:
                      Hp[x-1][i] =y*(Tf[x-1][i]-Tp[x-1][i-1])+Hp[x-
1][i-1]                         # internal nodes
                elif H_solid<=Hp[x-1][i-1]<=(H_solid + lfu):#if PCM
is in phase transition
                    if x==1:
                       Hp[x-1][i] =y*(Tx[i-1]-Tp[x-1][i-1])+ Hp[x-
1][i-1]
                    else:
                       Hp[x-1][i] =y*(Tf[x-1][i]-Tp[x-1][i-1])+ Hp[x-
1][i-1]
```

```
                else:      # if PCM in liquid state
                    if x==1:
                       Hp[x-1][i] = y*(Tx[i-1]-Tp[x-1][i-1])+Hp[x-
1][i-1]
                    else:
                       Hp[x-1][i] = y*(Tf[x-1][i]-Tp[x-1][i-1])+Hp[x-
1][i-1]
                if Hp[x-1][i]<H_solid:
                    Tp[x-1][i] = (Hp[x-1][i]-1000)/cps +85
                elif H_solid<=Hp[x-1][i]<=(H_solid + lfu):
                    Tp[x-1][i] =116.8 + 2*((Hp[x-1][i]-H_solid))/lfu
                else:
                    Tp[x-1][i] =118.8 + (Hp[x-1][i]-(H_solid
+lfu))/cpl
 ##Discharging mode
    else:
        for j in range (1,Nh+1):
                keff = Kp_solid                      #effective
thermal conductivity of PCM
                Uv   = 6*(1-ee)*(2+1.1*Re**0.6*pr**0.334)*
keff/(Dp**2)
                Af,Bf,Cf = dt*vf,keff/(pf*cf*Dp) ,Uv/(e*pf*cf)
                if j == 1:
                   Tf[j-1][i] = Af*(Tf[j-1][i-1]-T[i-1])+Bf*(Tf[j][i-
1]-2*Tf[j-1][i-1]+T[i-1])+Cf*(Tf[j-1][i-1]-Tp[j-1][i-1])+Tf[j-1][i-1]
                else:
                   Tf[j-1][i] = Af*(Tf[j-1][i-1]-Tf[j][i-
1])+Bf*(Tf[j][i-1]-2*Tf[j-1][i-1]+Tf[j-2][i-1])+Cf*(Tf[j-1][i-1]-Tp[j-
1][i-1])+Tf[j-1][i-1]
        for x in range (1,Nh+1):
```

```
                keff =Kp_solid         #effective thermal conductivity
                Uv = 6*(1-ee)*(2+1.1*Re**0.6*pr**0.334)*keff/(Dp**2)
                Ntu = Uv*A*H/(Mg*cpf)
                y = (Mg*cpf)*Ntu/(Ppcm*(1-ee)*A*H)
                if Hp[x-1][i-1]<(1000+cps*(116-85)):
                   if x==1:
                      Hp[x-1][i] =Hp[x-1][i-1]-y*(Tp[x-1][i-1]-Tx[i-
1])
                   else:
                      Hp[x-1][i] =Hp[x-1][i-1]-y*(Tp[x-1][i-1]-Tf[x-
1][i])
                elif H_solid<=Hp[x-1][i-1]<=(H_solid +lfu):
                    if x==1:
                       Hp[x-1][i] =Hp[x-1][i-1]-y*(Tp[x-1][i-1]-Tx[i-
1])
                    else:
                       Hp[x-1][i] =Hp[x-1][i-1]-y*(Tp[x-1][i-1]-Tf[x-
1][i])
                else:
                    if x==1:
                       Hp[x-1][i] = Hp[x-1][i-1]-y*(Tp[x-1][i-1]-Tx[i-
1])
                    else:
                       Hp[x-1][i] = Hp[x-1][i-1]-y*(Tp[x-1][i-1]-Tf[x-
1][i])
                if Hp[x-1][i]<H_solid:
                    Tp[x-1][i]    = (Hp[x-1][i]-1000)/cps +85
                elif H_solid<=Hp[x-1][i]<=(H_solid + lfu):
                    Tp[x-1][i]    =116.8 + 2*(Hp[x-1][i]-H_solid)/lfu
                else:
```

```
                    Tp[x-1][i] =118.8 + (Hp[x-1][i]-(H_solid +
lfu))/cpl
plt.subplots_adjust(right=0.75)
plt.subplots_adjust(top=1)
xan=linspace(0,24,nn)
plt.plot(xan,Tp[Nh-1][:],label='Layer Nh')
plt.plot(xan,Tp[10][:],label='Layer 20')
plt.plot(xan,Tp[10][:],label='Layer 10')
plt.plot(xan,Tp[0][:],label='Layer 1')
plt.title('winter, June 11')
plt.xlabel('Time(hr)')
plt.ylabel('Temperature of PCM')
plt.ylim([80,180])
legend(loc='best')
show()
```